https://doi.org/10.5194/egusphere-2025-5023
Preprint. Discussion started: 27 October 2025

A cross-site comparison of ecosystem- and plot-scale methane fluxes from wetlands and uplands

Tiia Määttä[1], Ankur Desai[2], Masahito Ueyama[3], Rodrigo Vargas[4], Eric J. Ward[5,6], Zhen Zhang[7], Gil Bohrer[8], Kyle Delwiche[9], Etienne Fluet-Chouinard[10], Järvi Järveoja[11], Sara Knox[12], Lulie Melling[13], Mats B. Nilsson[11], Matthias Peichl[11], Angela Che Ing Tang[14], Eeva-Stiina Tuittila[15], Jinsong Wang[16], Sheel Bansal[17], Sarah Feron[18], Manuel Helbig[19], Aino Korrensalo[20,21], Ken W. Krauss[22], Gavin McNicol[23], Shuli Niu[16], Zutao Ouyang[24], Kathleen Savage[25], Oliver Sonnentag[26], Robert Jackson[27,28], and Avni Malhotra[1,29]

[1] Department of Geography, Faculty of Science, University of Zürich, Winterthurerstrasse 190, 8057 Zürich, Switzerland
[2] Atmospheric and Oceanic Sciences, University of Wisconsin-Madison, Madison, WI, 53706, USA
[3] Osaka Metropolitan University, Osaka, Japan
[4] School of Life Sciences, Arizona State University, Tempe, AZ, 85287, USA
[5] University of Maryland, Earth System Science Interdisciplinary Center, College Park MD, USA
[6] NASA Goddard Space Flight Center, Biospheric Sciences Laboratory, Greenbelt MD, USA
[7] National Tibetan Plateau Data Center (TPDC), State Key Laboratory of Tibetan Plateau Earth System, Environment and Resource (TPESER), Institute of Tibetan Plateau Research, Chinese Academy of Sciences, Beijing, 100101, China
[8] Department of Civil, Environmental & Geodetic Engineering, The Ohio State University, Columbus, OH, 43210, USA
[9] Department of Environmental Science, Policy & Management, UC Berkeley, Berkeley, California, USA
[10] Earth System Sciences Division, Pacific Northwest National Laboratory, Richland, WA, USA
[11] Department of Forest Ecology and Management, Swedish University of Agricultural Sciences, Umeå, Sweden
[12] Department of Geography, McGill University, Montreal, Canada
[13] UN Sustainable Development Solutions Network, Asia Headquarters, Sunway University, 47500 Bandar Sunway, Selangor, Malaysia
[14] Department of Environmental Sciences, University of Toledo, Toledo, Ohio, USA
[15] School of Forest Sciences, Joensuu campus, University of Eastern Finland, Joensuu, Finland
[16] Key Laboratory of Ecosystem Network Observation and Modeling, Institute of Geographic Sciences and Natural Resources Research, Chinese Academy of Sciences, Beijing 100101, China
[17] U.S. Geological Survey, Northern Prairie Wildlife Research Center, Jamestown, ND USA
[18] University of Groningen, Leeuwarden, the Netherlands
[19] GFZ Helmholtz Centre for Geosciences, Potsdam, Germany
[20] Department of Environmental and Biological Sciences, University of Eastern Finland, Kuopio, Finland
[21] Natural Resources Institute Finland, Joensuu, Finland
[22] Louisiana Universities Marine Consortium (LUMCON), Chauvin, LA 70344, USA
[23] Department of Earth and Environmental Sciences, University of Illinois Chicago, Chicago, IL, USA
[24] College of Forestry, Wildlife and Environment, Auburn University, Auburn, AL, USA
[25] Woodwell Climate Research Center, Falmouth, USA
[26] Université de Montréal, Département de géographie, Montréal, QC, Canada
[27] Department of Earth System Science, Stanford University, Stanford, 94305, USA
[28] Woods Institute for the Environment and Precourt Institute for Energy, Stanford University, Stanford, 94305, USA
[29] Biological Sciences Division, Pacific Northwest National Laboratory, 902 Battelle Boulevard, Richland, WA, USA

Correspondence to: Tiia Määttä (tiia.maatta@geo.uzh.ch)

https://doi.org/10.5194/egusphere-2025-5023
Preprint. Discussion started: 27 October 2025

Abstract. Wetland and upland ecosystems play significant but opposing roles in the global methane (CH_4) budget, acting as natural sources and sinks, respectively. Two of the most common approaches for measuring CH_4 fluxes (FCH_4) are chambers, which capture temporally intermittent, fine-scale spatial heterogeneity (ca. 1 m^2), and eddy covariance (EC) towers, which cover a larger area (ca. 100-10000 m^2) at a longer term. Although chamber and EC observations have been combined in various syntheses and databases to estimate CH_4 budgets, a unified cross-site evaluation of FCH_4 estimates at plot and ecosystem scales is lacking. As a first step toward a systematic spatiotemporal scaling of EC tower and chamber footprints, we quantified the differences between site-level aggregate FCH_4 (EC vs chamber; ΔFCH_4) from ten wetland and upland sites at half-hourly, hourly, daily, weekly, monthly, and annual timescales. We found that ecosystem-scale median FCH_4 was consistently higher than plot-scale FCH_4 at all temporal scales, with the smallest difference at daily timescale (multi-site median ΔFCH_4: 1.36 nmol m^{-2} s^{-1}; ~104% higher ecosystem-scale than plot-scale FCH_4) and largest at annual scales (2.58 nmol m^{-2} s^{-1}; ~87% higher ecosystem-scale than plot-scale FCH_4). In general, the agreement between ecosystem- and plot-scale FCH_4 decreased with finer temporal resolution (from Spearman ρ=0.95 at annual scale to ρ=0.65 at half-hourly scale), while ΔFCH_4 variation was greatest at daily-to-annual scales. Key environmental predictors of ΔFCH_4 included plot-scale spatial heterogeneity, dominant vegetation type, vapor pressure deficit, atmospheric pressure, and friction velocity at the daily and monthly scales. Wind direction was a significant predictor only at the monthly scale, suggesting EC footprint effects. These findings suggest accounting for variation in EC footprint extent, chamber measurement placement and artifacts is key to reconciling multi-scale FCH_4 observations in diverse ecosystems and refining CH_4 budgets.

1 Introduction

Methane (CH_4), a potent greenhouse gas, is produced in wetlands and consumed in upland soils- respectively the largest natural CH_4 sources and sinks globally. However, the magnitude of these fluxes remains highly uncertain (IPCC, 2023; Saunois et al., 2024). Field measurements of CH_4 fluxes (FCH_4) are often conducted using enclosed chamber systems or eddy covariance (EC) towers (Bansal et al., 2023b). Chambers are typically deployed at point scale (<1 m^2) to capture plot-scale spatial heterogeneity in CH_4 source-sink dynamics within the study area (Livingston and Hutchinson, 1995; Morin et al., 2017; Virkkala et al., 2018). Chamber measurements can be manual or automated, the former is more labor-intensive and thus, results in a temporally sporadic sampling pattern (typically few per month), while the latter offers more consistent and long term temporal sampling (typically half hourly over seasons) but can be more spatially limited due to high instrumentation cost. Thus, chambers generally represent a lower fraction of the ecosystem (Barba et al., 2018; McGuire et al., 2012; Morin et al., 2014, 2017).

In contrast, EC towers continuously measure FCH_4 with high temporal resolution, typically half hourly, over seasons and years (Morin, 2019; Morin et al., 2017). The EC technique is based on the principle that the measured FCH_4 that originates from the tower footprint area (100-10000 m^2) is carried upwards and outward toward the sensor by turbulent diffusion (Aubinet et al., 2012; Morin et al., 2014). Therefore, a single half-hourly EC measurement represents a mixed observation at the ecosystem scale located over a somewhat uncertain footprint area, which changes from one observation to the other, and may include a mixture of distinctly different ecosystem and hydrological subtypes (defined as different "plots") (Chu et al., 2021; Xu et al., 2018). A chamber measurement represents a prescribed point with a well-known location and plot type but a small area. Averaging multiple chamber observations in the same plot (defined as "spatial replicates") increases the area representation of the chamber observation, but it is still several orders of magnitude smaller than EC measurements. While both approaches provide complementary perspectives on ecosystem FCH_4, the data provided by each method pose different challenges for model parameterization or evaluation of relevant ecosystem FCH_4 processes across spatial and temporal scales.

Many global and regional FCH_4 models are parameterized using EC FCH_4 data because of its consistent temporal sampling and because the EC reporting standard include environmental covariates (e.g., McNicol et al., 2023; Oikawa et al., 2024; Peltola et al., 2019; Ueyama et al., 2023b). Community-contributed datasets, such as FLUXNET-CH_4 (Delwiche et al., 2021; Knox et al., 2019), offer unprecedented opportunity to access EC FCH_4 data from around the globe. However, even large collaborations such as FLUXNET-CH_4 only cover a relatively small number of locations, from a global perspective, and is missing important coverage in key ecosystems (e.g., tropics; Delwiche et al., 2021; Zhu et al., 2024). Chamber FCH_4 data are cheaper and simpler to deploy and are therefore implemented in a larger number of sites globally. Thus, chambers provide a greater spatial site-level representation than EC sites and are needed to fill the missing data gaps. As a result, data from EC and chamber methods are sometimes compiled to augment syntheses and budget estimations (Hill and Vargas, 2022b; Kuhn et al., 2021; Yuan et al., 2024). Integration of plot-scale chamber FCH_4 data into ecosystem-scale EC datasets poses several challenges due to methodological differences (Hill and Vargas, 2022b). These challenges also apply to carbon dioxide (CO_2) measurements, with studies noting significant discrepancy between the two, partly due to manual chambers (and sometimes EC) often lacking nighttime measurements, biasing flux estimates (Barba et al., 2018; Phillips et al., 2017). To our knowledge, a systematic comparison of FCH_4 from these different scales across multiple sites, has not been conducted (but see Davidson et al. 2017).

Plot and ecosystem-scale FCH_4 are expected to differ due to the different FCH_4 source areas, measurement artifacts and uncertainties of the chamber and EC methods, and differences in their response to environmental FCH_4 drivers. In many comparison studies conducted in wetland and upland ecosystems, chamber FCH_4 is higher than EC FCH_4 (Chaichana et al., 2018; Clement et al., 1995; Davidson et al., 2017; Krauss et al., 2016; Marushchak et al., 2016; Meijide et al., 2011; Morin et al., 2017; Riutta et al., 2007), although some studies report the opposite (Budishchev et al., 2014; Forbrich et al., 2011; Hill and Vargas, 2022b; Schrier-Uijl et al., 2010; Wang et al., 2013) and others find that the direction of the difference varies between years (Korrensalo et al., 2018). The EC method integrates FCH_4 over the constantly moving and often spatially heterogeneous footprint, and the surface cover types within the footprint differ substantially in FCH_4 and, in wetlands, may include non-flooded areas where FCH_4 is expected to be near zero (Kutzbach et al., 2004; Riutta et al., 2007; Sha et al., 2011), which can introduce significant bias (Morin et al., 2017).

Since the attribution of surface cover type and location is better defined in chamber measurements, chamber FCH_4 sampling can offer more representative estimates of FCH_4 variability within a site (Bansal et al., 2023a). However, chambers only capture a small portion of the landscape, are often placed in high-emitting hotspots, do not sample over tall vegetation patches, and may incorporate sampling location biases (Bansal et al., 2023b), often leading to higher observed fluxes at the individual sampled plots, than the true, mean ecosystem-scale FCH_4 (but see Voigt et al., 2023). Environmental variables that influence FCH_4 variability, such as soil temperature, water table level (or water elevation in flooded sites), and net ecosystem CO_2 exchange, could also predict cross-scale FCH_4 differences given the different processes influencing FCH_4 at different spatial and temporal scales (Knox et al., 2021; Morin et al., 2014; Turetsky et al., 2014). EC observations are sensitive to environmental variables, such as wind speed and direction, that affect the extent and location of the observation footprint, while chamber measurements should be unaffected by these (Wang et al., 2013). While some studies have evaluated EC-chamber FCH_4 differences with spatially explicit FCH_4 upscaling or downscaling with the help of EC footprint modeling, many of these studies have been conducted in individual sites (e.g., Budishchev et al., 2014; Marushchak et al., 2016; Morin et al., 2017; Schrier-Uijl et al., 2010). Thus, an exploration of bulk-scale FCH_4 differences between ecosystem and plot-scale FCH_4 (based on spatiotemporal aggregations) and their controls across multiple sites can help in directing future research efforts utilizing EC footprint modeling to reconcile cross-scale FCH_4 differences.

To explore the differences between ecosystem and plot-scale FCH_4 (ΔFCH_4) measured by EC and chamber systems, respectively, and to identify the time scales and environmental conditions at which the two data types agree best, we 1) compared co-located and contemporaneous EC and chamber FCH_4 rates across multiple sites and examined how the differences ranged across temporal scales (half-hourly to annual), and 2) investigated the potential predictors of ΔFCH_4. We hypothesized that plot-scale FCH_4 would be higher than ecosystem-scale FCH_4 as chambers often selectively target FCH_4 hotspots and manual chamber measurements are often conducted at warmer daytime conditions. We expected that ΔFCH_4 is highest during daytime when most chamber measurements are conducted and plant activity is high, the latter of which is fully captured by towers but not always by manual chambers (Knox et al., 2021; Yu et al., 2013). This comparison of bulk FCH_4 rates is a key first step toward standardized harmonization of EC tower and chamber footprints to account for spatiotemporal heterogeneity across multiple sites.

We hypothesized that larger variance (suggesting higher spatio-temporal heterogeneity) observed in chambers and EC measurements would increase ΔFCH_4, and that the different temporal resolutions of manual and automated chambers would further contribute to ΔFCH_4. Finally, we expected that the temporal scale of data aggregation could influence the magnitude

https://doi.org/10.5194/egusphere-2025-5023
Preprint. Discussion started: 27 October 2025

of ΔFCH_4, and we hypothesized that ΔFCH_4 would be lower at coarser (seasonal to annual) than at finer (hourly to daily) temporal aggregations.

2 Methods

2.1 Study sites

We compiled ecosystem-scale (EC) and plot-scale (chamber) FCH_4 data from ten sites, representing different climatic conditions and ecosystem types (two uplands and eight wetlands; Fig. 1, Table 1). Each site differed in the number of days with both chamber and EC measurements (n=5-759), the number of chambers used (n=3-18), the year of observations (range across sites: 2012-2020), and whether the chambers were automated or manual (Table C1 and Fig. B1). The site selection was based on the availability of coincident EC and chamber FCH_4 data. EC data were obtained from the FLUXNET-CH_4 database (Delwiche et al., 2021; Knox et al., 2019) and chamber data were provided by site principal investigators in response to a call for data via the FLUXNET-CH_4 network. The sites are located in China, Finland, Sweden and the USA. Most sites have a humid continental (n=3) or subarctic climate (n=3), with others located in humid subtropical (n=3) and cold subtropical highland (n=1) regions (Table 1).

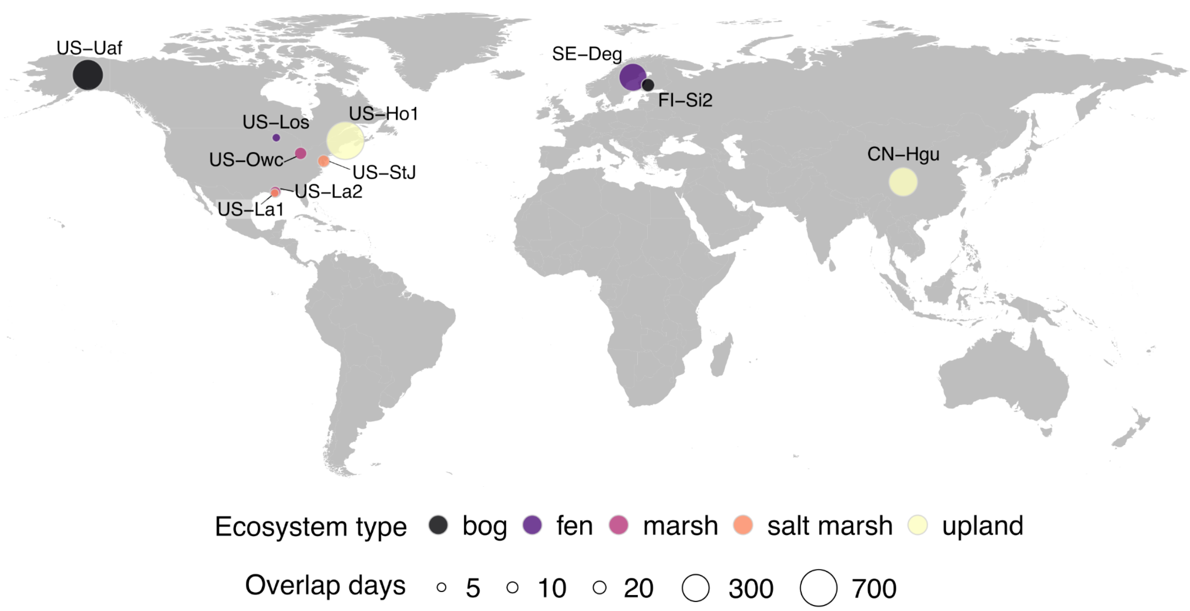

Figure 1. Map of study sites. Point colors indicate ecosystem type and point size reflects the number of overlap days between eddy covariance and chamber measurements (details in Table C1). Ecosystem type follows the site classification in the

https://doi.org/10.5194/egusphere-2025-5023
Preprint. Discussion started: 27 October 2025

FLUXNET-CH_4 database (Delwiche et al., 2021; Knox et al., 2019). Base map: Natural Earth (1:50 m Cultural Vectors; naturalearthdata.com), created with R package *maps* (Becker et al., 2023).

Table 1. Environmental characteristics of the study sites during the FCH_4 observation periods. Site classification, dominant vegetation, air temperature, precipitation, and water table level data were obtained from half-hourly FLUXNET-CH_4 and chamber datasets (Delwiche et al., 2021; Knox et al., 2019). Mean air temperature, total precipitation, and mean water table level were calculated over the EC-chamber overlap periods used in the analyses. Negative water table level indicates that water table level was below the soil surface. Köppen climate abbreviations: Cwc = cold subtropical highland, Dfc = subarctic, Dfb = warm-summer humid continental, Cfa = humid subtropical, Dwc = monsoon-influenced subarctic climate. Column abbreviations: TA = air temperature, P = total precipitation, WTL = water table level, Vegetation = site dominant vegetation type, Overlap days = number of days with both EC and chamber FCH_4 observations. In Overlap days, values marked with and without asterisk (*) represent automated and manual chambers, respectively.

FLUXNET-CH_4 ID	Site name	Climate (Köppen)	Site classification	TA (°C)	P (mm)	WTL (min, max; cm)	Vegetation	Overlap days	Chamber FCH_4 data ref.	EC FCH_4 data ref.
CN-Hgu	Hongyuan	Cwc	upland (alpine meadow)	2.6	386	-	Aerenchymatous	363*	Wang et al. (2021)	Niu and Chen (2020)
FI-Si2	Siikaneva-2 Bog	Dfc	bog	14.6	14	-11.6 (-39, 15.2)	*Sphagnum* moss	26	Korrensalo et al. (2018)	Alekseychik et al. (2021); Vesala et al. (2020)
SE-Deg	Degerö	Dfc	fen	4.7	394	-1.35 (-10.2, 0.8)	*Sphagnum* moss	338*	Bond-Lamberty et al. (2020); Järveoja et al. (2018)	Nilsson and Peichl (2020)

https://doi.org/10.5194/egusphere-2025-5023
Preprint. Discussion started: 27 October 2025

US-Ho1	Howland Forest	Dfb	upland (needleleaf forest)	6.9	838	-53.6 (-112, 8.19)	Tree	759*	Richardson et al. (2019)	Richardson and Hollinger (2020)
US-La1	Pointe-aux-Chenes Brackish Marsh	Cfa	salt marsh	24.7	9	-0.99 (-13.3, 3.13)	Aerenchymatous	5	Krauss et al. (2016)	Holm et al. (2020a)
US-La2	Salvador WMA Freshwater Marsh	Cfa	marsh	26	15	1.33 (-8.79, 24.1)	Aerenchymatous	10	Krauss et al. (2016)	Holm et al. (2020b)
US-Los	Lost Creek	Dfb	fen	18.4	92	-11.2 (-16.1, -4.89)	Ericaceous shrub	5	Desai (2025b)	Desai (2025a); Desai and Thom (2020)
US-Owc	Old Woman Creek	Dfb	marsh	15.2	468	73.9 (35, 120)	Aerenchymatous	18	Bohrer et al. (2019)	Bohrer et al. (2020)
US-StJ	St Jones Reserve	Cfa	salt marsh	20	520	30.1 (-39, 102)	Aerenchymatous	16	Hill and Vargas (2022a)	Hill and Vargas (2022b); Vázquez-Lule and Vargas (2021)

https://doi.org/10.5194/egusphere-2025-5023
Preprint. Discussion started: 27 October 2025

US-Uaf	University of Alaska, Fairbanks	Dwc	bog	-0.2	262	-12.5 (-37.8, 12.9)	*Sphagnum* moss	458*	Ueyama et al. (2022)	Iwata et al. (2020)

2.2 Datasets and data compilation

2.2.1 Chamber and EC CH_4 flux data

The plot-scale chamber FCH_4 data for each site were obtained from the site principal investigators. Each dataset included FCH_4 (varying units) and additional environmental variables, such as soil temperature and water table level. Chamber datasets comprised measurements from both manual (n=6 sites; taken 1-3 times per month) and automated chamber methods (n=4 sites; taken at half-hourly or hourly intervals, see Table C1; Subke et al., 2021). Chamber fluxes for all sites were calculated by the data providers using linear regression of change in CH_4 concentration over time (details in Text A1). None of the chamber FCH_4 data were gap-filled, and in most cases, ebullition events had been filtered out by the data providers (Text A1). We designated CH_4 emission with positive, and CH_4 uptake with negative signs.

The ecosystem-scale EC datasets for each site (except US-StJ, see below) were obtained from the FLUXNET-CH_4 database (Delwiche et al., 2021; Knox et al., 2019), and include both gap-filled and non-gap-filled FCH_4 values (nmol m^{-2} s^{-1}) at a half-hourly resolution along with various meteorological and environmental variables. We used gap-filled EC FCH_4 in the analyses, but excluded data during long data gaps (>2 months) when the gap-filled values may be a significant source of uncertainty (Delwiche et al., 2021). Gap-filling was performed using artificial neural networks (ANN; Knox et al. 2019) which have shown good performance for FCH_4 data gap-filling (Irvin et al., 2021; Knox et al., 2016, 2019).

CN-Hgu EC FCH_4 data showed anomalous extreme CH_4 uptake and isolated extreme positive FCH_4 spikes. Therefore, we filtered out EC FCH_4 values where 1) CH_4 uptake exceeded -100 nmol m^{-2} s^{-1} (empirically determined threshold; Chen et al., 2019, 2020), 2) nighttime (incoming shortwave radiation < 10 W m^{-2}; Morin et al., 2014) friction velocity < 0.1 m s^{-1} (Chen et al., 2019, 2020), and 3) single extreme positive FCH_4 spikes occurred beyond the monthly 99.5th FCH_4 percentile where nighttime air temperature was within 1 °C of its dew point (calculated with Magnus formula and Alduchov & Eskridge constants; Alduchov and Eskridge, 1996; Lawrence, 2005) and the open-path gas analyzer may have had condensation

https://doi.org/10.5194/egusphere-2025-5023
Preprint. Discussion started: 27 October 2025

(Heusinkveld et al., 2008). Additional extreme FCH_4 (FCH_4 = 862 nmol m^{-2} s^{-1}) associated with friction velocity = 0.93 m s^{-1} and wind speed = 0.05 m s^{-1} was removed as an outlier. After filtering, the CN-Hgu dataset was 70% of the original.

For US-StJ, we obtained EC FCH_4 data from the data providers (Hill and Vargas, 2022b; Vázquez-Lule and Vargas, 2021). As ANN-gap-filled EC FCH_4 values were not available at US-StJ, we used only non-gap-filled EC FCH_4. EC FCH_4 were processed by the data providers following AmeriFlux protocols (Chu et al., 2023; Hill and Vargas, 2022b; Vázquez-Lule and Vargas, 2021).

2.2.2 Environmental data

For all sites (except US-StJ), environmental data were obtained from the FLUXNET-CH_4 EC data product, including ANN-gap-filled net ecosystem CO_2 exchange (NEE), friction velocity (u*), wind direction (WD), gap-filled wind speed, gap-filled vapor pressure deficit (VPD), and gap-filled air pressure (PA) (Delwiche et al. 2021; Knox et al. 2019). Soil temperature (TS; topmost 2-10 cm depth) data was obtained from FLUXNET-CH_4 and site-specific chamber datasets when available. If a site had TS observations from both chamber and FLUXNET-CH_4 datasets, a mean of both was taken to obtain a site-level TS. Similarly, site-level water table level (WTL) was obtained by utilizing either FLUXNET-CH_4 or chamber-associated WTL measurements, or by taking their mean.

Environmental data for US-StJ were obtained from the data providers (Hill and Vargas, 2022b; Vázquez-Lule and Vargas, 2021). PA, VPD, wind speed, WD, and u* were not gap-filled, while TS and WTL were gap-filled based on their linear relationships with water temperature and water table level, respectively (Hill and Vargas, 2022b). NEE was gap-filled using marginal distribution sampling moving look-up tables (Hill and Vargas, 2022b).

See a summary of environmental data in Table C2.

2.3 Data processing and harmonization

The chamber datasets were harmonized to a similar structure, and FCH_4 units were standardized to nmol m^{-2} s^{-1}, matching the units used in the FLUXNET-CH_4 EC FCH_4 data. Then, EC and chamber datasets were combined using common timestamps (Fig. 2). To evaluate differences across temporal aggregations, we aggregated data at six temporal scales: 1. half-hourly (automated chamber data only; CN-Hgu, SE-Deg, US-Ho1, US-Uaf; n=4 sites), 2. hourly (CN-Hgu, SE-Deg, US-Ho1, US-Uaf; n=4 sites), 3. daily (all sites, n=10 sites), 4. weekly (n=10 sites), 5. monthly (n=10 sites), and 6. annual (n=10 sites) (Fig. 2). Note that most sites did not include snow-covered periods, and the datasets primarily represent the snow-free season.

The data were aggregated from the timestamp-aligned data by taking the median of FCH_4 measurements (non-normally distributed), mean of NEE (normally distributed) and wind *u* and *v* components (see 2.4.2), and median of the rest of the environment and meteorological variables (non-normally distributed). Half-hourly aggregation was created by taking the median of chamber measurements for each EC timestamp. To check for robustness of our results from the median-based

https://doi.org/10.5194/egusphere-2025-5023
Preprint. Discussion started: 27 October 2025

temporal aggregations, we also created temporal aggregations based on FCH_4 means. In addition, we calculated cumulative sums (mg CH_4 m^{-2}) of chamber and EC FCH_4 at daily, weekly, monthly, and annual scales to see how EC-chamber differences scale up to ecosystem CH_4 budgets. As the chamber FCH_4 data from FI-Si2, US-La1, and US-La2 lacked hourly timestamps, we estimated daily cumulative FCH_4 for these sites by using the daily median or mean chamber FCH_4 and multiplied it by 48 while EC cumulative FCH_4 was calculated based on half-hourly EC FCH_4 from FLUXNET-CH_4. As this is not an accurate estimate of daily cumulative chamber FCH_4 for EC-chamber FCH_4 comparisons, we included these sites only in site-specific analyses and excluded them from cross-site analyses.

The difference between ecosystem and plot-scale FCH_4 was calculated as the row-wise difference between instantaneous EC FCH_4 and chamber FCH_4 (ΔFCH_4) in each aggregated dataset by subtracting chamber FCH_4 from the corresponding EC FCH_4 on the same timestamp. For supplementary analyses, we calculated the difference between cumulative EC FCH_4 and chamber FCH_4 at daily, weekly, monthly, and annual scales.

2.4 Statistical analyses

2.4.1 Differences between ecosystem and plot-scale FCH_4 observations

We used non-parametric statistics to analyze the FCH_4 data (EC, chamber and ΔFCH_4), because the data were skewed and non-normal. To test the statistical significance ($\alpha = 0.05$) of ΔFCH_4 and to assess ΔFCH_4 differences between chamber types at different temporal scales, we used Wilcoxon-Mann-Whitney tests (*wilcox.test* from *stats*; R Core Team 2024). Since the mean-based temporal aggregations were used as a sensitivity check, only descriptive statistics and Wilcoxon-Mann-Whitney tests were conducted for the mean-based aggregations (results in Table C3). Similarly, cumulative FCH_4 were analyzed with descriptive statistics and Wilcoxon-Mann-Whitney tests (results in Table C4). The rest of the methods described here were conducted on the median-based temporal aggregations of instantaneous FCH_4.

To estimate the slopes of the EC FCH_4 - chamber FCH_4 relationship, we also built simple linear mixed effects models with site as the random effect using function *lme* from package *nlme* (Pinheiro et al., 2000, 2023). For better interpretability of model slopes (in contrast to Yeo-Johnson-transformed values, see 2.4.2) and to meet the residual normality assumptions of linear mixed modeling, we transformed EC FCH_4 with inverse hyperbolic sine (Table C5). Due to non-convergence and residual non-normality, half-hourly and hourly scales were not assessed for EC-chamber FCH_4 slopes. We also used Spearman correlations to assess the direction and strength of the relationship between EC FCH_4 and chamber FCH_4, manual and automated chamber FCH_4, as well as FCH_4 magnitude (row-wise mean of EC and chamber FCH_4) and absolute ΔFCH_4.

We used Kruskal-Wallis tests (*kruskal.test* from *stats*; R Core Team 2024) to test for differences in ΔFCH_4 across hours and months (treated as categorical variables) within each temporal aggregation (half-hourly, hourly, daily, weekly, monthly, and annual). Then, we identified the significantly differing groups using the Conover-Iman post hoc test (function *conover.test* from package *conover.test*; Dinno, 2024).

https://doi.org/10.5194/egusphere-2025-5023
Preprint. Discussion started: 27 October 2025

2.4.2 Predictors of FCH_4 differences between ecosystem and plot scales

We built linear mixed models to estimate the predictors of ΔFCH_4. To meet the assumptions of linear mixed modeling and to improve residual diagnostics (normality and homoscedasticity of residuals) for model inference, we applied Yeo-Johnson power transformation (Yeo and Johnson, 2000) to absolute ΔFCH_4 values using the function *yeojohnson* from *bestNormalize* (Peterson, 2021). This transformation can be applied to zero values, and it improved our residual diagnostics, which were important for model inference. All models were built with the function *lme* from *nlme* (Pinheiro et al., 2000, 2023).

To evaluate potential predictors of ΔFCH_4, we included environmental and temporal variables available in the FLUXNET-CH_4 and chamber datasets in the models. The predictor selection was based on literature. They included: TS (°C), WTL (cm), PA (kPa), u* (m s^{-1}), WD (degrees), VPD (hPa), NEE (μmol CO_2 m^{-2} s^{-1}), month (categorical), site dominant vegetation (VEG; categorical; "tree", "ericaceous shrub", "aerenchymatous", "brown moss", and "*Sphagnum* moss"; taken from Delwiche et al., 2021), and hour (categorical; only with half-hourly and hourly datasets). We included EC-specific variables, such as u* and WD, as proxies for EC footprint to assess how variables contributing to the EC footprint may affect ΔFCH_4. While two of the VEG classes (tree and ericaceous shrub) were only represented in one site, preliminary linear regression model comparisons showed that VEG explained a large proportion of the ΔFCH_4 variance (R^2 = 0.4-0.7), and its inclusion in linear mixed models substantially improved model fit. Therefore, we included VEG as a fixed effect, while acknowledging that for tree and ericaceous shrub classes, the estimated effect may be related to the site rather than vegetation.

In all models, the reference level in VEG was *Sphagnum* moss, 0 in Hour, and May in Month. As WD is a circular variable (0°=360°), we represented WD as a continuous function of wind direction and speed by separating WD into orthogonal *u* and *v* wind components (uWD and vWD, respectively), which were averaged from the half-hourly EC datasets in hourly, daily, weekly, monthly, and annual aggregations (Text A2). As a result, uWD represents the strength of west-east wind while vWD represents the strength of north-south wind. This representation avoided discontinuity at 360°/0° and potential multicollinearity between model predictors.

For improved model convergence and β-coefficient calculations, Yeo-Johnson-transformed absolute ΔFCH_4 and all predictors were centered and scaled, except hour, month and VEG, which were categorical variables and were included without centering and scaling. To account for multicollinearity, we chose predictors based on Pearson correlation matrices (threshold $|r|<0.7$) and checked variance inflation factors (VIF; threshold ≤ 3) using the function *vif* from *car* (Fox and Weisberg, 2018). Due to multicollinearity (VIF>3), we built two separate half-hourly models containing either month or TS, two weekly models without NEE or VPD, and a monthly model without VPD and TS. WTL data was not available for CN-Hgu, and thus, this site was excluded from the models.

After accounting for temporal autocorrelation and residual variance (Text A3), we used backward variable selection based on likelihood ratio tests (AIC and *p*-values) together with type I ANOVA tests to determine significant predictors of Yeo-Johnson-transformed absolute ΔFCH_4. During variable selection, the models were fitted with maximum likelihood, and the final models

https://doi.org/10.5194/egusphere-2025-5023
Preprint. Discussion started: 27 October 2025

were refitted with restricted maximum likelihood for statistical inference. Model marginal and conditional R^2 were calculated with the function *r.squaredGLMM* from package *MuMIn* (Bartoń, 2024).

We built linear mixed effects models to investigate the effect of spatio-temporal FCH_4 variation on ΔFCH_4. To represent the FCH_4 variation between individual chambers within each site, we calculated the interquartile range (IQR) of chamber FCH_4 from an unaggregated dataset per each site and temporal scale unit (i.e., per day, week, month, or year). To see whether temporal variation within each temporal scale unit in EC FCH_4 may affect absolute ΔFCH_4, we also calculated EC FCH_4 IQR per each site and temporal scale unit. In the models, log-transformed absolute ΔFCH_4 was the response variable, and either log (+0.01)-transformed chamber IQR or log (+0.01)-transformed EC IQR was the explanatory variable, or both were included as explanatory variables to assess their relative effects on absolute ΔFCH_4.

All data processing and statistical analyses were carried out using R v4.3.3 (R Core Team, 2024).

https://doi.org/10.5194/egusphere-2025-5023
Preprint. Discussion started: 27 October 2025

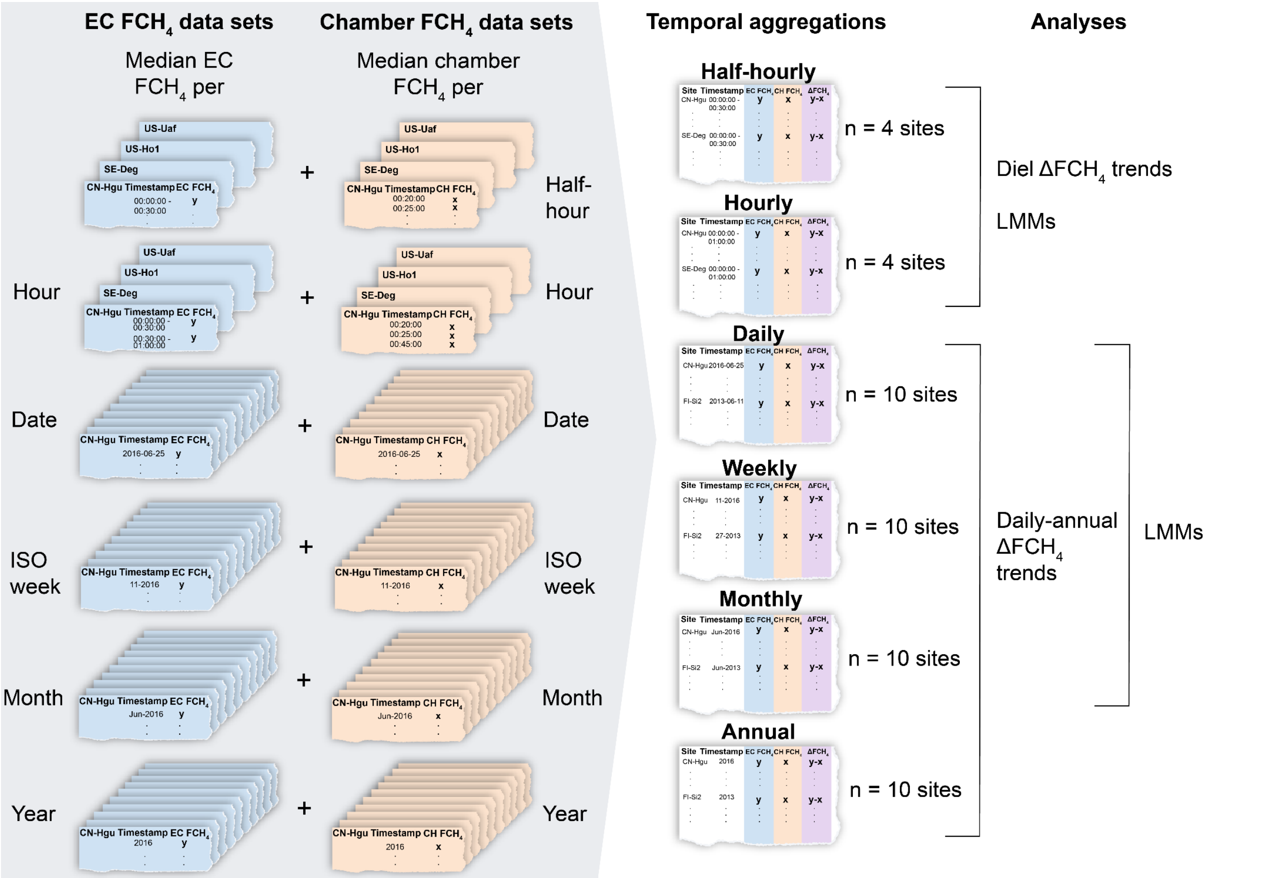

Figure 2. Overview of the main data aggregation workflow. Site-specific EC FCH_4 (blue) and chamber FCH_4 (orange) datasets were combined by taking the median FCH_4 per timestamp (half-hour to annual scale). ISO week is the week number according to the ISO-8601 standard. Then, site-level datasets were combined into multi-site datasets at six temporal scales: half-hourly, hourly, daily, weekly, monthly, and annual. Half-hourly EC FCH_4 data was not aggregated as it was already in half-hourly scale. ΔFCH_4 (purple) was calculated by subtracting median chamber instantaneous FCH_4 from median EC instantaneous FCH_4 per timestamp per site, and this measure was used in all analyses and linear mixed effects models (LMMs). Note that we also created temporal aggregations by taking the mean of EC and chamber FCH_4, and these data sets were used as a sensitivity check with descriptive statistics and pairwise comparisons.

https://doi.org/10.5194/egusphere-2025-5023
Preprint. Discussion started: 27 October 2025

3 Results

3.1 Ecosystem and plot-scale FCH_4 differ most at finer temporal aggregations

Ecosystem- (EC) and plot-scale (chamber) FCH_4 differed significantly at all the temporal aggregations shorter than monthly scale (Table 2). Median ecosystem FCH_4 was higher than plot-scale FCH_4 at all temporal aggregations (half-hourly to annual: 102%, 109%, 104%, 90%, 58%, and 87% higher, respectively). However, the coefficient of variation (CV, %) for ΔFCH_4 was large particularly in daily and weekly aggregations. Across temporal aggregations and site-years, CH_4 emissions ($FCH_4 > 0$) above the 90th percentile contributed a larger share of total plot-scale FCH_4 than ecosystem-scale FCH_4 (Table 2, Fig. B2), possibly indicating more CH_4 emission hot spots and hot moments at the plot scale. Our observed trend persisted when we aggregated chamber and EC FCH_4 data with means instead of medians (Table C3), where median ΔFCH_4 ranged between 0.28 (annual) and 1.23 (half-hourly) but mean ΔFCH_4 turned increasingly negative from daily (-1.16 nmol m^2 s^{-1}) to annual (-70.94 nmol m^2 s^{-1}) scales, highlighting plot-scale CH_4 emission hotspots and hot moments as possible ΔFCH_4 drivers which may have been more attenuated in the median-based aggregations. Ecosystem and plot-scale FCH_4 were positively correlated across temporal aggregations, with annual aggregation having the best agreement, while the worst agreements were in half-hourly and hourly aggregations (Fig. 3). In linear mixed models, a 1 nmol m^{-2} s^{-1} increase in plot-scale FCH_4 was associated with an ecosystem FCH_4 increase of 0.007 nmol m^{-2} s^{-1} (p=0.03) at daily plot-scale FCH_4 median (0.06 nmol m^{-2} s^{-1}), 0.01 nmol m^{-2} s^{-1} (p=0.066) at weekly plot-scale FCH_4 median (0.51 nmol m^{-2} s^{-1}), 0.009 nmol m^{-2} s^{-1} (p=0.183) at monthly plot-scale FCH_4 median (4.07 nmol m^{-2} s^{-1}), and 0.019 (p=0.044) at annual plot-scale FCH_4 median (6.55 nmol m^{-2} s^{-1}; see Table C4 for details).

https://doi.org/10.5194/egusphere-2025-5023
Preprint. Discussion started: 27 October 2025

Table 2. Ecosystem (EC) and plot-scale (chamber) FCH_4 difference (ΔFCH_4) at different temporal aggregations. A positive ΔFCH_4 indicates higher ecosystem than plot-scale FCH_4 and vice versa. The EC and chamber data sample sizes in Wilcoxon-Mann-Whitney tests are reported as n_{EC} and n_{CH}, respectively. The 90th percentiles (p90, without parentheses) and proportion (%, in parentheses) of chamber and EC CH_4 emission observations (where FCH_4>p90 and FCH_4>0) of the total chamber or EC FCH_4 sum show the contribution of high CH_4 emissions to total CH_4 emissions. Abbreviations: IQR = interquartile range, SD = standard deviation, CV = coefficient of variation.

Aggregation	**ΔFCH_4 median (IQR), *nmol m⁻² s⁻¹***	**ΔFCH_4 mean (SD), *nmol m⁻² s⁻¹***	**ΔFCH_4 CV (%)**	**Chamber FCH_4 p90, *nmol m^2 s^{-1}* (% of total FCH_4)**	**EC FCH_4 p90, *nmol m^2 s^{-1}* (% of total FCH_4)**	**Wilcoxon-Mann-Whitney test**
Half-hourly	1.4 (5.67)	5.61 (17.71)	196	33.44 (46)	64.31 (44)	$p<0.001$ (n_{EC}=74482, n_{CH}=74482)
Hourly	1.41 (5.28)	6.08 (15.34)	191	45.76 (47)	63.92 (44)	$p<0.001$ (n_{EC}=40072, n_{CH}=40072)
Daily	1.36 (4.27)	4.01 (81.49)	674	43.18 (75)	68.5 (60)	$p<0.001$ (n_{EC}=1879, n_{CH}=1879)
Weekly	1.44 (5.29)	-0.62 (105.8)	467	112.64 (76)	78.08 (63)	$p<0.001$ (n_{EC}=349, n_{CH}=349)
Monthly	1.46 (14.82)	-8.14 (151.18)	350	247.77 (69)	219.98 (64)	$p=0.082$ (n_{EC}=121, n_{CH}=121)
Annual	2.58 (24.59)	-1.37 (63.6)	194	220.35 (64)	250.78 (57)	$p=0.507$ (n_{EC}=22, n_{CH}=22)

https://doi.org/10.5194/egusphere-2025-5023
Preprint. Discussion started: 27 October 2025

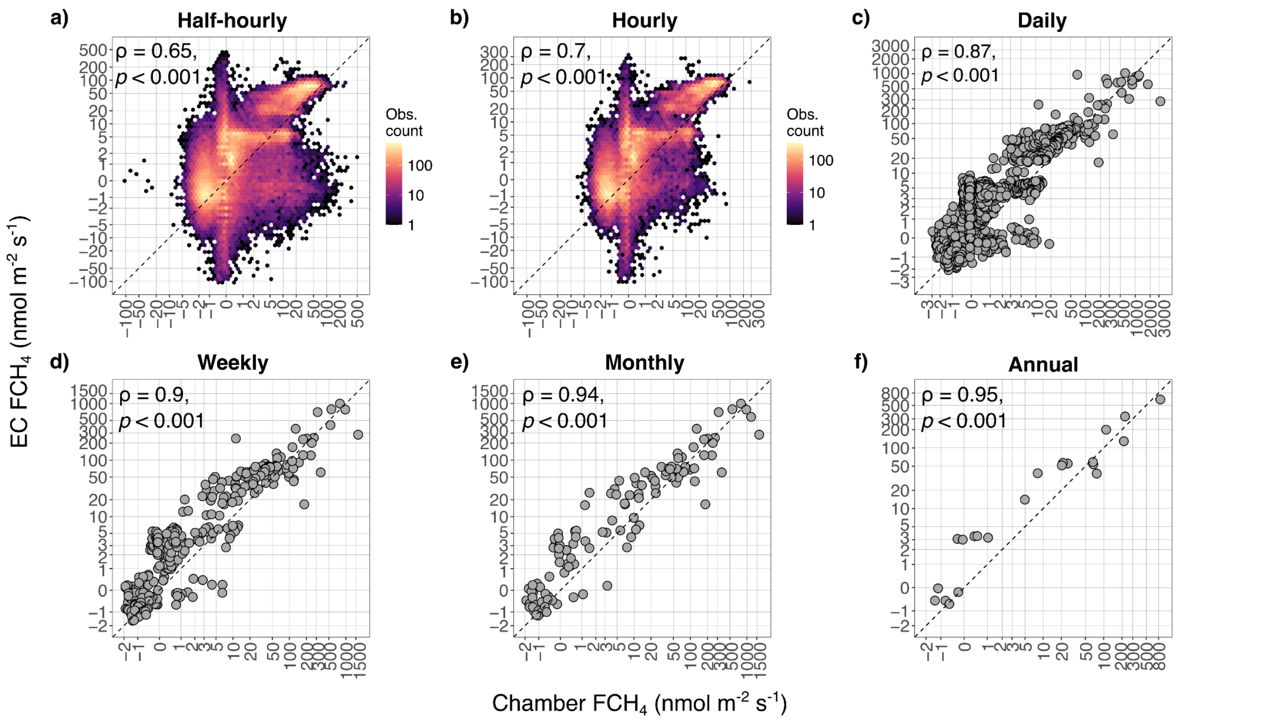

Figure 3. Agreement between ecosystem (EC) and plot-scale (chamber) FCH4 improves from finer to coarser temporal aggregations (a-f), as indicated by Spearman correlation coefficients (ρ; calculated with untransformed data). For visualization, the plot axes (a-f) were transformed with inverse hyperbolic sine to spread out points in the low FCH4 range and retain negative values (see untransformed plots in B3). In a) and b) the points for half-hourly (n=74482) and hourly (n=40072) aggregations are shown in hexagonal density clouds with log10-transformed color range to highlight trends in high point density areas (colors represent number of observations per hexagon). The high observation densities in a) and b) reveal site-specific trends in the discrepancy between ecosystem and plot scales (e.g., at x=0 and y=5). For daily (c), weekly (d), monthly (e), and annual (f) aggregations, sample sizes were n = 1879, 349, 121, and 22, respectively. The dashed line represents 1:1 line.

Ecosystem and plot-scale FCH4 differed between hours, months, and sites. In support of our hypotheses, the highest ΔFCH4 occurred between 5 AM and 3 PM (p<0.001; B4-B7), with maximum median ΔFCH4 at 9 AM (2.01 nmol m^{-2} s^{-1}, IQR: 6.16; half-hourly scale) and minimum at 8 PM (0.9 nmol m^{-2} s^{-1}, IQR: 4.16; half-hourly scale). However, the diel ΔFCH4 trends varied between sites and months (p<0.001; Fig. B8-B12). The highest absolute ΔFCH4 (with observations from all sites) was in August, September, and October (half-hourly to daily p<0.001; Fig. B13). In addition, ΔFCH4 varied in both magnitude and

https://doi.org/10.5194/egusphere-2025-5023
Preprint. Discussion started: 27 October 2025

direction within and between sites (Kruskal-Wallis p<0.001; half-hourly to monthly scale), with most medians being positive (Tables C6-C11 and B14-B15). The difference between cumulative sums of ecosystem and plot-scale FCH_4 increased from daily to annual scales but the seasonal and inter-annual trends varied between sites (Table B4, Fig. B16). The largest absolute ΔFCH_4 medians and CVs were consistently found in US-Owc (median: -108.22 nmol m^{-2} s^{-1}, CV: 169%; daily scale), while the lowest absolute ΔFCH_4 and FCH_4 were consistently found in US-Ho1 (median ΔFCH_4 <1 nmol m^{-2} s^{-1}; Tables C6-C11).

Flux magnitude, measured as the mean between EC and chamber FCH_4 (FCH_{4_mean}), was generally positively related to ΔFCH_4 but negative relationships existed when FCH_{4_mean}<0 (i.e., net uptake). The positive FCH_4 magnitude and absolute ΔFCH_4 relationship became stronger at coarser temporal resolutions (Spearman p<0.001; Fig. 4). In all aggregations, the higher ΔFCH_4 came from higher ecosystem than plot-scale FCH_4 (≥70% of all observations when FCH_{4_mean}>0; result not shown). In half-hourly and hourly aggregations, ΔFCH_4 and FCH_{4_mean} were negatively or positively related when FCH_{4_mean} suggested net uptake or emission, respectively (Fig. 4a and b). When FCH_{4_mean}<0, ecosystem-scale FCH_4 was generally higher than plot-scale FCH_4 (57% and 58% of all observations when FCH_{4_mean}<0 in half-hourly and hourly aggregations, respectively; result not shown). However, most of the highest observations originate from CN-Hgu. Sites also differed in whether the trends in negative FCH_4 came from higher plot or ecosystem-scale FCH_4: for example, at US-Uaf, 100% of ΔFCH_4 observations at FCH_{4_mean}<0 consisted of higher plot-scale FCH_4 while ca. 66% of hourly and half-hourly observations (FCH_{4_mean}<0) in US-Ho1 came from higher ecosystem-scale FCH_4.

https://doi.org/10.5194/egusphere-2025-5023
Preprint. Discussion started: 27 October 2025

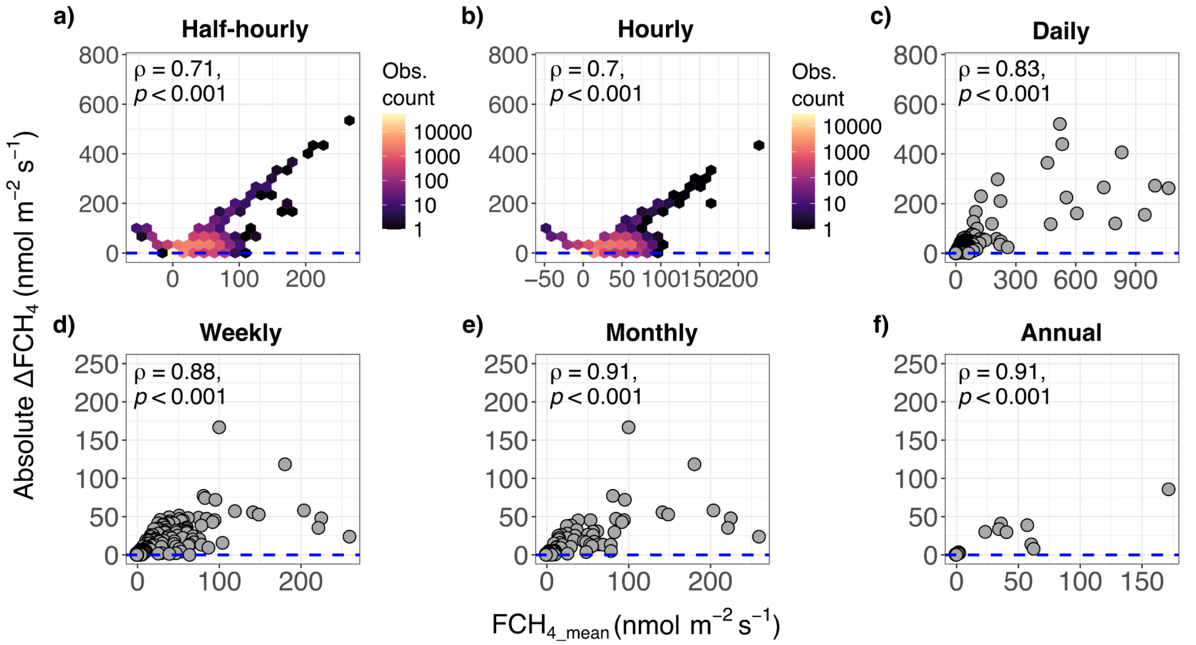

Figure 4. The absolute difference between ecosystem-scale (EC) and plot-scale (chamber) FCH_4 (ΔFCH_4) increases with FCH_4 magnitude (FCH_{4_mean}). FCH_{4_mean} is the row-wise mean of EC FCH_4 and chamber FCH_4. In a) and b) half-hourly and hourly points are shown in hexagonal density clouds with a log-transformed color range to highlight trends in high point density areas (colors represent number of observations per hexagon). Plots c-f show daily, weekly, monthly and annual aggregations, respectively. The blue dashed line represents ΔFCH_4=0 meaning complete agreement between ecosystem and plot-scale FCH_4. Higher Spearman correlation coefficient (ρ, α=0.05) represents stronger deviation from ΔFCH_4=0. For visualization, outliers were removed from daily (n=3), weekly (n=10), monthly (n=8) and annual (n=1) plots but the Spearman correlations are based on original data. See plots with outliers in Fig. B17.

3.2 Predictors of ecosystem and plot-scale FCH_4 differences

3.2.1 Atmospheric pressure, friction velocity and wind direction drive daily-to-monthly FCH_4 differences between ecosystem and plot scales

The significance and effect size of ΔFCH_4 predictors varied across temporal aggregations, with site-dominant vegetation type having the highest effect sizes at the daily-to-monthly scale (Table 3). Dominance of aerenchymatous vegetation had relatively high effect sizes (|β-coefficient|>0.68). However, only one site was classified as tree-dominated (US-Ho1) and ericaceous shrub-dominated (US-Los), while three were aerenchymatous and two were *Sphagnum*-moss dominated. Thus, we were unable to separate true vegetation-related effects from site effects.

PA and u* were significant ΔFCH_4 predictors at the daily and monthly scales (but weekly PA p=0.057), while VPD was significant only at the daily scale. However, the effect sizes were relatively low (β-coefficient≤0.25; Table 3). Wind direction

https://doi.org/10.5194/egusphere-2025-5023
Preprint. Discussion started: 27 October 2025

(uWD) was a significant ΔFCH_4 predictor only in the monthly scale. Month was a significant predictor only in the final half-hourly-daily models, where August and July had the highest effect sizes (β-coefficient>0.41), while morning hours, particularly 5 AM, were most important in the half-hourly-hourly models (5 AM β-coefficient>0.08). However, the fixed effects in the final half-hourly and hourly models explained a very small proportion of the total variation (marginal R^2<0.05, Tables S12-S13).

Table 3. Linear mixed effects model results identifying environmental predictors of ecosystem and plot-scale FCH_4 difference (ΔFCH_4) at different temporal scales. Fixed effects are listed in decreasing order based on their β-coefficients. Significant predictors are highlighted in bold. Half-hourly and hourly models had very low marginal R^2 (<0.05) and were excluded from this table. See half-hourly and hourly models in Table C13 and full models in Table C14. Abbreviations: SE = standard error, Df = degrees of freedom, VEG = site dominant vegetation, PA = air pressure (kPa), u* = friction velocity (m s^{-1}), WTL = water table level (cm), TS = soil temperature (°C), NEE = net ecosystem CO_2 exchange (μmol CO_2 m^{-2} s^{-1}), VPD = vapor pressure deficit (hPa), vWD = *v* wind component (m s^{-1}), uWD = *u* wind component (m s^{-1}).

Dataset	Predictors	β-coefficient	SE	*p*-value (t-test)	Marginal R^2	Conditional R^2	Df	Random effect variation explained, %
Daily (n=9 sites)	Intercept	0.4867	0.361	0.1779	0.5346	0.9265	1363	
	Fixed effects							
	VEG							
	- Tree	-1.4718	0.6767	0.0816			5	
	- Aerenchymatous	1.0111	0.4723	0.0852			5	
	Month							
	- Jul	0.4939	0.1685	**0.0043**			87	
	- Aug	0.4577	0.1696	**0.0084**			87	
	VEG							

https://doi.org/10.5194/egusphere-2025-5023
Preprint. Discussion started: 27 October 2025

	-Ericaceous shrub	0.4333	0.7104	0.5686			5	
	Month							
	- Sep	0.2851	0.1656	0.0886			87	
	- Apr	0.234	0.3683	0.5269			87	
	- Dec	0.2281	0.5059	0.6533			87	
	- Oct	0.1884	0.1689	0.2677			87	
	- Jun	0.1595	0.1658	0.3389			87	
	- Nov	0.1118	0.2356	0.6363			87	
	- Mar	-0.0735	0.5003	0.8835			87	
	TS	-0.0525	0.0269	0.051			1371	
	VPD	-0.0457	0.0109	**0**			1371	
	u*	0.0342	0.0076	**0**			1371	
	PA	-0.0259	0.0072	**0**			1371	
	uWD	0.0052	0.0066	0.4305			1371	
	vWD	0.0043	0.007	0.5423			1371	
	NEE	0.0017	0.0104	0.8679			1371	
	WTL	0.0012	0.0376	0.9745			1371	
	Random effects							
	Site							59.59
	Year-month							24.62
Weekly								
(n=9 sites)	Intercept	0.5066	0.3402	0.1381	0.5554	0.8351	178	
	Fixed effects							

https://doi.org/10.5194/egusphere-2025-5023
Preprint. Discussion started: 27 October 2025

	VEG							
	- Tree	-1.3455	0.6772	0.1036			3	
	- Aerenchymatous	0.8552	0.4642	0.1248			3	
	-Ericaceous shrub	0.5256	0.6837	0.4767			3	
	PA	-0.0716	0.0374	0.0572			178	
	Random effects							
	Site							62.91
	Year-month							$1.05e^{-05}$
Monthly	Intercept	-0.2243	0.3145	0.4778	0.6599	0.8788	80	
(n=9	**Fixed effects**							
sites)	Month							
	- Mar	1.4967	1.4236	0.2962			80	
	VEG							
	- Aerenchymatous	1.2901	0.4307	**0.0303**			5	
	-Ericaceous shrub	0.7673	0.6684	0.3029			5	
	Month							
	- **Apr**	0.6774	0.2947	**0.0241**			80	
	VEG							
	- Tree	-0.5482	0.5955	0.3995			5	
	PA	-0.2535	0.1046	**0.0177**			80	
	uWD	0.2322	0.0666	**0.0008**			80	
	u*	-0.1875	0.0774	**0.0176**			80	

https://doi.org/10.5194/egusphere-2025-5023
Preprint. Discussion started: 27 October 2025

Month					
- Oct	-0.1805	0.1432	0.2111	80	
WTL	0.1375	0.0809	0.0931	80	
Month					
- Dec	0.1258	0.3948	0.7509	80	
NEE	0.1069	0.0664	0.1114	80	
Month					
- Sep	0.0963	0.1475	0.5158	80	
vWD	0.0686	0.0501	0.1747	80	
Month					
- Jul	0.0608	0.1465	0.6789	80	
- Jun	0.0461	0.1408	0.7442	80	
- Nov	-0.0404	0.2062	0.8453	80	
- Aug	0.021	0.1456	0.8857	80	
Random effects					
Site					64.35

3.2.2 Spatial FCH_4 variation increases ecosystem and plot-scale FCH_4 difference

Spatial variation between FCH_4 measurements by individual chambers increased absolute ΔFCH_4 (Fig. 5). The increasing trend between chamber IQR (log +0.01) and absolute ΔFCH_4 (log) became clearer in coarser temporal scales, where a unit (*e*-fold; ca. 2.7x) increase in monthly and annual chamber FCH_4 variation (IQR +0.01) was associated with ca. 51% and 63% increase in absolute ΔFCH_4, respectively (marginal $R^2 \geq 0.31$, $p \leq 0.01$). Temporal EC FCH_4 variation (e.g., within date in daily scale) did not lead to strong increases in absolute ΔFCH_4 at daily-to-monthly aggregations (marginal $R^2 < 0.01$), but the annual mixed effects model showed a ca. 198% increase in absolute ΔFCH_4 with a unit increase in EC FCH_4 IQR (+0.01; marginal

https://doi.org/10.5194/egusphere-2025-5023
Preprint. Discussion started: 27 October 2025

R^2=0.82). Models with both chamber and EC IQR (log +0.01) as explanatory variables showed significant chamber IQR at daily-to-monthly aggregations (p<0.001, marginal R^2=0.06-0.31) and significant EC IQR at daily scale (p=0.005). In contrast, the annual model had a nonsignificant chamber IQR and significant EC IQR (p=0.001, marginal R^2=0.81). The sites also differed in the strength and direction of the relationship between chamber and EC FCH_4 variation and ΔFCH_4 (Fig. 5).

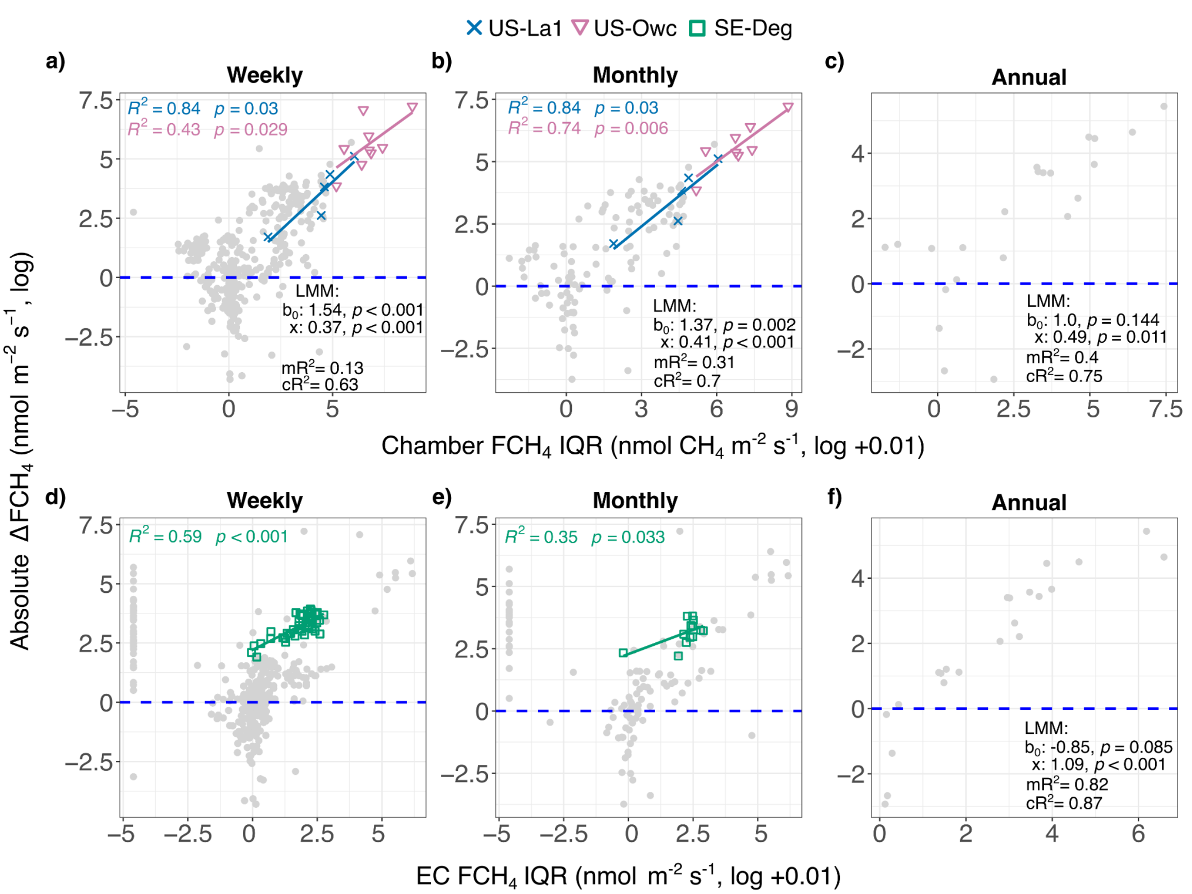

Figure 5. Variation in FCH_4 between individual chambers and eddy covariance (EC) timestamps increases absolute ΔFCH_4. a-c) Relationship between chamber FCH_4 variation (variation between individual chambers per aggregation timestamp, represented by interquartile range; IQR) and absolute ΔFCH_4 at weekly (a), monthly (b) and annual (c) scales. d-f) Relationship between EC timestamp FCH_4 variation (represented by IQR) and absolute ΔFCH_4 at weekly (d), monthly (e) and annual (f) scales. Linear mixed effects model (LMM) results: b_0 = model intercept, x = predictor (chamber or EC FCH_4 log IQR +0.01) of log absolute ΔFCH_4, p = predictor significance (preceded by model coefficient estimates), mR^2 and cR^2 = marginal and conditional R^2, respectively. In d) and e) LMM results are not shown due to low marginal R^2 ($mR^2 \leq 0.06$). Daily scale is not shown due to the low number (n=1) of sites with significant relationships and low marginal R^2 ($mR^2 \leq 0.06$). Linear regressions,

https://doi.org/10.5194/egusphere-2025-5023
Preprint. Discussion started: 27 October 2025

R^2s and p-values are only shown for sites with significant IQR predictor and R^2>0.2 and are shown in different colors and shapes (gray points: nonsignificant and R^2≤0.2 sites). The dashed blue line indicates ΔFCH_4=0. See version with untransformed data in Fig. B18.

3.2.3 Ecosystem and plot-scale FCH_4 difference does not significantly vary among chamber types

We did not find significant differences in ΔFCH_4 between automated and manual chambers at all aggregations (Wilcoxon-Mann-Whitney; daily p=0.948, weekly p=0.361, monthly p=0.565, annual p=0.722). However, ΔFCH_4 in manual chambers had higher variation than automated chambers in daily (CV_{manual}=284%, $CV_{automated}$=181%), weekly (CV_{manual}=262%, $CV_{automated}$=181%), and monthly (CV_{manual}=240%, $CV_{automated}$=182%) aggregations. The correlations between chamber FCH_4 and EC FCH_4 for both automated and manual chambers were strong at daily-to-annual aggregations (ρ>0.7, Fig. B19).

4 Discussion

4.1 Ecosystem-scale FCH_4 is higher than plot-scale FCH_4 at all temporal scales

Contrary to our hypothesis, across all temporal aggregations, ecosystem-scale (EC) FCH_4 was higher than at the plot scale (chamber). Higher EC FCH_4 than chamber FCH_4 have been observed in an arctic peatland with area-weighted chamber FCH_4 (Budishchev et al., 2014), a managed peat meadow with upscaled chamber FCH_4 (Schrier-Uijl et al., 2010), a peatland with down-scaled EC FCH_4 (Forbrich et al., 2011), a temperate forest with spatial chamber FCH_4 averages (Wang et al., 2013), and a temperate salt marsh with spatio-temporal chamber and EC FCH_4 averages (Hill and Vargas, 2022b), while other studies at individual sites have observed higher chamber FCH_4 (upscaled to ecosystem-level with different methods) than EC FCH_4 (Chaichana et al., 2018; Clement et al., 1995; Davidson et al., 2017; Krauss et al., 2016; Marushchak et al., 2016; Meijide et al., 2011; Morin et al., 2017; Riutta et al., 2007). Nonetheless, the median difference was relatively low across sites and temporal aggregations (min 1.36 daily, max 2.58 nmol m^{-2} s^{-1} annual), with CV ranging from a minimum of 191% (hourly) to a maximum of 674% (daily; Table 2), indicating relatively good agreement between ecosystem and plot-scale FCH_4 across sites but with large variation around perfect agreement. While our higher ecosystem than plot-scale FCH_4 trend was robust across temporal scales, due to the limited data availability (n=10 sites), our results might reflect site differences and generalizations should be tested when more data becomes available.

We found the best general agreement between instantaneous ecosystem and plot-scale FCH_4 in the monthly and annual aggregations, with the agreement improving from fine to coarse temporal resolutions, as expected. The improved agreement is likely a result of the data aggregation, which reduces the influence of inter-daily FCH_4 variability. In addition, mean ΔFCH_4 in weekly, monthly and annual aggregations was negative, indicating higher plot-scale than ecosystem-scale FCH_4, and the

CV for the weekly aggregation in particular was large (467%). Our results suggest that high CH_4 emissions and FCH_4 variability in plot-scale measurements are associated with higher ΔFCH_4, particularly at time scales longer than daily (Table 2 and Fig. B2); suggesting that combining plot- and ecosystem-scale FCH_4 data at heterogeneous sites is particularly problematic at coarse temporal scales. This may highlight the importance of selective chamber placement on high-emitting locations and time periods within the study sites. However, our results based on cumulative FCH_4 (Table C4) also show that ecosystem-scale cumulative FCH_4 are generally higher than at plot scale. Therefore, site-level CH_4 budgets calculated with ecosystem-scale FCH_4 data can exceed plot-scale estimates despite localized plot-scale CH_4 emission peaks (with site-specific variation; Fig. B16).

In general, the spatio-temporal variation of EC footprint and chamber measurement artifacts may have contributed to the higher ecosystem-scale FCH_4. Chamber measurements are challenged by tall vegetation, and in most cases chambers that observe ebullition events are discarded, and therefore, the EC footprints may have covered high-CH_4-emitting areas (i.e., CH_4 emission hot spots), such as *Typha* sp.-dominated vegetation patches, and ebullition events (i.e., CH_4 emission hot moments) more often than chambers, leading to higher ecosystem-scale FCH_4. This has been demonstrated in spatially heterogeneous areas, where CH_4 emission hot spots within EC footprints may be important ΔFCH_4 drivers (Desai et al., 2015; Rey-Sanchez et al., 2025; Xu et al., 2018), and at least in some sites, the majority of FCH_4 is contributed through ebullition (Villa et al., 2021). In addition, FCH_4 hot spots and hot moments can vary in both space and time, and manual chamber FCH_4 measurements (n=6 sites) are often conducted sporadically, during daytime and in weekly or monthly campaigns, resulting in large uncertainties related to spatio-temporal FCH_4, and possibly ΔFCH_4, variation across temporal scales (Anthony and Silver, 2021, 2023; Vargas and Le, 2023). The EC footprint effects could be further highlighted by the increasing ΔFCH_4 with increasing FCH_4 (Fig. 4), and similar trends were observed in a rice paddy (Meijide et al., 2011). However, ΔFCH_4 in low FCH_4 is likely not detected well due to EC and chamber detection limits, the reported ranges of which cover the minimum absolute ΔFCH_4 of 0-0.05 nmol m^{-2} s^{-1} (Desai et al., 2015; Erkkilä et al., 2018; Kroon et al., 2007, 2010; Richardson et al., 2019; Smeets et al., 2009). Altogether, the mismatch in EC footprint and chamber measurement coverage could be an important ΔFCH_4 driver, as FCH_4 between surface cover types and within them can vary strongly even within the same growing season (Voigt et al., 2023), highlighting the need to account for EC footprint representativeness as well as chamber measurement location and frequency when combining plot and ecosystem-scale FCH_4 data.

4.2 Atmospheric pressure, friction velocity and vapor pressure deficit predict daily and weekly FCH_4 difference between ecosystem and plot scales

PA, u* and VPD were important daily and weekly-scale ΔFCH_4 predictors. PA can be a strong predictor of daily and multiday FCH_4 (Knox et al., 2021), and ΔFCH_4 decreased with higher PA (weekly PA p=0.057). As drops in PA have been associated with ebullitive FCH_4 in wetlands (Knox et al., 2021; Nadeau et al., 2013; Sachs et al., 2008; Tokida et al., 2007) and as unvented closed chambers can alter chamber air pressure (Jentzsch et al., 2025) and most ebullition events were filtered out from chamber FCH_4 data (Text A1), EC may have captured FCH_4 pulses during falling PA that chamber data did not include.

Friction velocity may have increased ΔFCH_4 mainly via effects on CH_4 ebullition in open water (Wille et al., 2008), which EC detected but chambers excluded. However, EC FCH_4 can be underestimated in low u* which could also have led to subsequent decreases in ΔFCH_4 (Aubinet, 2008; Baldocchi, 2003). The strong effect size of site dominant vegetation and the negative VPD effect may reflect species- and site-specific stomatal conductance and CH_4 transport (Cernusak et al., 2018; Grossiord et al., 2020). The importance of plant activity may be further supported by the marginally-significant TS (p=0.051) which may have acted as a proxy for increased plant activity particularly in July and August (p<0.01), the peak growing season months in the northern hemisphere. Chamber artifacts may have also contributed to the u* and VPD effects: short chamber deployments in high u* and low WTL may have underestimated chamber FCH_4 (Lai et al., 2012), while longer measurements (e.g. FI-Si2, US-La1 and US-La2: >30 min) in high WTL may have kept stomata open and increased CH_4 transport and chamber FCH_4 (Knapp and Yavitt, 1992; Langensiepen et al., 2012). However, given the limited sample size in the models (n=9 sites), these results may be strongly influenced by site selection.

As expected, greater variation in FCH_4 between chambers led to higher ΔFCH_4 especially at the weekly to annual scales. Indeed, chamber FCH_4 can vary strongly between individual chambers (Davidson et al., 2002) but FCH_4 variation can be even stronger between chamber patches (due to differences in vegetation and microtopography) than within them (Stewart et al., 2024), a factor which was not included in our analyses. Similar to CH_4, spatial variation in chamber-based soil CO_2 respiration measurements has been estimated as an important driver of the discrepancies between ecosystem and soil CO_2 respiration observations and their varying directions, indicating that chambers may capture soil respiration hot spots and moments that EC does not (Phillips et al., 2017). Chambers capturing these CH_4 emission hot spots and hot moments may have led to the large ΔFCH_4 CVs and negative mean ΔFCH_4 particularly in the daily and weekly aggregations in both median and mean-based temporal aggregations (Table 2 and Table C3). The spatial variation between chambers could have also contributed to chamber FCH_4 random errors and ΔFCH_4 patterns in Fig. 4 (Levy et al., 2011). Nevertheless, despite the possible importance of chamber CH_4 emission hot spots and moments in driving ΔFCH_4, cumulative plot-scale FCH_4 seem to be increasingly overcome by higher ecosystem-scale FCH_4 at coarser temporal scales, but with site-specific trends (Table C4, Fig. B16). Between-chamber variation explained ΔFCH_4 best at US-La1 (but n=5) and US-Owc, and spatial FCH_4 heterogeneity is high particularly at US-Owc (Rey-Sanchez et al., 2018; Villa et al., 2021), which may explain these trends. In contrast, SE-Deg has a relatively homogeneous vegetation composition (Järveoja et al., 2018), which is probably the reason why EC FCH_4 variation had a better fit than between-chamber FCH_4 variation (Fig. 5). The increasing absolute ΔFCH_4 with between-chamber FCH_4 variation may result from the EC footprint capturing patches that only a portion of the chamber measurements may represent. This may be highlighted in sites with manual chamber measurements which were conducted 1-3 times a month and during daytime when FCH_4 are often higher than at nighttime (Koebsch et al., 2015; Long et al., 2010; Parmentier et al., 2011) (e.g., US-La1; Fig. 5). Therefore, using representative chamber patches and measurement times to upscale chamber FCH_4 to the EC footprint could potentially decrease ΔFCH_4 (Schrier-Uijl et al., 2010; Vargas and Le, 2023).

4.3 Wind direction, atmospheric pressure and friction velocity drive monthly ecosystem and plot-scale FCH_4 differences

At the monthly scale ΔFCH_4 was best explained by wind direction (uWD), PA and u*. Wind direction has been an important EC FCH_4 predictor in wetlands similar to the sites of this study in multiday (2.7-21.3 days) and seasonal (42.7-341 days) scales (Knox et al., 2021). In general, the significant uWD may indicate monthly-scale variation in EC footprint and the possibly systematically different land cover coverage than that of chambers within the study sites, but footprint-aware analyses with a larger sample size are required to confirm these hypotheses. PA and u* are considered to be more influential FCH_4 drivers in the diel to multiday scales, so, together with uWD, they may instead represent seasonality in ΔFCH_4, driven by continental-scale air pressure systems or regional land-sea winds (Griebel et al., 2016; Montaldo and Oren, 2016; Rebmann et al., 2005). The high effect size and significance of aerenchymatous vegetation may further suggest a role of seasonal plant activity with higher CH_4-emitting or -consuming aerenchymatous plant biomass in growing season months (Knox et al., 2021; Niu et al., 2011), but this could also be related to site-specificity in monthly ΔFCH_4 patterns (conditional R^2=0.88). Site-specificity may also be highlighted by the significant April in the monthly model, as only three out of nine sites had observations in April (Fig. B1).

Monthly and annual ΔFCH_4 trends may have also reflected seasonal snow and ice thaw dynamics, as well as changes in the chamber measurement system. The higher ecosystem-scale FCH_4 at CN-Hgu and US-Ho1 in cooler months (Fig. B14) may have resulted from spring snowmelt releasing stored CH_4 below the ice and snow cover (Hargreaves et al., 2001; Morin et al., 2017; Rinne et al., 2007; Zhang et al., 2012) which might have been captured by EC but not by chambers. However, only four sites had data from November, December and March (Fig. B1). Therefore, sites with full year co-occurring chamber and EC FCH_4 coverage are needed to investigate the seasonal ΔFCH_4 dynamics further. Changes in the chamber measurement system also likely contributed to monthly and interannual ΔFCH_4. In US-Ho1 and US-Uaf, the number of chambers per chamber surface cover class varied between years and months: due to instrument malfunction or chamber replacements, in some timestamps spatial chamber medians did not include CH_4-emitting or -consuming patches while EC did, leading to a large monthly- and annual-scale ΔFCH_4 variation (Richardson et al., 2019; Ueyama et al., 2023a).

4.4 FCH_4 difference between ecosystem and plot scales is highest in the morning and at noon

As we expected, our diel analyses revealed higher ΔFCH_4 and ecosystem-scale FCH_4 from morning to noon (max ΔFCH_4 at 9 AM) and lower in the evening and at night (min ΔFCH_4 at 8 PM), but the trends varied strongly between sites and months. Higher daytime FCH_4 has been observed particularly during growing seasons (Koebsch et al., 2015; Long et al., 2010; Parmentier et al., 2011), and higher diurnal EC FCH_4 than chamber FCH_4 also by Yu et al. (2013). Ecosystem FCH_4 seemed to be driving the monthly diel ΔFCH_4 fluctuations particularly in July with noon and August with morning FCH_4 peaks, while plot scale showed less diel fluctuation (Fig. B8-B12), possibly as a result of the spatial aggregation of chamber measurements. Our findings of increasing absolute ΔFCH_4 with FCH_4 (Fig. 4) may reflect these differences, as EC and chamber FCH_4 random error can increase with flux magnitude (Hollinger and Richardson, 2005; Knox et al., 2019; Richardson et al., 2006, 2008),

https://doi.org/10.5194/egusphere-2025-5023
Preprint. Discussion started: 27 October 2025

and may also be associated with diel variation in turbulence, EC footprint, and spatial FCH_4 heterogeneity (Hollinger and Richardson, 2005; Knox et al., 2021; Levy et al., 2011), and vary between sites (Delwiche et al., 2021; Richardson et al., 2006). However, the diel-scale mixed models had very low explanatory power and high site-specificity (conditional R^2>0.79), making it difficult to identify drivers for the observed ΔFCH_4 trends. Thus, more sites with hourly chamber FCH_4 measurements are needed to disentangle the diel ΔFCH_4 predictors.

The high daytime ΔFCH_4 (CN-Hgu, SE-Deg, US-Ho1) could have resulted from diel variation in u* and VPD. High daytime u* can enhance ebullition, CH_4 volatilization and release of stored CH_4 from nocturnal boundary layer (Baldocchi, 2003; Long et al., 2010; Morin et al., 2014; Sachs et al., 2008; Wille et al., 2008). Related to VPD, pressurized plant-mediated CH_4 transport typically peaks in the late morning to afternoon, as temperature and humidity gradients between cooler belowground tissues and warmer, drier aboveground air enhance internal-external pressure differences that drive gas flow through aerenchyma. However, very high VPD can induce stomatal closure, thereby reducing CH_4 transport (van den Berg et al., 2020; Knox et al., 2021; Morin et al., 2014; Vroom et al., 2022; Whiting and Chanton, 1996). Enhanced stomatal conductance under high solar radiation may have also increased diffusive plant-mediated CH_4 transport (van der Nat et al., 1998), leading to higher daytime ecosystem-scale FCH_4 than plot-scale FCH_4 as dark chambers possibly closed the stomata. However, longer chamber deployment can decrease VPD within the chamber, and re-open the stomata (Knapp and Yavitt, 1992; Langensiepen et al., 2012). The high nighttime ΔFCH_4 (US-Uaf) could have been driven by u*: the nighttime EC footprint may have covered high-CH_4-emitting areas when u* was low and EC footprint larger (Baldocchi et al., 2012; Chu et al., 2021; Vesala et al., 2008). Aerenchymatous vegetation may have also decreased daytime ecosystem-scale FCH_4 by increasing rhizospheric oxidation and CH_4 consumption under high solar radiation, VPD, and soil temperature (Cho et al., 2012; Zhao et al., 2021). However, further footprint-aware research on diel ΔFCH_4 patterns is needed to explore these hypotheses.

4.5 Plot-scale FCH_4 may have been underestimated due to chamber artifacts

EC and chamber techniques fundamentally differ in how ecosystem FCH_4 is measured, which could influence ΔFCH_4. Gas analyzers used for EC can be divided into open- and closed-path analyzers, the former of which is more sensitive to weather conditions, while the latter is influenced by the choice of the air pump and time lags between sonic anemometer and the gas analyzer (Baldocchi, 2003; Detto et al., 2011). However, the random and systematic errors associated with open- and closed-path EC gas analyzers do not contribute significantly to the total EC FCH_4 random error, which may be more affected by the movement of EC footprint and turbulence (Deventer et al., 2019; Knox et al., 2019; Peltola et al., 2014). Thus, the two analyzers should agree relatively well in practice and they can be combined in multi-site syntheses (Detto et al., 2011; Deventer et al., 2019; Peltola et al., 2014). However, detecting upland CH_4 uptake rates accurately with open-path analyzers is challenging due to uptake rates often falling within the instrument's detection limits (Chamberlain et al., 2017; Iwata et al., 2014). Of the two upland sites included in this study, these artifacts may have affected the results from CN-Hgu where EC FCH_4 were measured with an open-path gas analyzer.

As manual and automated chambers differ in temporal representation, the nonsignificant differences between automated and manual chambers in ΔFCH_4 were surprising. The nonsignificant differences are also reflected in the strong correlations between automated and manual chamber FCH_4 and EC FCH_4 (Fig. B19), and similar nonsignificant differences between automated and manual chambers were found in a Tibetan wetland (Yu et al., 2013). The spatial medians of manual chamber FCH_4 may have reduced the spatial FCH_4 variation common for manual chambers, and roughly correspond to the smaller spatial FCH_4 variation of automated chambers. However, the higher ΔFCH_4 variation of manual chambers could have resulted from chamber measurements being conducted 1-3 times a month leading to data gaps (Morin et al., 2014, 2017). Thus, care should be taken when combining manual chamber FCH_4 data with EC FCH_4 data in multi-site syntheses.

Chamber FCH_4 measurement and calculation methodology may have contributed to the generally lower plot-scale FCH_4. All chamber FCH_4 data was calculated using linear regression which may underestimate FCH_4 (Forbrich et al., 2010; Korkiakoski et al., 2017; Levy et al., 2011; Nakano, 2004; Pihlatie et al., 2013). High-precision CH_4 analyzers, such as cavity ring-down spectrometers and near-infrared laser gas analyzers, could capture nonlinear CH_4 concentration gradients which linear regression fails to do (Forbrich et al., 2010). With gas chromatography, the underestimation and related uncertainties may become even greater due to smaller sample sizes and difficulty in detecting low-quality FCH_4 measurements during chamber measurements (Christiansen et al., 2015; Levy et al., 2011). In sites which used gas chromatography, the number of samples was 4-7 per chamber deployment (e.g., FI-Si2, US-Owc), while sites that used high-precision CH_4 analyzers (CN-Hgu, SE-Deg, US-Ho1, US-Uaf) had ca. 1 Hz sampling interval, resulting in vastly different sample sizes per chamber deployment between sites, and thus higher uncertainties in chamber FCH_4. However, linear regression can be statistically more robust for comparing chamber FCH_4 from different sites with varying soil properties (Venterea et al., 2009). Furthermore, depending on chamber design, chambers can alter soil conditions (e.g., soil moisture) which may also contribute to ΔFCH_4 (Bansal et al., 2023b; Subke et al., 2021). It may be valuable to compare chamber and EC FCH_4 using both linear and exponential fits for chamber FCH_4 to better understand ΔFCH_4 trends across sites.

4.6 Limitations and uncertainties

The main uncertainties and limitations in our study arose from the sample size, chamber FCH_4 data and EC footprint. As we were able to include only ten sites in the analyses, our results are limited by the site-specific climate, vegetation, and methodology. Thus, in order to produce results that would be better generalizable to other sites and regions (e.g., tropics), future studies could include more sites from a variety of climates and dominant vegetation types. Since we used spatial medians of chamber FCH_4 measurements instead of upscaled chamber FCH_4 in the analyses to investigate cross-scale FCH_4 differences, the results should not be taken as indication of systematic methodological differences between EC and chamber FCH_4. Thus, the next steps could include comparing EC and chamber methods by upscaling chamber FCH_4 to the EC footprint level, or downscaling EC FCH_4 to chamber level, using footprint models and indices of footprint spatial heterogeneity based on fine-scale land cover classification (Hartley et al., 2015; Metzger, 2018; Räsänen et al., 2021; Tuovinen et al., 2019; Xu et al.,

https://doi.org/10.5194/egusphere-2025-5023
Preprint. Discussion started: 27 October 2025

2018). Future studies could apply high-resolution (e.g., 1-2 m) remotely-sensed data together with field surveys to determine chamber patch classes which could be used in upscaling chamber FCH_4 to the EC footprint level (Davidson et al., 2017; Forbrich et al., 2011; Morin et al., 2017; Rey-Sanchez et al., 2018; Schrier-Uijl et al., 2010; Stewart et al., 2024; Tuovinen et al., 2019), or downscaling EC FCH_4 to land cover classes (Forbrich et al., 2011; Rößger et al., 2019). By comparing footprint- and patch-weighted chamber FCH_4 to EC FCH_4, we would expect ΔFCH_4 to decrease or chamber FCH_4 exceed EC FCH_4 due to the incorporation of footprint FCH_4 heterogeneity (Budishchev et al., 2014; Schrier-Uijl et al., 2010). As our results may indicate FCH_4 hot spots and moments within the study sites as a possible ΔFCH_4 driver, identifying FCH_4 hot spots within the EC footprint with the aid of footprint-weighted FCH_4 maps (Rey-Sanchez et al., 2022) could also assist in finding representative chamber FCH_4 locations to reconcile the ecosystem and plot-scale FCH_4 differences. In addition, our cross-scale FCH_4 comparisons may contain large uncertainties due to differences in chamber FCH_4 outlier removal (Text A1) (Jentzsch et al., 2025; Levy et al., 2011). To minimize these uncertainties in future comparison studies, it is therefore recommended to use chamber FCH_4 data that has been processed in as standardized a way as possible.

5 Conclusions

We explored the differences between ecosystem-scale (eddy covariance, EC) and plot-scale (chamber, spatially-aggregated median) instantaneous CH_4 flux (FCH_4) across ten wetland and upland sites and in different temporal aggregations. Contrary to our expectations, we observed significantly higher median ecosystem FCH_4 than plot-scale FCH_4 across all temporal scales. However, the median FCH_4 difference between ecosystem and plot-scales (ΔFCH_4) remained relatively low. Ecosystem and plot-scale FCH_4 correlated strongly from daily to annual scales, which indicates that ecosystem and plot-scale FCH_4 observations could be combined in multi-site analyses at coarse temporal scales. However, care must be taken when combining cross-scale FCH_4 data, as variation in (based on instantaneous FCH_4) and magnitude of ΔFCH_4 (based on cumulative FCH_4) was large at daily to annual scales, and the agreement was worst at the half-hourly to hourly scales. In addition, ΔFCH_4 increased with FCH_4 magnitude at all temporal scales, suggesting that combining ecosystem- and plot-scale FCH_4 in high CH_4-emission ecosystems, such as wetlands, could lead to large FCH_4 uncertainties.

We attribute the higher ecosystem-scale FCH_4 than plot-scale FCH_4 mainly to the combination of selective chamber placement and the spatio-temporal dynamics of the EC footprint which may have captured CH_4 emission events that were not detected by chambers. Our results highlight the importance of monthly and seasonal variation in variables related to plant activity, atmospheric pressure, wind direction, and friction velocity as drivers of ΔFCH_4 across sites. Between-chamber FCH_4 variation also led to higher ΔFCH_4, which highlights the mismatch of chamber and EC footprint coverage of the study sites as a ΔFCH_4 driver. Nevertheless, ΔFCH_4 seems to vary between sites, warranting further research on ΔFCH_4 controls within and across ecosystem types. Based on our findings, we recommend the following:

- Cross-site efforts to upscale chamber FCH_4 to EC footprint level, or conversely, to downscale EC FCH_4 to chamber scale, using chamber measurements stratified by surface cover classes which take into account for vegetation and soil characteristics
- Further investigation of diel ΔFCH_4 dynamics from a higher number of sites with automated chamber measurements, particularly related to the spatial representativeness of the chamber measurements in relation to the EC footprint and chamber artifacts on the observed FCH_4
- More widely adopted, standardized methods for examining heterogeneity of FCH_4 in EC footprints, which can inform representative chamber and EC tower placement within the study sites (e.g., EC footprint modeling and targeted manual chamber sampling; Rey-Sanchez et al., 2022, Barba et al., 2018)
- Systematic bias and uncertainty of chamber and EC FCH_4 observations should be incorporated into model evaluation and parameterization studies

As syntheses and databases are increasingly utilizing both plot- and ecosystem-scale FCH_4 measurements, it is important to understand their differences across multiple sites. Taking these differences into account in future studies will improve ecosystem CH_4 budget estimates.

Appendices

Appendix A: Supplementary texts (Text A1-A3)

Text A1.

Quality control summary for chamber FCH_4 data sets. Data quality control and possible outlier removal was done by data providers prior to sharing chamber FCH_4 data, and a summary of the methods are listed here. For more details, please see the site-specific references.

<u>CN-Hgu</u>

FCH_4 was measured using dark chambers without a pressure vent or fan. FCH_4 was corrected for air temperature but not for air pressure. After each measurement, the computer system immediately calculated FCH_4 rate by using a linear regression model, and recorded the regression coefficients, R^2, and *p*-values (Wang et al. 2022). Low-quality data were excluded when $R^2<0.9$. Ebullition is not a significant CH_4 source at the studied site and thus ebullition events were not removed.

<u>FI-Si2</u>

Nonlinearities in the FCH_4 data resulting from ebullition events and chamber leakages were removed during quality control. As a result, 10.4 % of the flux values were excluded as outliers (Korrensalo et al. 2018). The chambers had a fan and the air temperature used for FCH_4 calculations was measured inside the chamber during the measurements. The chambers were dark.

SE-Deg

The chamber FCH_4 data was corrected for air density (including air temperature) but not for air pressure. Low-quality data were removed based on R^2 and RMSE values (flux values with both $R^2<0.95$ and RMSE>0.02) of the fitted linear regression. Ebullition events were removed (but CH_4 ebullition is not considered a significant CH_4 source at the site). Air temperature was measured inside the chamber. The chambers did not have a pressure vent or a fan but the sample air is circulated back from the analyzer to the chamber and the air flow back into the chamber provides some mixing of the headspace air. FCH_4 was not separately corrected for H_2O dilution, but the dry mixing ratio from LGR was used for FCH_4 calculation. FCH_4 was measured using both dark (n=4) and transparent (n=4) chambers. See further details of the chamber measurement system in Järveoja et al. (2018).

US-Ho1

During data quality checks, all data points that had $R^2<0.9$ in the fitted linear regression were removed. All data known to have been affected by disturbances, such as instrument failures, calibrations and testing, were also removed from the data set. Chamber FCH_4 was corrected for air temperature and pressure (Richardson et al. 2019). Ebullition events were not removed. Chambers had a pressure vent but no fan. Air temperature and pressure were measured beside the chamber. The chamber FCH_4 was calculated based on the H_2O dilution-corrected FCH_4 provided by IRGA. The chambers were dark.

US-La1 and US-La2

No ebullition was detected in chamber FCH_4 measurements, and thus no ebullition events were removed. Air temperature was measured inside and outside of the chamber and used for the FCH_4 calculations. Chambers had no pressure vent nor a fan, but air was mixed manually by sucking and injecting air with the sampling syringe (Krauss et al. 2016). The chambers were dark.

US-Los

No specific outlier removal was performed but most mean $R^2>0.9$ for CH_4 flux across replicates. About 15% of observations had $R^2<0.66$. Ebullition events were not removed. The chambers had a small battery-powered fan and a small vent. Air temperature and pressure from outside the chamber were used to calculate the FCH_4. H_2O dilution corrections were obtained from LGR and used for the FCH_4 calculations. The chambers were dark.

US-Owc

Outliers were removed based on R^2 values from linear regression ($R^2\leq0.85$). The whole chamber measurement was discarded if more than three points were removed based on the R^2 values. Ebullition events were not included in the data following this quality control processing. Chambers had a pressure vent to prevent air pressure fluctuations within the chamber (Rey-Sanchez et al. 2018). Air temperature was measured inside the chamber. FCH_4 was corrected for pressure and air temperature. The chambers were dark.

https://doi.org/10.5194/egusphere-2025-5023
Preprint. Discussion started: 27 October 2025

US-StJ

Outliers were removed based on R^2 values from linear regression (R^2<0.9) for simultaneously measured CO_2 fluxes, and data that passed these quality control steps were assumed to apply to CH_4 flux as well (Hill and Vargas 2022). Ebullition events were removed. The chambers were dark and included a small fan for air mixing.

US-Uaf

FCH_4 was calculated by taking into account air temperature and pressure which were measured outside of the chamber. The CH_4 concentration was corrected for H_2O dilution. Chambers had a pressure vent but no fan. The chambers were dark. Ebullition events were estimated negligible at this site and thus no ebullition removal was conducted.

Text A2.

Wind *u* and *v* component calculation.

Wind direction was separated into *u* (calculated with sine; equation 1) and *v* (calculated with cosine; equation 2) component vectors which combine both wind speed and direction for each half-hour measurement period.

$$u = -WS * sin[\frac{2\pi * WD}{360}] \quad (1)$$

$$v = -WS * cos[\frac{2\pi * WD}{360}], \quad (2)$$

where WS is wind speed (m s^{-1}) and WD is wind direction in decimal degrees.

The *u* and *v* component averages were then calculated by taking the mean over the temporal unit in each aggregation (e.g. hour or day), resulting in temporally-aggregated *u* and *v* components in m s^{-1}.

Text A3.

Details of linear mixed effects models.

Temporal autocorrelation and residual variance structures were examined and chosen based on Akaike Information Criteria (AIC) and residual diagnostics, with more emphasis on the latter. Temporal autocorrelation was modeled using an autoregressive structure of order 1 (AR1) in the daily, weekly, and monthly models. To meet the requirements of the corAR1 argument in R, random effects in these models were nested to account for site-specific sampling times (e.g., daily model:

https://doi.org/10.5194/egusphere-2025-5023
Preprint. Discussion started: 27 October 2025

random = ~1 | Site/YearMonth, correlation = corAR1(form = ~ Day | Site/YearMonth)). The nesting allowed for the inclusion of temporal autocorrelation within each temporal scale, for example "YearMonth", at the site level, reducing residual temporal autocorrelation compared to models with un-nested random effects. However, incorporating AR1 in the half-hourly model did not improve model fit or reduce residual variance and was therefore excluded. In addition, despite improvements in AIC in the hourly model, inclusion of AR1 led to model non-convergence and it had to be excluded from the model, leading to higher AIC but temporal autocorrelation and residual normality and variance heterogeneity were still acceptable when the random effect was nested (*Site/Date*).

Heterogeneous residual variance caused by some of the predictors was modeled in some of the models using an exponential variance structure (*varExp*; half-hourly and hourly: VPD, u*, PA; daily: PA and TS; weekly: PA; monthly: uWD, u*), as well as variance per stratum (*varIdent*; weekly: Year). We also tested other variance structures but, according to AIC and residual diagnostics, exponential variance structure led to best model fit and some of the other structures led to model non-convergence. Despite our efforts to account for the residual variance heterogeneity, some heterogeneity remained in the models while AIC and general model residual heterogeneity improved.

Appendix B: Supplementary figures (Figures B1-B19)

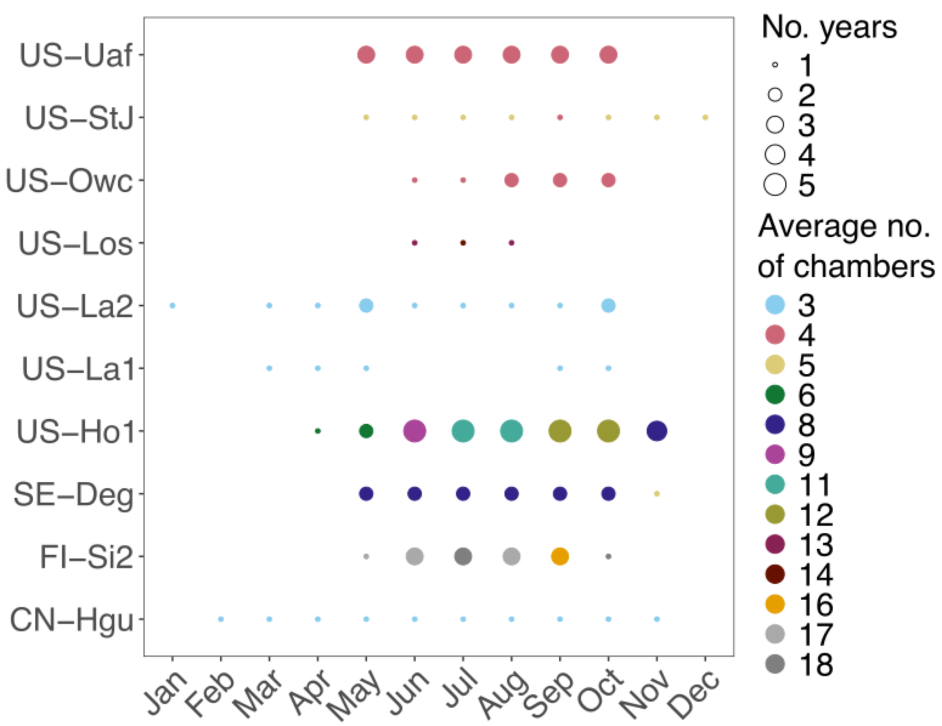

https://doi.org/10.5194/egusphere-2025-5023
Preprint. Discussion started: 27 October 2025

Figure B1. Number of individual chambers and years per month per site. The size of the point describes the number of years and color the average number of individual chambers used within each month across years.

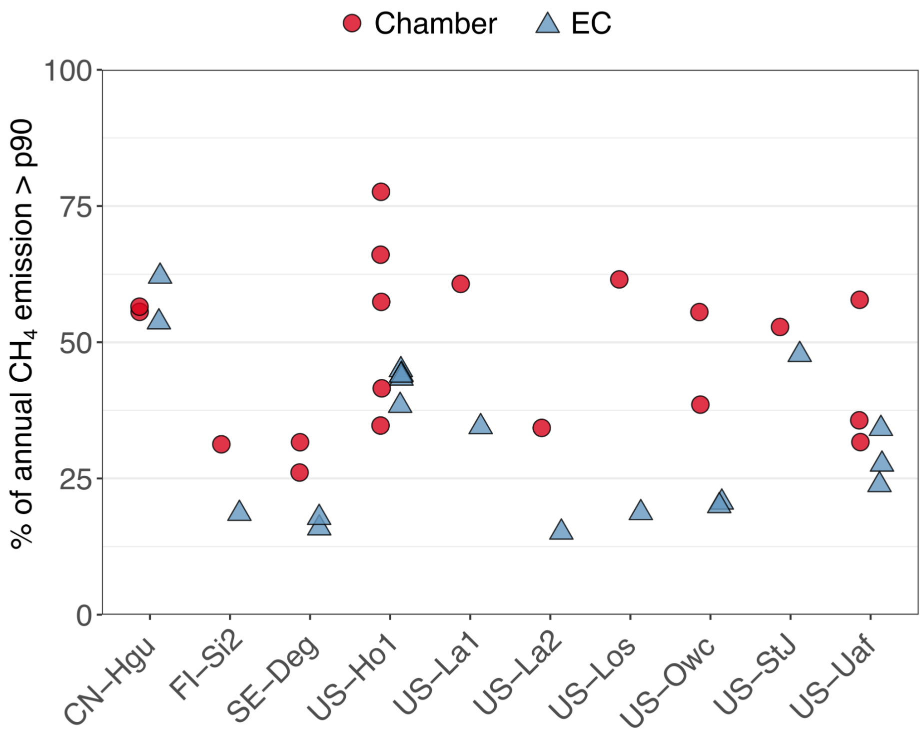

Figure B2. Contribution of high CH_4 emissions to annual CH_4 emissions per site in the unaggregated data set. For each site and year, high CH_4 emissions were estimated as FCH_4 above the 90th percentile (p90) and their proportion (%) of the total annual CH_4 emission was calculated separately for chamber (red circle) and EC (blue triangle). In the unaggregated data set, all EC FCH_4 data is in the half-hourly scale, but the chamber data measurement frequency varies across sites (see Table S1).

https://doi.org/10.5194/egusphere-2025-5023
Preprint. Discussion started: 27 October 2025

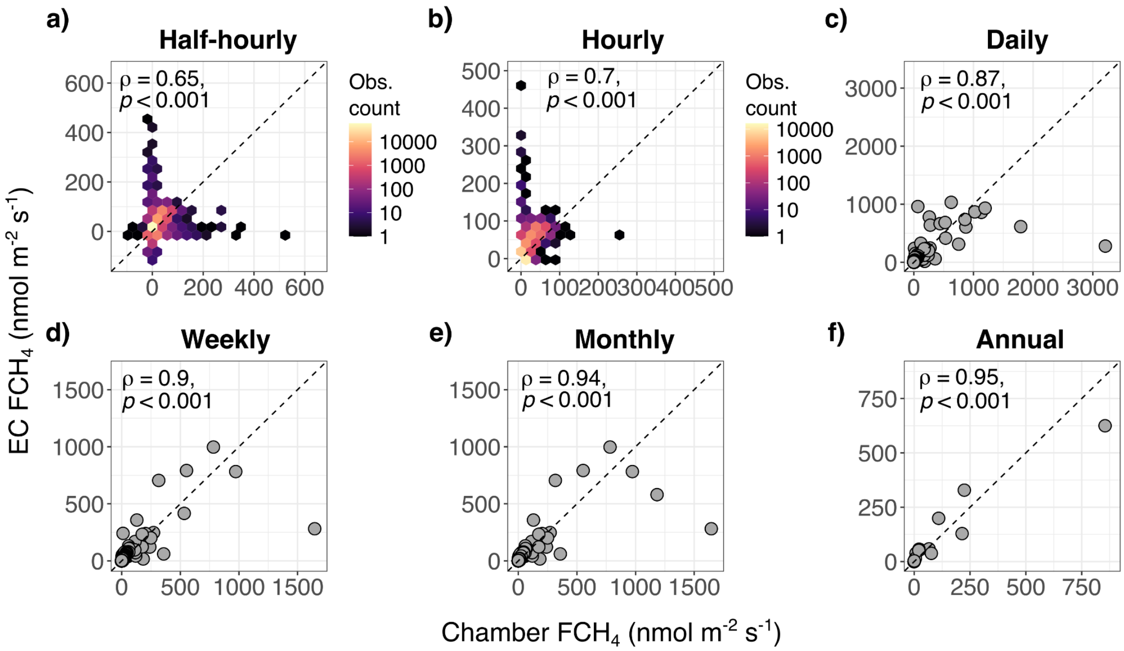

Figure B3. Relationship between EC FCH_4 and chamber FCH_4 with untransformed plot axes. Higher Spearman correlation coefficients (ρ) indicate stronger agreement between EC FCH_4 and chamber FCH_4. In a) and b) the points for half-hourly (n=74482) and hourly (n=40072) aggregations are shown in hexagonal density clouds with a log-transformed color range to highlight trends in high point density areas (colors represent number of observations per hexagon). For daily (c), weekly (d), monthly (e), and annual (f) aggregations, sample sizes were n = 1879, 349, 121, and 22, respectively. The dashed line represents 1:1 line.

https://doi.org/10.5194/egusphere-2025-5023
Preprint. Discussion started: 27 October 2025

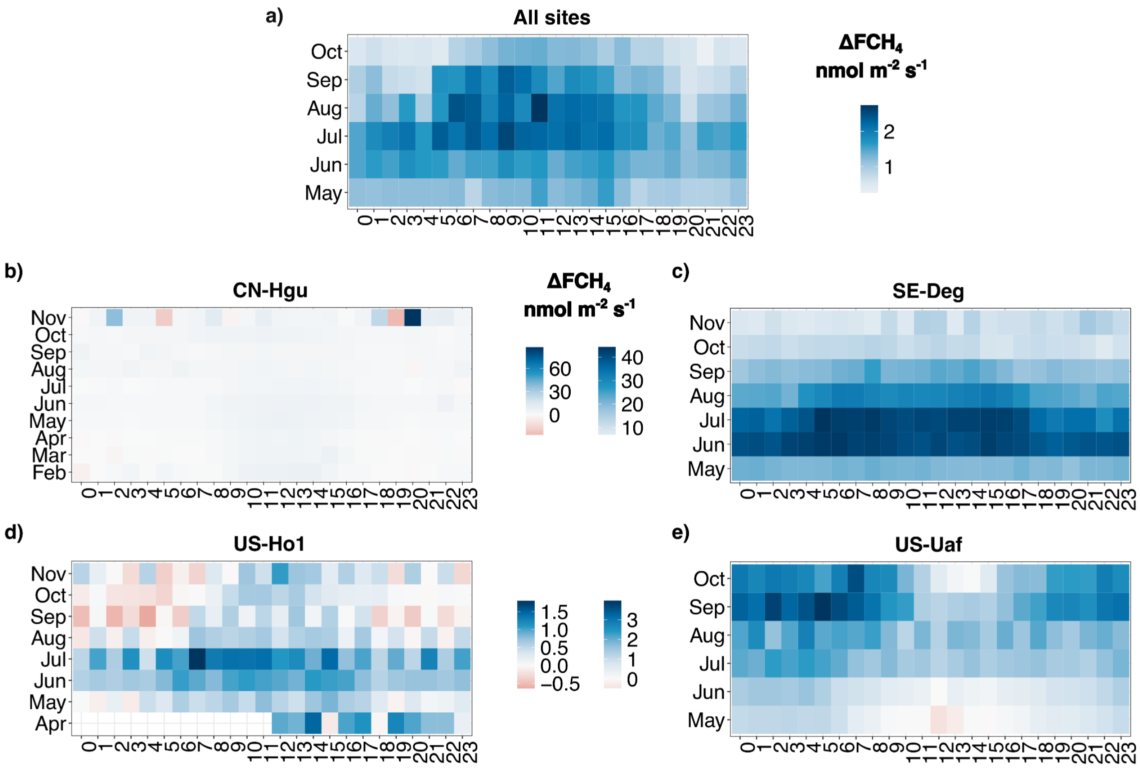

795

Figure B4. Heatmaps of hourly median ΔFCH_4 across months in the half-hourly aggregation. Positive ΔFCH_4 (blue) represents higher EC FCH_4 than chamber FCH_4, and negative (red) higher chamber FCH_4 than EC FCH_4. X axis represents hours of day (24 h) and y axis months. a) Data set containing all sites (n=4 sites). Only months which were included in all sites are shown (May-October). b) CN-Hgu (all months), c) SE-Deg (all months), d) US-Ho1 (all months), e) US-Uaf (all months).

800

https://doi.org/10.5194/egusphere-2025-5023
Preprint. Discussion started: 27 October 2025

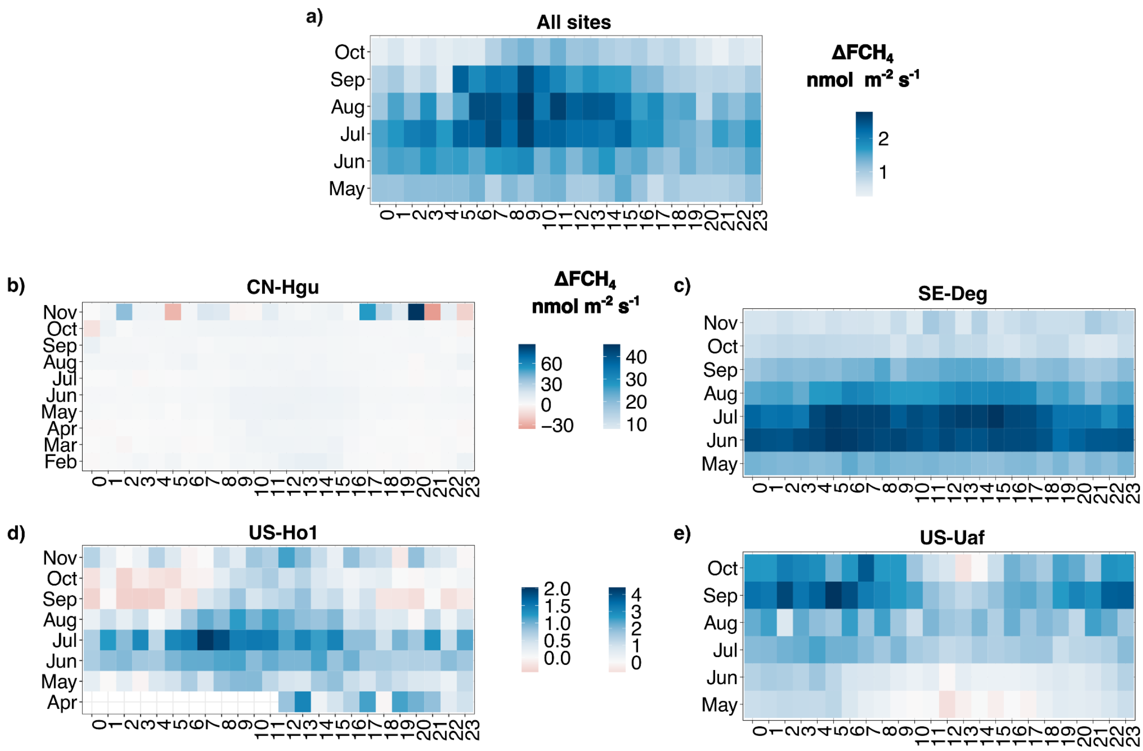

Figure B5. Heatmaps of hourly median ΔFCH4 across months in the hourly aggregation. Positive ΔFCH4 (blue) represents higher EC FCH4 than chamber FCH4, and negative (red) higher chamber FCH4 than EC FCH4. X axis represents hours of day (24 h) and y axis months. a) Data set containing all sites (n=4 sites). Only months which were included in all sites are shown
805 (May-October). b) CN-Hgu (all months), c) SE-Deg (all months), d) US-Ho1 (all months), e) US-Uaf (all months).

https://doi.org/10.5194/egusphere-2025-5023
Preprint. Discussion started: 27 October 2025

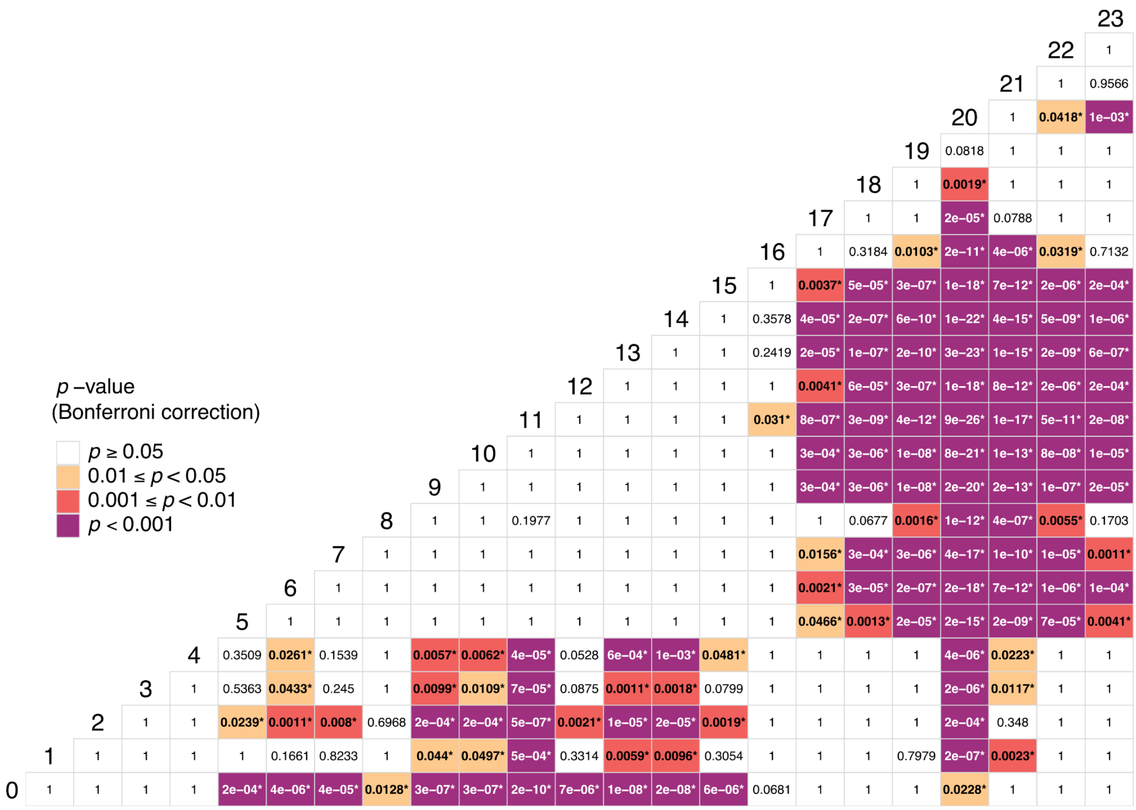

Figure B6. Significance levels (Bonferroni-adjusted p-values) of Conover-Iman multiple pairwise comparisons in ΔFCH_4 in the half-hourly aggregation containing sites with automated chamber measurements (n=4 sites). Numbers on the diagonal line are labels for the hourly bins, starting from 0-1 and ending in 23-24. Different colors represent the Bonferroni-adjusted p-values, with reference to an overall significance threshold of $\alpha = 0.05$. Numbers inside the tiles are Bonferroni-adjusted p-values of the pairwise comparisons at four decimal places. Values in bold and asterisk (*) represent p-values that remain significant after Bonferroni correction.

https://doi.org/10.5194/egusphere-2025-5023
Preprint. Discussion started: 27 October 2025

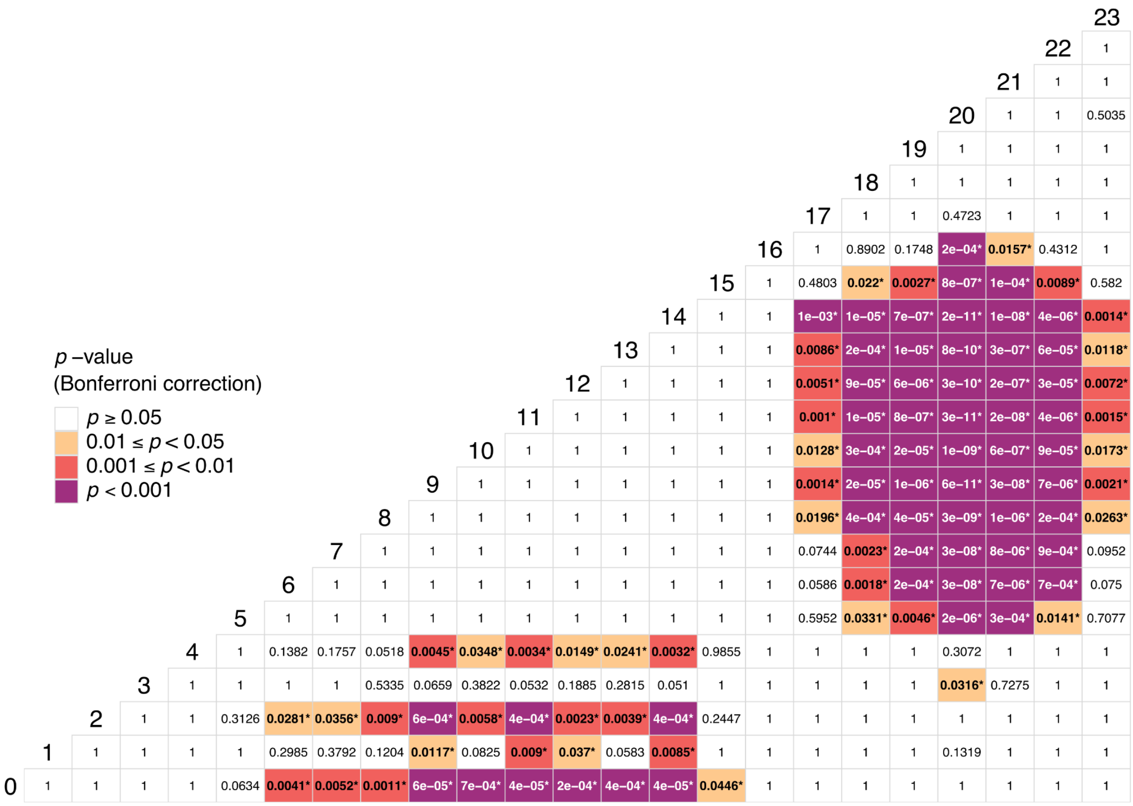

Figure B7. Significance levels (Bonferroni-adjusted *p*-values) of Conover-Iman multiple pairwise comparisons in ΔFCH_4 in the hourly aggregation containing sites with automated chamber measurements (n=4 sites). Numbers on the diagonal line are labels for the hourly bins, starting from 0-1 and ending in 23-24. Different colors represent the Bonferroni-adjusted *p*-values, with reference to an overall significance threshold of $\alpha = 0.05$. Numbers inside the tiles are Bonferroni-adjusted *p*-values of the pairwise comparisons at four decimal places. Values in bold and asterisk (*) represent *p*-values that remain significant after Bonferroni correction.

https://doi.org/10.5194/egusphere-2025-5023
Preprint. Discussion started: 27 October 2025

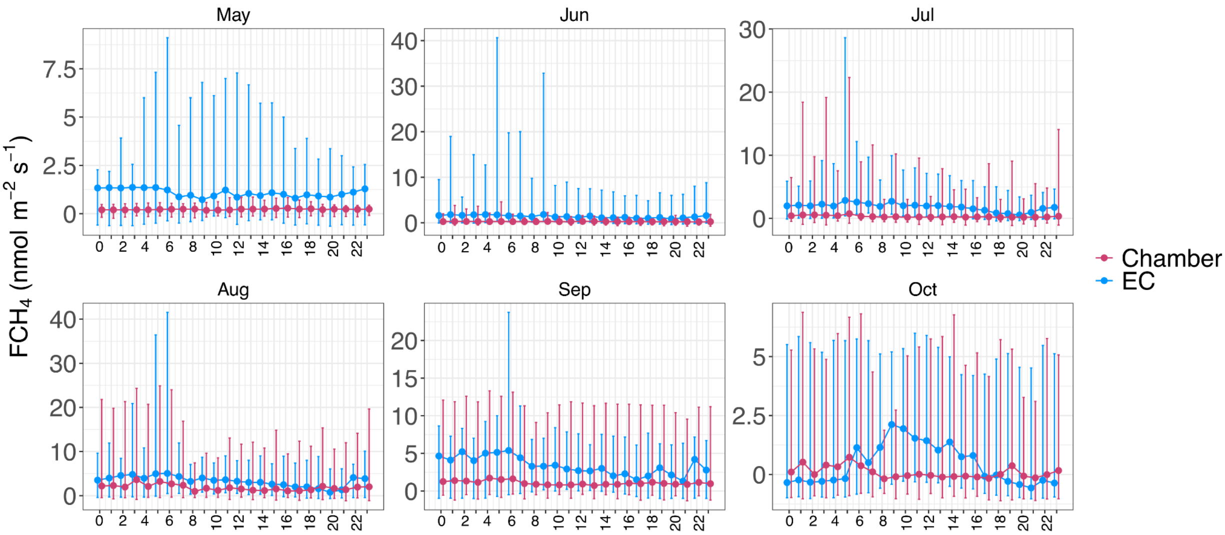

825 **Figure B8.** Hourly median chamber (red) and EC FCH4 (blue) per month in the half-hourly data set. Variation around the median is represented by the interquartile range (between 25% and 75%). Only months containing all sites (n=4) with automated chamber measurements are shown.

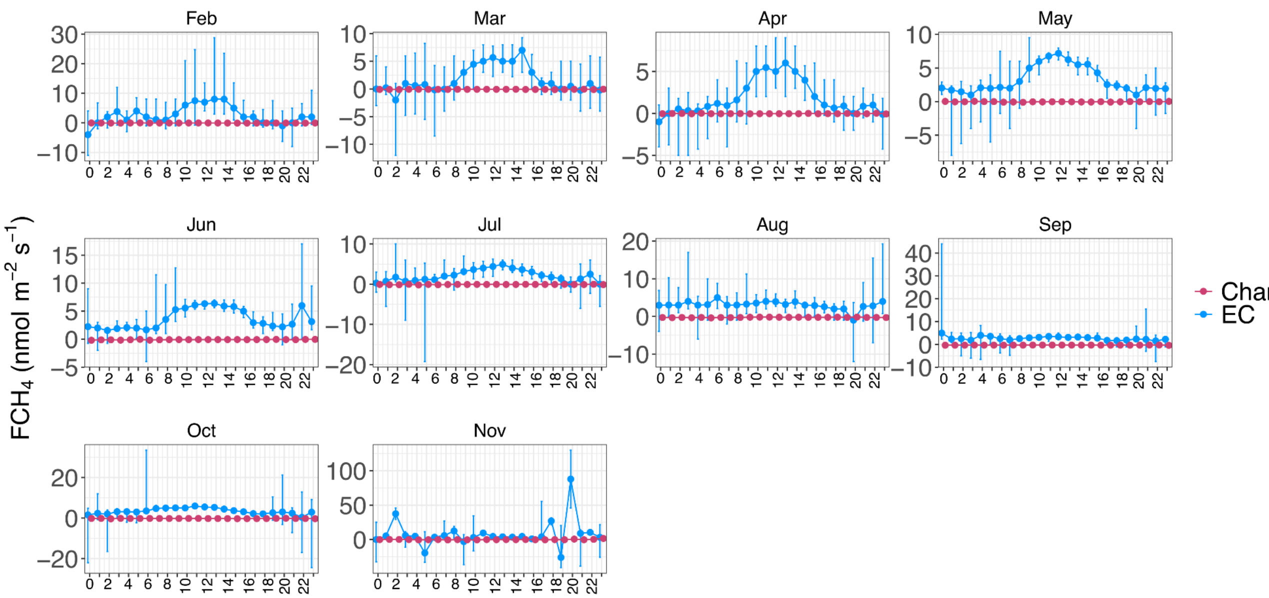

830 **Figure B9.** Hourly median chamber (red) and EC FCH4 (blue) per month at CN-Hgu in the half-hourly dataset. Variation around the median is represented by the interquartile range (between 25% and 75%).

https://doi.org/10.5194/egusphere-2025-5023
Preprint. Discussion started: 27 October 2025

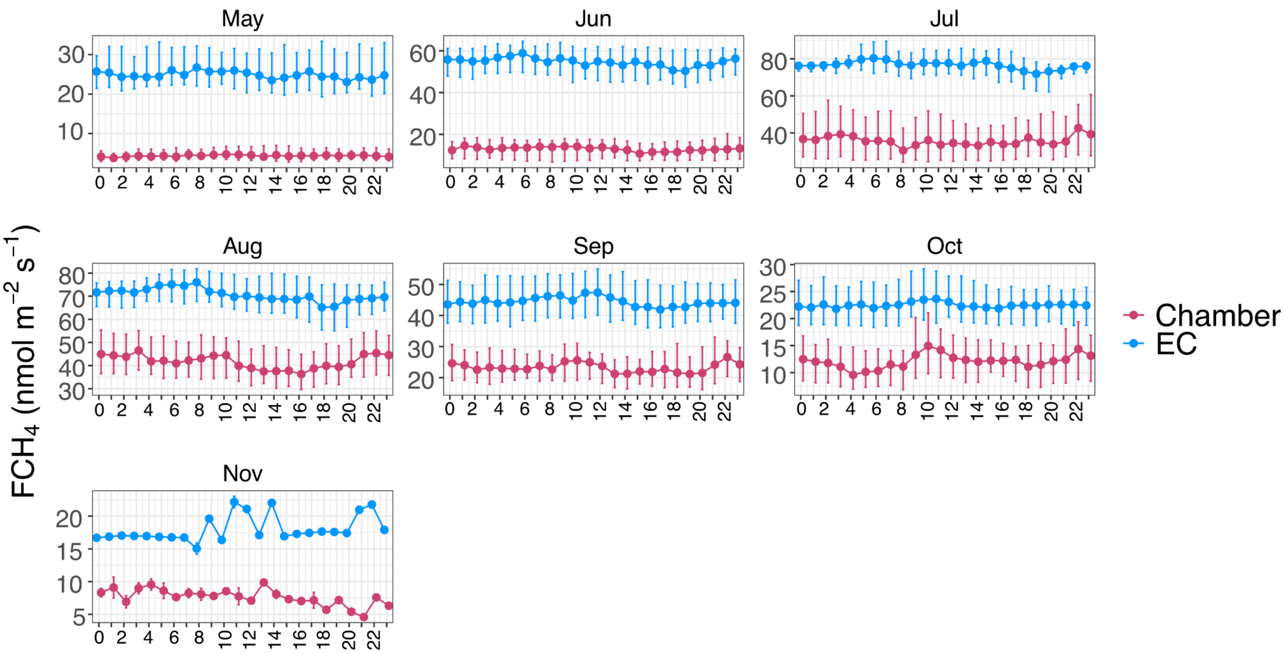

Figure B10. Hourly median chamber (red) and EC FCH4 (blue) per month at SE-Deg in the half-hourly dataset. Variation around the median is represented by the interquartile range (between 25% and 75%).

835

https://doi.org/10.5194/egusphere-2025-5023
Preprint. Discussion started: 27 October 2025

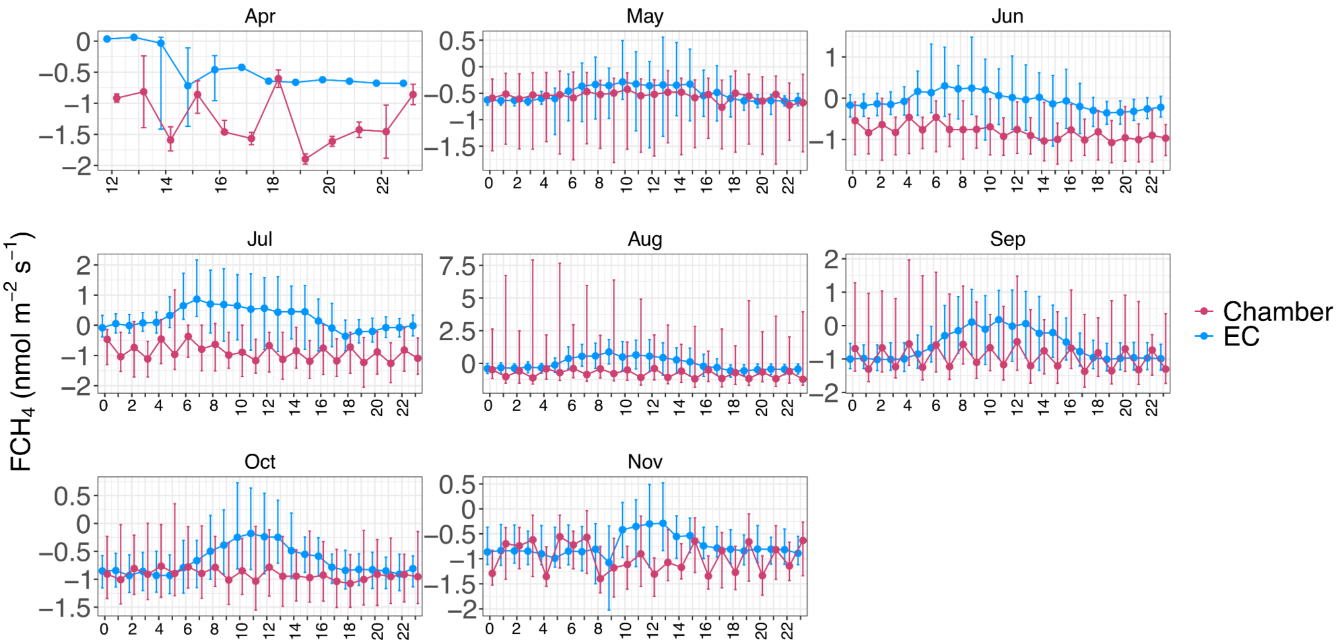

Figure B11. Hourly median chamber (red) and EC FCH_4 (blue) per month at US-Ho1 in the half-hourly dataset. Variation around the median is represented by the interquartile range (between 25% and 75%).

840

https://doi.org/10.5194/egusphere-2025-5023
Preprint. Discussion started: 27 October 2025

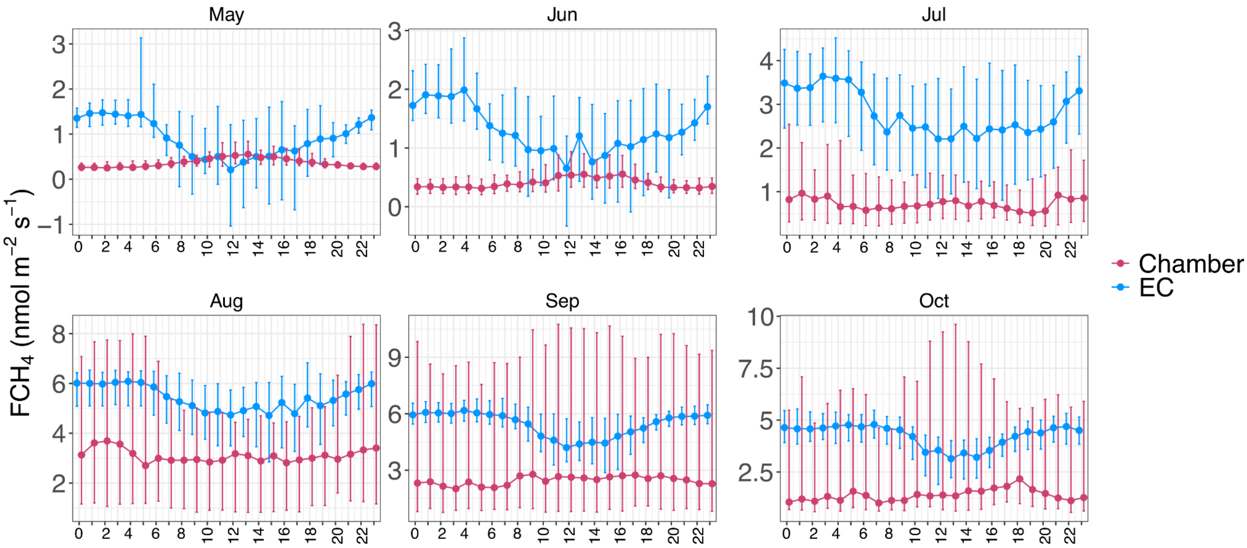

845 **Figure B12.** Hourly median chamber (red) and EC FCH_4 (blue) per month at US-Uaf in the half-hourly dataset. Variation around the median is represented by the interquartile range (between 25% and 75%).

https://doi.org/10.5194/egusphere-2025-5023
Preprint. Discussion started: 27 October 2025

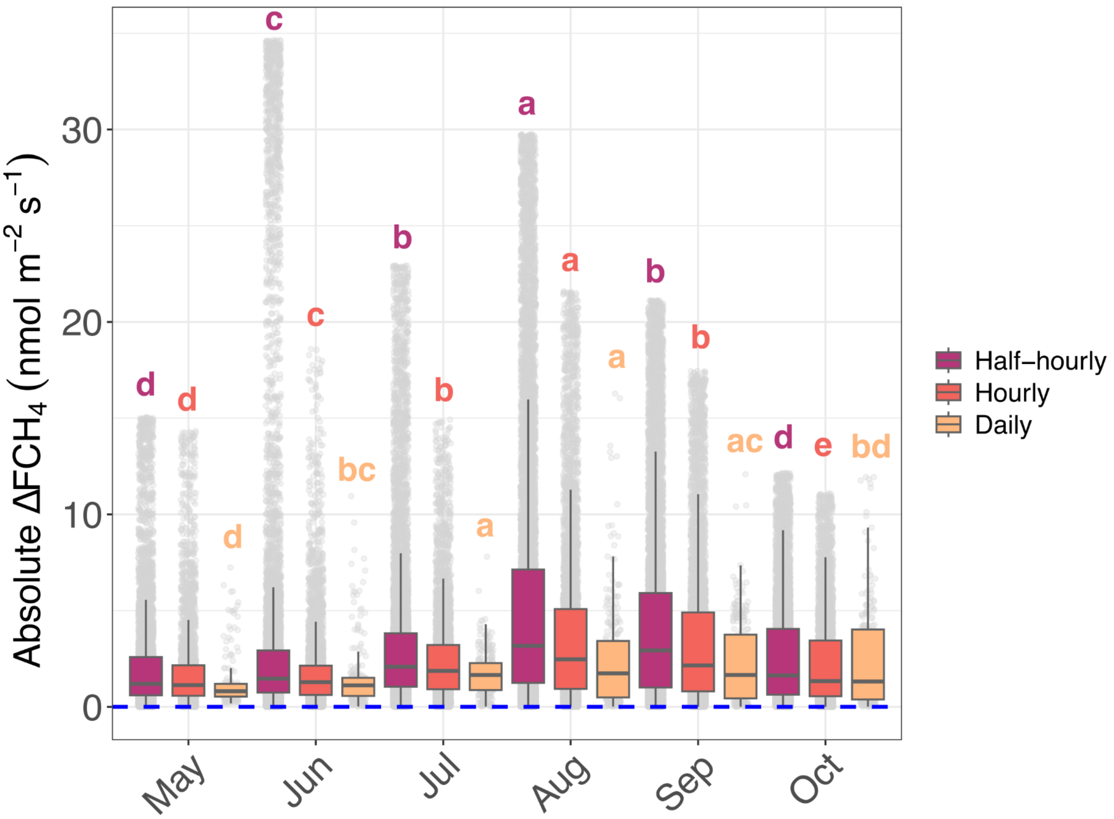

Figure B13. Absolute EC-chamber FCH4 differences (ΔFCH4) between months in half-hourly, hourly and daily aggregations. Different colors represent different temporal aggregations and gray points show the underlying data. For visualization, we filtered out data points 1.5 x IQR below the first quartile and 1.5 x IQR above the third quartile but statistics were based on the original data. The letters indicate whether ΔFCH4 differs significantly between months: months that share at least one shared letter are not significantly different (*p*>0.05) while months with different letters differ significantly (*p*≤0.05). Pairwise comparisons were conducted with the Conover-Iman post hoc test. While there was data in other months, the May-October period was chosen for this figure due to these months including either all (n=4; half-hourly and hourly aggregations) or almost all sites (n=7 or 8 sites; daily aggregation). Weekly and monthly aggregations did not have significant ΔFCH4 differences between months (Kruskal-Wallis *p*>0.05) and are not shown in this figure.

https://doi.org/10.5194/egusphere-2025-5023
Preprint. Discussion started: 27 October 2025

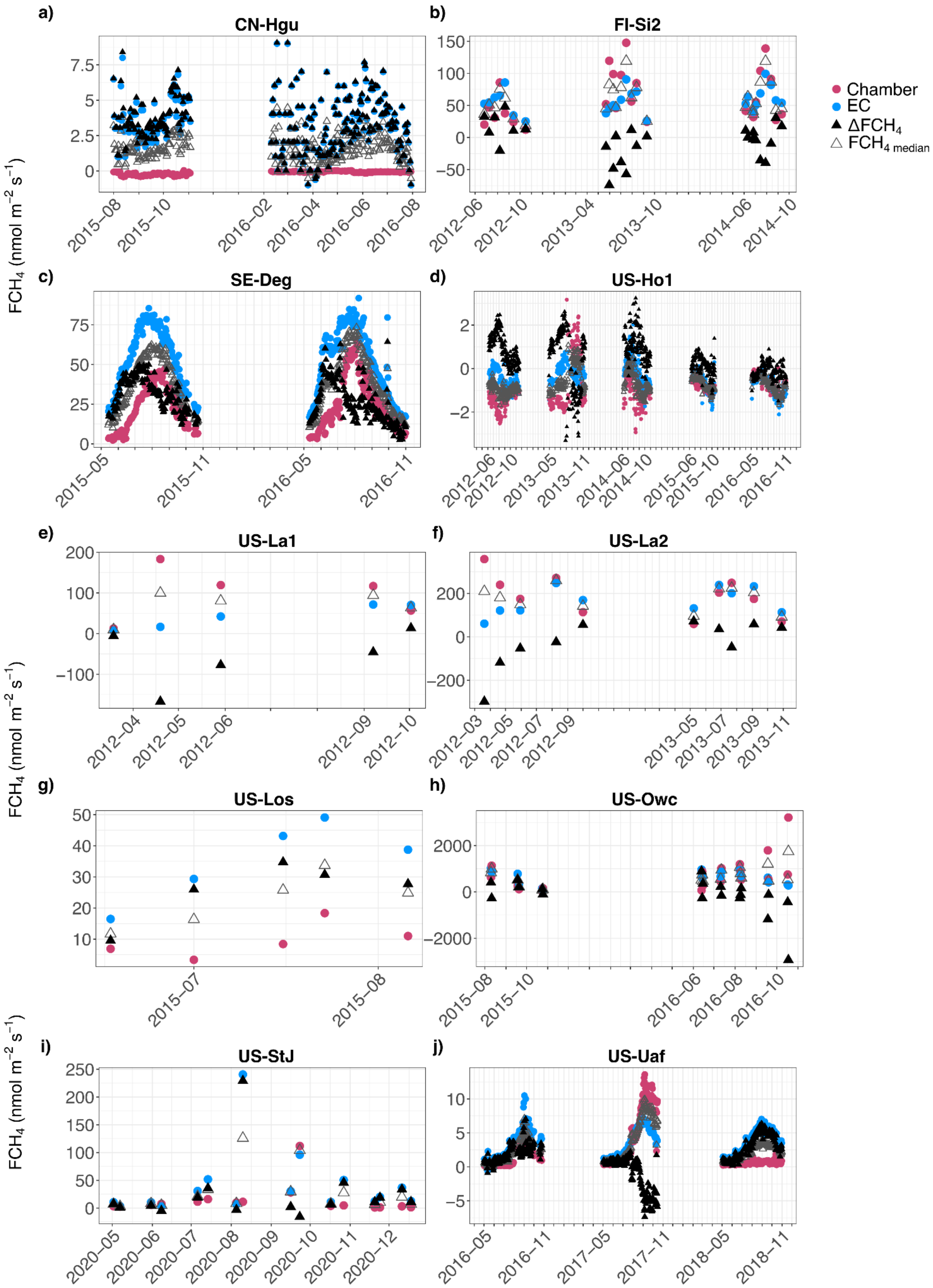

https://doi.org/10.5194/egusphere-2025-5023
Preprint. Discussion started: 27 October 2025

Figure B14. Site-specific trends in daily EC and chamber FCH_4, EC-chamber median FCH_4 ($\Delta FCH_{4\ median}$), and EC-chamber difference (ΔFCH_4) (a to j). Red circles represent chamber and blue EC FCH_4 measurements. Black triangle is ΔFCH_4 and the hollow light gray triangle is $\Delta FCH_{4\ median}$. In d) 46 outlier points from 2013 were removed to improve visualization (see US-Ho1 with outliers in Fig. S10). Negative ΔFCH_4 indicates higher chamber FCH_4 than EC FCH_4, and positive higher EC FCH_4 than chamber FCH_4.

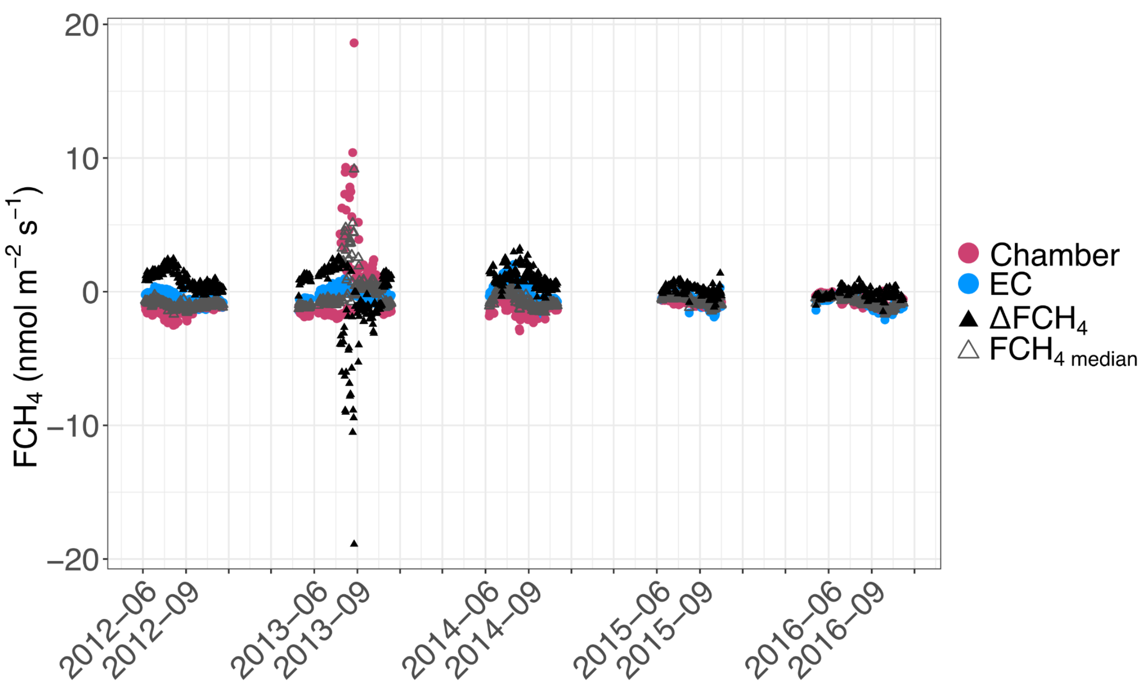

Figure B15. US-Ho1: trends in daily EC and chamber FCH_4, EC-chamber median FCH_4 ($\Delta FCH_{4\ median}$), and EC-chamber difference (ΔFCH_4), with 46 outliers in 2013. Red circles represent chamber and blue EC FCH_4 measurements. Black triangle is ΔFCH_4 and the hollow light gray triangle is $\Delta FCH_{4\ median}$. Negative ΔFCH_4 indicates higher chamber FCH_4 than EC FCH_4, and positive higher EC FCH_4 than chamber FCH_4.

https://doi.org/10.5194/egusphere-2025-5023
Preprint. Discussion started: 27 October 2025

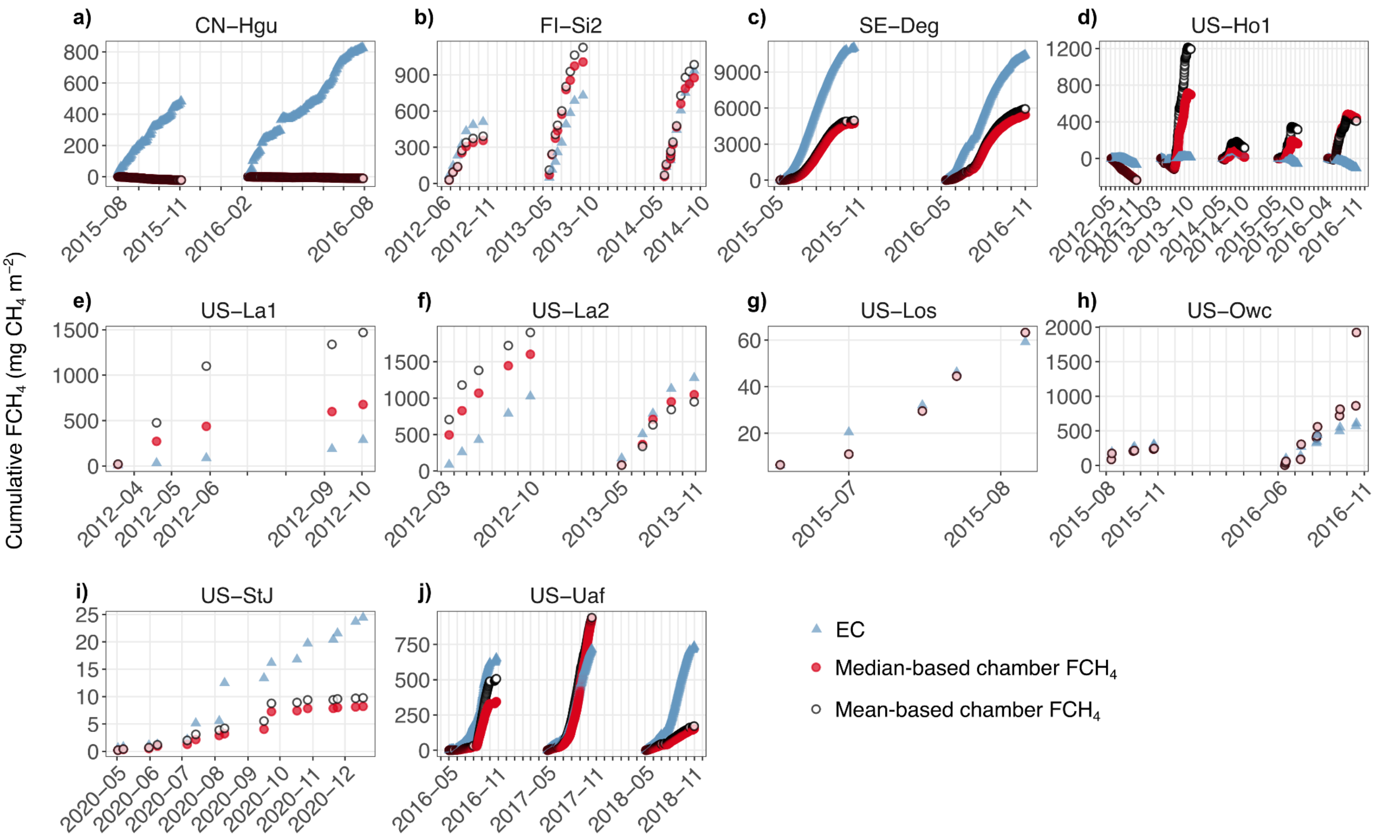

Figure B16. Cumulative sums of ecosystem-scale (EC) and plot-scale (chamber) FCH4 at the daily scale across sites (a-j). Blue triangles represent EC, red points chamber FCH4 calculated from the median-based aggregation, and white points chamber FCH4 calculated from the mean-based aggregation. Note that since the chamber FCH4 data at FI-Si2, US-La1, and US-La2 lacked hourly timestamps, we roughly estimated daily cumulative FCH4 by using the daily chamber FCH4 median or mean for all 24 hours of the measurement date (EC cumulative FCH4 was calculated based on daily half-hourly FCH4 from FLUXNET-CH4), and these estimates should thus be interpreted with caution.

https://doi.org/10.5194/egusphere-2025-5023
Preprint. Discussion started: 27 October 2025

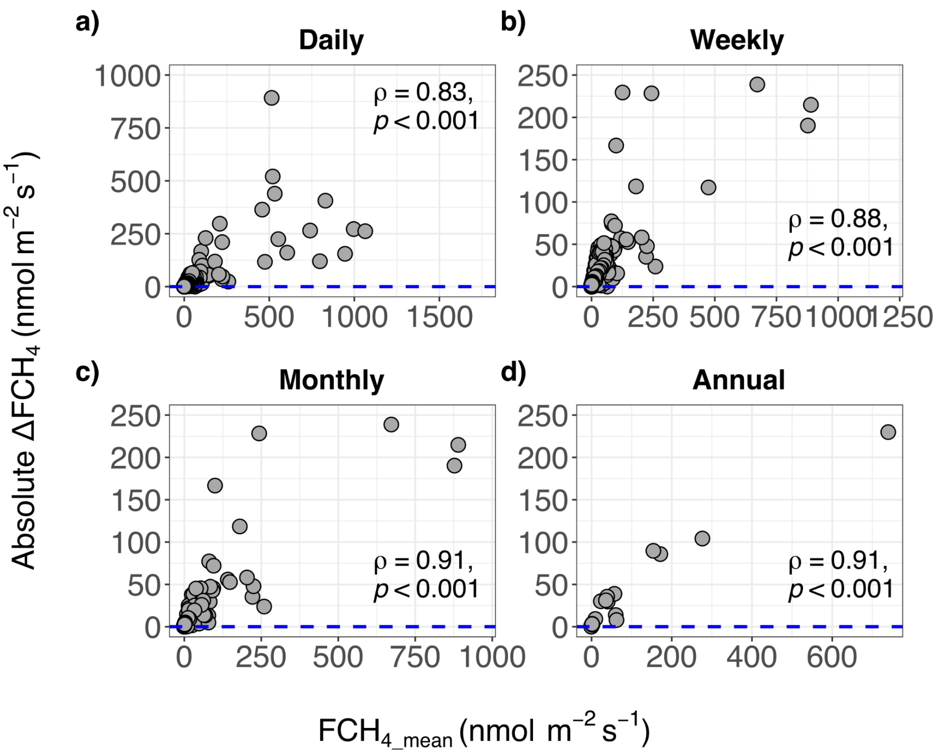

895 **Figure B17.** The relationship between FCH_4 magnitude and absolute ΔFCH_4 with outliers in daily (a), weekly (b), monthly (c) and annual (d) scales. FCH_{4_mean} is the row-wise mean of EC FCH_4 and chamber FCH_4, and EC-chamber FCH_4 difference (ΔFCH_4) was calculated by subtracting chamber FCH_4 from EC FCH_4. Positive ΔFCH_4 indicates higher EC FCH_4 than chamber FCH_4 and negative values higher chamber FCH_4 than EC FCH_4. The blue dashed line represents the line of equality where EC FCH_4 and chamber FCH_4 are equal. ρ represents Spearman correlation coefficient, followed by its statistical significance ($\alpha = 0.05$). Higher ρ represents stronger deviation from the line of equality, i.e. $\Delta FCH_4=0$ while perfect agreement between chamber and EC FCH_4 would result in ρ=0.

https://doi.org/10.5194/egusphere-2025-5023
Preprint. Discussion started: 27 October 2025

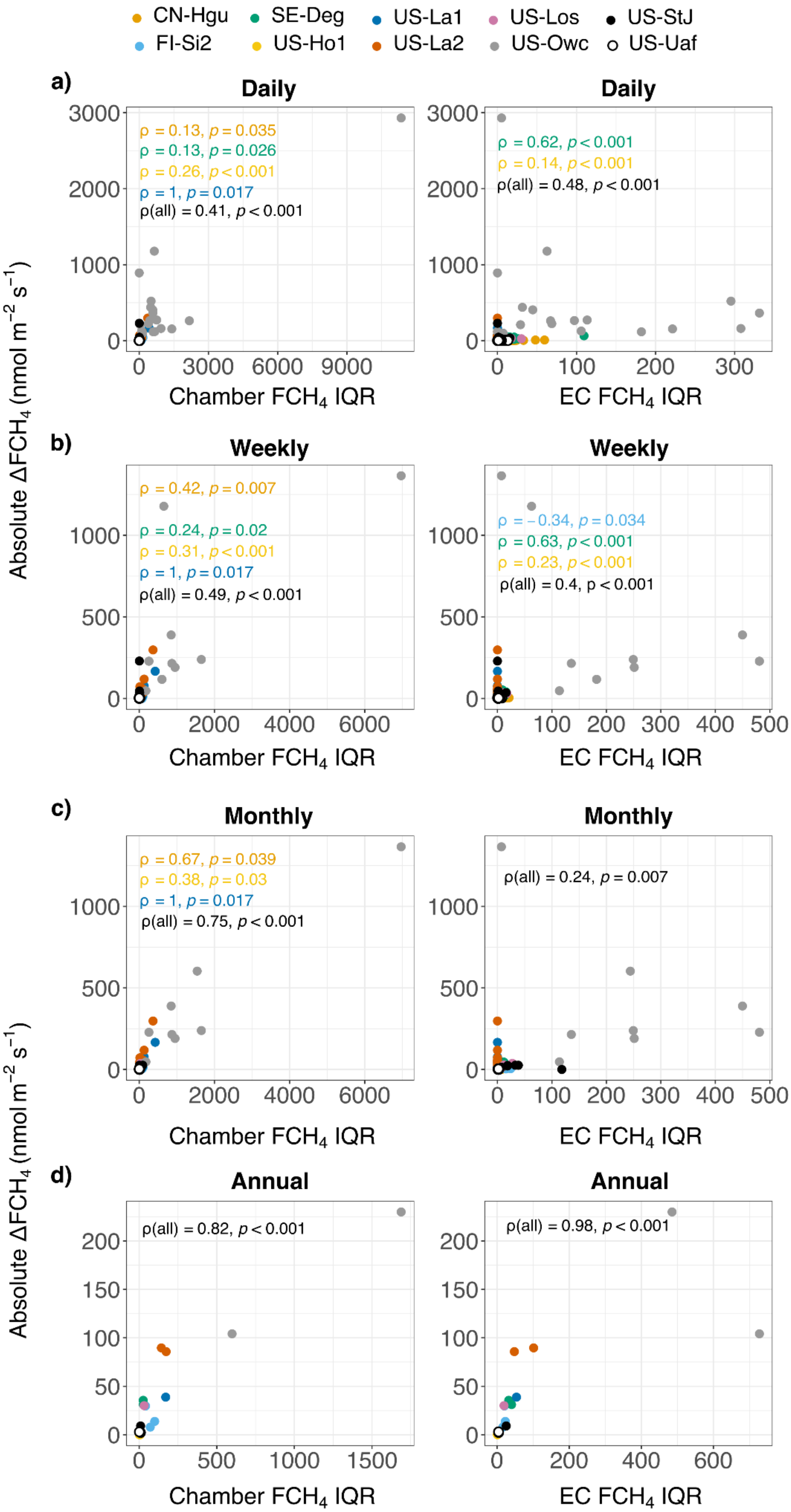

https://doi.org/10.5194/egusphere-2025-5023
Preprint. Discussion started: 27 October 2025

Figure B18. Untransformed absolute ΔFCH_4, chamber and EC FCH_4 IQR in daily (a), weekly (b), monthly (c), and annual (d) aggregations. Different colors represent individual sites. Plots in the left panel show the relationship between daily variation in FCH_4 between individual chambers within each site and site-level absolute ΔFCH_4. The right side panel shows the same but with daily variation in EC FCH_4. The strength and general direction of the relationship was measured with Spearman correlation coefficient (ρ). "ρ(all)" refers to the Spearman correlation for the whole dataset.

https://doi.org/10.5194/egusphere-2025-5023
Preprint. Discussion started: 27 October 2025

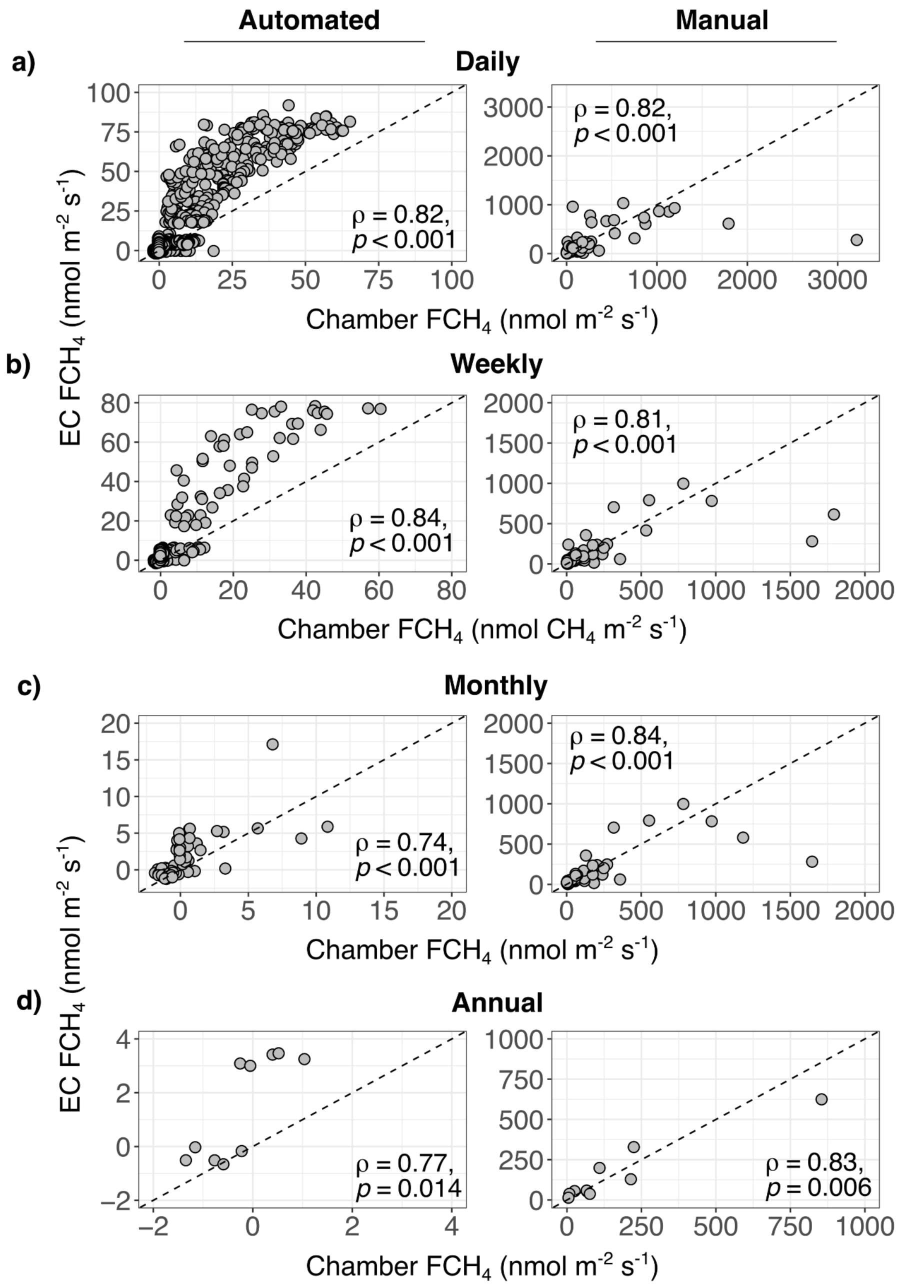

Figure B19. Automated (left panel) and manual (right panel) chamber FCH_4 had strong positive relationships with EC FCH_4 across sites and temporal scales (a to d). The dashed line represents the 1:1 line, and ρ Spearman correlation coefficient of the relationship. Automated chambers were included in four sites (CN-Hgu, SE-Deg, US-Ho1, and US-Uaf) and manual chambers in six sites (FI-Si2, US-La1, US-La2, US-Los, US-Owc, and US-StJ). Half-hourly and hourly plots are in Fig. 3. Note different x and y axis scales.

https://doi.org/10.5194/egusphere-2025-5023
Preprint. Discussion started: 27 October 2025

Appendix C: Supplementary tables (Tables C1-C14)

Table C1. Methodological and data details of the site chamber (CH) and eddy covariance (EC) measurement systems. “CH method” refers to whether the chambers are manual or automated, and whether chambers were dark or transparent to sunlight. CH meas. frequency = chamber measurement frequency. CH-EC overlap is the total duration of overlap between chamber and EC measurements in days (note: the measurements are spread out over different seasons and years; see S3). Gap-filled EC is the percentage of ANN-gap-filled EC FCH_4 values of all EC FCH_4 values per site (in the unaggregated data set). Further details of the CH and EC measurement systems can be found in the corresponding references. Abbreviations in “CH analyzer”: LI-COR = LI-COR Biosciences, Nebraska, USA; Picarro = Picarro Inc., Santa Clara, CA, USA; Los Gatos = Los Gatos Research Inc., San Jose, CA, USA; Aerodyne = TILDAS CS, Aerodyne Research Inc., Billerica, MA, USA; Varian = Varian, Inc., Palo Alto, CA, USA; Shimadzu = Shimadzu Scientific Instruments, Kyoto, Japan.

https://doi.org/10.5194/egusphere-2025-5023
Preprint. Discussion started: 27 October 2025

FLUXNET-CH$_4$ ID	Location (lat, lon)	CH method	CH analyzer	EC analyzer	EC tower height (m)	No. of CH	CH meas. frequency	EC-CH start, end year	EC-CH overlap days	Gap-filled EC (%)	CH data ref.	EC data ref.
CN-Hgu	32.845278, 102.59	automated, dark	near infrared laser gas analyzer (model 915-0011, Los Gatos)	open-path infrared gas analyzer (LI-7700; LI-COR)	3	3	56 min	2015, 2016	363	44	Wang et al. (2021)	Niu and Chen (2020)
FI-Si2	61.8372, 24.1967	manual, dark	gas chromatograph (Agilent Technologies 7890A) and liquid handler (Gilson GX-271)	open-path gas analyzer (LI-7700, LI-COR)	2.4	18	1-3 x month	2012, 2014	26	5	Korrensalo et al. (2018)	Alekseychik et al. (2021), Vesala et al. (2020)
SE-Deg	64.182029, 19.556539	automated, dark and transparent	cavity ring-down spectrometer (model GGA-24EP, Los Gatos)	Closed-path gas analyzer (Model 911-0011-0004, Los Gatos)	3	4	1 hour	2015, 2016	338	31	Bond-Lamberty et al. (2020), Järveoja et al. (2018)	Nilsson and Peichl (2020)
US-Ho1	45.2041, -68.7402	automated, dark	cavity ring-down spectrometer (model G2121-i; Picarro) & Aerodyne Quantum Cascade Laser (Aerodyne)	Closed-path gas analyzer (model G2311-f, Picarro cavity ring-down spectrometer)	31	20	ca. 1 hour (varied between years and chambers)	2012, 2016	759	52	Richardson et al. (2019)	Richardson and Hollinger (2020)
US-La1	29.5013, -90.4449	manual, dark	gas chromatograph (model CP-3800, Varian)	open-path gas analyzer (LI-7700, LI-COR)	3.4	3	1 x month	2012, 2012	5	0	Krauss et al. (2016)	Holm et al. (2020a)

https://doi.org/10.5194/egusphere-2025-5023
Preprint. Discussion started: 27 October 2025

US-La2	29.8587, -90.2869	manual, dark	gas chromatograph (model CP-3800, Varian)	open -path gas analyzer (LI-7700, LI-COR)	3.6	3	1 x month	2012, 2013	10	10	Krauss et al. (2016)	Holm et al. (2020b)
US-Los	46.0827, -89.9792	manual, dark	near-infrared laser gas analyzer (Los Gatos UGGA)	open-path gas analyzer (LI-7700, LI-COR)	10.2	14	1-3 x month	2015, 2015	5	31	Desai (2025b)	Desai (2025a), Desai and Thom (2020)
US-Owc	41.37951667, -82.5124667	manual, dark	gas chromatograph (GC-2014, Shimadzu)	open-path gas analyzer (LI-7700, LI-COR)	2.7	4	1 x month	2015, 2016	18	50	Bohrer et al. (2019)	Bohrer et al. (2020)
US-StJ	39.08821106, -75.43722534	manual, dark	near-infrared laser gas analyzer (Los Gatos)	open-path gas analyzer (LI-7700, LI-COR)	3.5	5	1-2 x month	2020	16	0	Hill and Vargas (2022)	Vargas (2018)
US-Uaf	64.86627, -147.85553	automated, dark	near-infrared laser gas analyzer (Los Gatos)	closed-path gas analyzer (RMT200 Fast Methane Analyzer or Greenhouse Gas Analyzer, Los Gatos)	6	5	30 min	2016, 2018	458	59	Ueyama et al. (2022)	Iwata et al. (2020)

https://doi.org/10.5194/egusphere-2025-5023
Preprint. Discussion started: 27 October 2025

Table C2. Details of the used environmental data. FLUXNET-CH_4 soil temperature data was from the topmost soil depths (2-10 cm below soil surface). Abbreviations: NEE = net ecosystem exchange, u* = friction velocity, WD = wind direction, WS = wind speed, VPD = vapor pressure deficit, PA = air pressure, WTL = water table level, TS = soil temperature, ANN = artificial neural network, MDS = marginal distribution sampling.

Site	Environmental variable	Data	Data reference
CN-Hgu	NEE	Half-hourly FLUXNET-CH_4: ANN-gap-filled	Delwiche et al. (2021); Knox et al. (2019)
	u*	Half-hourly FLUXNET-CH_4: ANN-gap-filled	
	WD	Half-hourly FLUXNET-CH_4: ANN-gap-filled	
	WS	Half-hourly FLUXNET-CH_4: gap-filled	
	VPD	Half-hourly FLUXNET-CH_4: gap-filled	
	PA	Half-hourly FLUXNET-CH_4: gap-filled	
	WTL	-	-
	TS	Half-hourly FLUXNET-CH_4	Delwiche et al. (2021); Knox et al. (2019)
FI-Si2	NEE	Half-hourly FLUXNET-CH_4: ANN-gap-filled	Delwiche et al. (2021); Knox et al. (2019)
	u*	Half-hourly FLUXNET-CH_4: ANN-gap-filled	
	WD	Half-hourly FLUXNET-CH_4: ANN-gap-filled	
	WS	Half-hourly FLUXNET-CH_4: gap-filled	
	VPD	Half-hourly FLUXNET-CH_4: gap-filled	

https://doi.org/10.5194/egusphere-2025-5023
Preprint. Discussion started: 27 October 2025

	PA	Half-hourly FLUXNET-CH_4: gap-filled	
	WTL	Mean of daily gap-filled FLUXNET-CH_4 WTL and chamber-associated WTL	Delwiche et al. (2021); Knox et al. (2019), Korrensalo et al. (2018)
	TS	Chamber-associated TS	Korrensalo et al. (2018)
SE-Deg	NEE	Half-hourly FLUXNET-CH_4: ANN-gap-filled	Delwiche et al. (2021); Knox et al. (2019)
	u*	Half-hourly FLUXNET-CH_4: ANN-gap-filled	
	WD	Half-hourly FLUXNET-CH_4: ANN-gap-filled	
	WS	Half-hourly FLUXNET-CH_4: gap-filled	
	VPD	Half-hourly FLUXNET-CH_4: gap-filled	
	PA	Half-hourly FLUXNET-CH_4: gap-filled	
	WTL	Mean of half-hourly gap-filled FLUXNET-CH_4 WTL and chamber-associated WTL	Delwiche et al. (2021); Knox et al. (2019); Järveoja et al. (2018); Bond-Lamberty et al. (2020)
	TS	Mean of half-hourly FLUXNET-CH_4 TS and chamber-associated TS	
US-Ho1	NEE	Half-hourly FLUXNET-CH_4: ANN-gap-filled	Delwiche et al. (2021); Knox et al. (2019)
	u*	Half-hourly FLUXNET-CH_4: ANN-gap-filled	
	WD	Half-hourly FLUXNET-CH_4: ANN-gap-filled	
	WS	Half-hourly FLUXNET-CH_4: gap-filled	
	VPD	Half-hourly FLUXNET-CH_4: gap-	

https://doi.org/10.5194/egusphere-2025-5023
Preprint. Discussion started: 27 October 2025

		filled	
	PA	Half-hourly FLUXNET-CH_4: gap-filled	
	WTL	Half-hourly FLUXNET-CH_4: gap-filled	
	TS	Chamber-associated TS	Richardson et al. (2019)
US-La1 & US-La2	NEE	Half-hourly FLUXNET-CH_4: ANN-gap-filled	Delwiche et al. (2021); Knox et al. (2019)
	u*	Half-hourly FLUXNET-CH_4: ANN-gap-filled	
	WD	Half-hourly FLUXNET-CH_4: ANN-gap-filled	
	WS	Half-hourly FLUXNET-CH_4: gap-filled	
	VPD	Half-hourly FLUXNET-CH_4: gap-filled	
	PA	Half-hourly FLUXNET-CH_4: gap-filled	
	WTL	Mean of daily FLUXNET-CH_4 WTL and chamber-associated WTL	Delwiche et al. (2021); Knox et al. (2019); Krauss et al. (2016)
	TS	Mean of daily gap-filled FLUXNET-CH_4 TS and chamber-associated TS	
US-Los	NEE	Half-hourly FLUXNET-CH_4: ANN-gap-filled	Delwiche et al. (2021); Knox et al. (2019)
	u*	Half-hourly FLUXNET-CH_4: ANN-gap-filled	
	WD	Half-hourly FLUXNET-CH_4: ANN-gap-filled	
	WS	Half-hourly FLUXNET-CH_4: gap-filled	
	VPD	Half-hourly FLUXNET-CH_4: gap-	

https://doi.org/10.5194/egusphere-2025-5023
Preprint. Discussion started: 27 October 2025

		filled	
	PA	Half-hourly FLUXNET-CH_4: gap-filled	Delwiche et al. (2021); Knox et al. (2019); Pugh et al. (2018)
	WTL	Mean of half-hourly gap-filled FLUXNET-CH_4 WTL and chamber-associated WTL	
	TS	Mean of half-hourly FLUXNET-CH_4 TS and chamber-associated TS	
US-Owc	NEE	Half-hourly FLUXNET-CH_4: ANN-gap-filled	Delwiche et al. (2021); Knox et al. (2019)
	u*	Half-hourly FLUXNET-CH_4: ANN-gap-filled	
	WD	Half-hourly FLUXNET-CH_4: ANN-gap-filled	
	WS	Half-hourly FLUXNET-CH_4: gap-filled	
	VPD	Half-hourly FLUXNET-CH_4: gap-filled	
	PA	Half-hourly FLUXNET-CH_4: gap-filled	
	WTL	Mean of half-hourly gap-filled FLUXNET-CH_4 WTL and chamber-associated WTL	Delwiche et al. (2021); Knox et al. (2019); Bohrer et al. (2019)
	TS	Half-hourly FLUXNET-CH_4 TS	Delwiche et al. (2021); Knox et al. (2019)
US-StJ	NEE	Half-hourly: MDS-gap-filled	Hill and Vargas (2022); Vargas (2018)
	u*	Half-hourly: not gap-filled	
	WD	Half-hourly: not gap-filled	

https://doi.org/10.5194/egusphere-2025-5023
Preprint. Discussion started: 27 October 2025

	WS	Half-hourly: not gap-filled	
	VPD	Half-hourly: not gap-filled	
	PA	Half-hourly: not gap-filled	
	WTL	Half-hourly: gap-filled with a linear relationship with NOAA water table level	
	TS	Half-hourly: gap-filled with a linear relationship with water temperature	
US-Uaf	NEE	Half-hourly FLUXNET-CH_4: ANN-gap-filled	Delwiche et al. (2021); Knox et al. (2019)
	u*	Half-hourly FLUXNET-CH_4: ANN-gap-filled	
	WD	Half-hourly FLUXNET-CH_4: ANN-gap-filled	
	WS	Half-hourly FLUXNET-CH_4: gap-filled	
	VPD	Half-hourly FLUXNET-CH_4: gap-filled	
	PA	Half-hourly FLUXNET-CH_4: gap-filled	
	WTL	Mean of half-hourly gap-filled FLUXNET-CH_4 WTL and chamber-associated WTL	Delwiche et al. (2021); Knox et al. (2019); Ueyama et al. (2023)
	TS	Mean of half-hourly FLUXNET-CH_4 TS and chamber-associated TS	

940

https://doi.org/10.5194/egusphere-2025-5023
Preprint. Discussion started: 27 October 2025

Table C3. Descriptive statistics and Wilcoxon-Mann-Whitney test results based on temporal aggregations from chamber and EC FCH_4 means instead of medians. Proportions of annual chamber and EC CH_4 emission (i.e., $FCH_4 \leq 0$ excluded) above the 90th percentile (p90) are reported to highlight the contribution of high CH_4 emission values to FCH_4. Abbreviations: IQR = interquartile range, SD = standard deviation, CV = coefficient of variation (%), EC = eddy covariance.

Data set	ΔFCH_4 median (IQR), *nmol m⁻² s⁻¹*	ΔFCH_4 mean (SD), *nmol m⁻² s⁻¹*	ΔFCH_4 CV (%)	Wilcoxon-Mann-Whitney test	Chamber FCH_4 p90 (% of total FCH_4)	EC FCH_4 p90 (% of total FCH_4)
Half-hourly	1.23 (5.74)	4.84 (18.56)	206	$p<0.001$ ($n_{EC}=74482$, $n_{CH}=74482$)	36.42 (46)	64.31 (44)
Hourly	1.19 (5.42)	4.76 (16.28)	198	$p<0.001$ ($n_{EC}=40072$, $n_{CH}=40072$)	36.62 (46)	75.81 (24)
Daily	1.11 (4.77)	-1.16 (170.67)	1106	$p<0.001$ ($n_{EC}=1879$, $n_{CH}=1879$)	43.47 (78)	66.67 (60)
Weekly	1.03 (6.73)	-19.55 (284.31)	770	$p=0.015$ ($n_{EC}=349$, $n_{CH}=349$)	98.12 (82)	77.82 (64)
Monthly	1.05 (13.15)	-58.55 (472.15)	566	$p=0.511$ ($n_{EC}=121$, $n_{CH}=121$)	315.38 (78)	218.47 (63)
Annual	0.28 (16.93)	-70.94 (311.86)	333	$p=0.972$ ($n_{EC}=22$, $n_{CH}=22$)	307.19 (72)	251.67 (60)

https://doi.org/10.5194/egusphere-2025-5023
Preprint. Discussion started: 27 October 2025

Table C4. Descriptive statistics and Wilcoxon-Mann-Whitney test results for ΔFCH_4 based on cumulative EC and chamber FCH_4 (mg CH_4 m^{-2}) at daily to annual aggregations (note: cumulative FCH_4 were calculated only for exact EC-chamber FCH_4 timestamps and do not represent cumulative sums for ecosystem CH_4 budget calculations). Due to a lack of hourly timestamps in the chamber FCH_4 data at FI-Si2, US-La1 and US-La2, these three sites were excluded from this table, resulting in n=7 sites. Results are given separately for data sets based on median (left) and mean (right) aggregations of chamber and EC FCH_4 at each temporal scale. The EC and chamber data sample sizes in Wilcoxon-Mann-Whitney tests are reported as n_{EC} and n_{CH}, respectively. Abbreviations: IQR = interquartile range, SD = standard deviation, CV = coefficient of variation (%).

	Median-based aggregation				**Mean-based aggregation**			
Data set	**ΔFCH_4 median (IQR), *mg CH_4 m^{-2}***	**ΔFCH_4 mean (SD), *mg CH_4 m^{-2}***	**ΔFCH_4 CV (%)**	**Wilcoxon-Mann-Whitney test**	**ΔFCH_4 median (IQR), *mg CH_4 m^{-2}***	**ΔFCH_4 mean (SD), *mg CH_4 m^{-2}***	**ΔFCH_4 CV (%)**	**Wilcoxon-Mann-Whitney test**
Daily	1.29 (5.5)	5.88 (29.22)	303	$p<0.001$ (n_{EC}=1838, n_{CH}=1838)	1.15 (5.47)	4.99 (29.1)	305	$p<0.001$ (n_{EC}=1838, n_{CH}=1838)
Weekly	6.39 (32.68)	34.65 (117.8)	212	$p=0.006$ (n_{EC}=312, n_{CH}=312)	5.53 (32.52)	29.37 (116.05)	211	$p=0.028$ (n_{EC}=312, n_{CH}=312)
Monthly	13.4 (93.83)	117.5 (385.22)	213	$p=0.314$ (n_{EC}=92, n_{CH}=92)	8.85 (88.37)	99.62 (385.22)	209	$p=0.485$ (n_{EC}=92, n_{CH}=92)
Annual	37.1 (742.78)	675.63 (2024.37)	193	$p=0.897$ (n_{EC}=16, n_{CH}=16)	35.23 (781.38)	572.81 (1945.22)	188	$p=0.897$ (n_{EC}=16, n_{CH}=16)

https://doi.org/10.5194/egusphere-2025-5023
Preprint. Discussion started: 27 October 2025

Table C5. Linear mixed effects model results for assessing the slopes between EC FCH_4 and chamber FCH_4. To meet residual normality assumptions of linear mixed models, EC FCH_4 was transformed with inverse hyperbolic sine (IHS) and the fixed effect estimates, *p*-values and standard errors (SE) are in transformed scale. Average marginal effects (AME) and their 95% confidence intervals (CI) are reported in the back-transformed units (nmol m^{-2} s^{-1}) and represent the average change in EC FCH_4 with a 1 nmol m^{-2} s^{-1} increase in chamber FCH_4 across all chamber FCH_4 observations. AME CIs were obtained with parametric simulation from the fixed effect estimate and covariance. Half-hourly and hourly models are not included due to non-convergence and residual non-normality.

Model	Fixed effect	Estimate β (IHS scale)	*p*-value	SE	AME (95% CI)
Daily	Intercept	3.647	<0.001	0.657	0.007 (0.0006-0.032)
	Chamber FCH_4	0.0004	0.031	0.0002	
Weekly	Intercept	3.612	<0.001	0.645	0.011 (-0.0007-0.049)
	Chamber FCH_4	0.0006	0.066	0.0003	
Monthly	Intercept	3.591	<0.001	0.646	0.009 (-0.005-0.049)
	Chamber FCH_4	0.0005	0.183	0.0004	
Annual	Intercept	3.653	<0.001	0.636	0.02 (0.002-0.088)
	Chamber FCH_4	0.001	0.044	0.0004	

https://doi.org/10.5194/egusphere-2025-5023
Preprint. Discussion started: 27 October 2025

Table C6. Wilcoxon-Mann-Whitney test results for half-hourly aggregation. The EC and chamber data sample sizes in Wilcoxon Mann-Whitney tests are reported as n_{EC} and n_{CH}, respectively. Proportions of annual chamber and EC CH_4 emission (i.e., $FCH_4 \leq 0$ excluded) above the 90th percentile (p90) are reported as the mean of year-specific 90th percentiles (not in parentheses) and percentages (in parentheses). This data set contains chamber measurements only from automated chambers (n=4 sites). Abbreviations: IQR = interquartile range, CV = coefficient of variation (%).

Site	Mean EC FCH_4 (SD), *nmol m⁻²s⁻¹*	Mean chamber FCH_4 (SD), *nmol m⁻²s⁻¹*	Median EC FCH_4 (IQR, CV), *nmol m⁻²s⁻¹*	Median chamber FCH_4 (IQR, CV), *nmol m⁻²s⁻¹*	Median ΔFCH_4 (IQR, CV), *nmol m⁻²s⁻¹*	Chamber FCH_4 p90 (% of total FCH_4)	EC FCH_4 p90 (% of total FCH_4)	Wilcoxon-Mann-Whitney test
CN-Hgu	4.73 (25.36)	-0.12 (0.35)	3.0 (6.0, 241)	-0.1 (0.24, 165)	3.12 (6.04, 239)	0.63 (55)	20 (58)	$p<0.001$ (n_{EC} = 9571, n_{CH} = 9571)
SE-Deg	53.18 (22.31)	25.19 (18.24)	54.1 (36.28, 42)	21.61 (24.24, 72)	26.94 (23.98, 62)	50.5 (25)	79.85 (17)	$p<0.001$ (n_{EC} = 13987, n_{CH} = 13987)
US-Ho1	-0.21 (1.84)	1.21 (10.47)	-0.4 (1.32, 158)	-0.89 (1.44, 334)	0.38 (2.36, 311)	18.06 (49)	3.24 (43)	$p<0.001$ (n_{EC} = 30716, n_{CH} = 30716)
US-Uaf	3.61 (4.35)	2.45 (3.58)	3.39 (4.17, 107)	0.78 (2.32, 146)	1.22 (3.76, 146)	5.73 (36)	6.99 (29)	$p<0.001$ (n_{EC} = 20208, n_{CH} = 20208)

https://doi.org/10.5194/egusphere-2025-5023
Preprint. Discussion started: 27 October 2025

Table C7. Wilcoxon-Mann-Whitney test results for hourly aggregation. The EC and chamber data sample sizes in Wilcoxon Mann-Whitney tests are reported as n_{EC} and n_{CH}, respectively. Proportions of annual chamber and EC CH_4 emission (i.e., $FCH_4 \leq 0$ excluded) above the 90th percentile (p90) are reported as the mean of year-specific 90th percentiles (not in parentheses) and percentages (in parentheses). This data set contains chamber measurements only from automated chambers (n=4 sites). Abbreviations: IQR = interquartile range, CV = coefficient of variation (%).

Site	**Mean EC FCH_4 (SD),** *nmol CH_4 $m^{-2}s^{-1}$*	**Mean chamber FCH_4 (SD),** *nmol CH_4 $m^{-2}s^{-1}$*	**Median EC FCH_4 (IQR, CV),** *nmol CH_4 $m^{-2}s^{-1}$*	**Median chamber FCH_4 (IQR, CV),** *nmol CH_4 $m^{-2}s^{-1}$*	**Median ΔFCH_4 (IQR, CV),** *nmol CH_4 $m^{-2}s^{-1}$*	**Chamber FCH_4 p90 (% of total FCH_4)**	**EC FCH_4 p90 (% of total FCH_4)**	**Wilcoxon-Mann-Whitney test**
CN-Hgu	4.56 (22.87)	-0.11 (0.26)	3.0 (6.11, 229)	-0.09 (0.2, 145)	3.08 (5.99, 227)	0.6 (54)	19.75 (56)	*p*<0.001 (n_{EC} = 5305, n_{CH} = 5305)
SE-Deg	53.17 (22.05)	25.11 (17.42)	54.41 (36.28, 41)	21.6 (25.34, 69)	26.9 (23.04, 51)	49.59 (23)	79.67 (17)	*p*<0.001 (n_{EC} = 7243, n_{CH} = 7243)
US-Ho1	-0.21 (1.53)	-0.37 (3.05)	-0.36 (1.23, 149)	-0.95 (1.27, 192)	0.47 (1.95, 188)	7.43 (53)	2.82 (41)	*p*<0.001 (n_{EC} = 17215, n_{CH} = 17215)
US-Uaf	3.61 (3.71)	2.37 (3.53)	3.32 (4.04, 96)	0.73 (2.17, 149)	1.28 (3.55, 137)	5.47 (35)	7.02 (27)	*p*<0.001 (n_{EC} = 10309, n_{CH} = 10309)

https://doi.org/10.5194/egusphere-2025-5023
Preprint. Discussion started: 27 October 2025

Table C8. Wilcoxon-Mann-Whitney test results for daily aggregation. The EC and chamber data sample sizes in Wilcoxon-Mann-Whitney tests are reported as n_{EC} and n_{CH}, respectively. Proportions of annual chamber and EC CH_4 emission (i.e., $FCH_4 \leq 0$ excluded) above the 90th percentile (p90) are reported as the mean of year-specific 90th percentiles (not in parentheses) and percentages (in parentheses). This dataset contains all sites (n=10). Note: due to small sample sizes (n=5) in US-La1 and US-Los, the Wilcoxon-Mann-Whitney test results should be interpreted with caution. Abbreviations: IQR = interquartile range, CV = coefficient of variation (%).

Site	**Mean EC FCH_4 (SD),** ***nmol CH_4 $m^{-2}s^{-1}$***	**Mean chamber FCH_4 (SD),** ***nmol CH_4 $m^{-2}s^{-1}$***	**Median EC FCH_4 (IQR, CV),** ***nmol CH_4 $m^{-2}s^{-1}$***	**Median chamber FCH_4 (IQR, CV),** ***nmol CH_4 $m^{-2}s^{-1}$***	**Median ΔFCH_4 (IQR, CV),** ***nmol CH_4 $m^{-2}s^{-1}$***	**Chamber FCH_4 p90 (% of total FCH_4)**	**EC FCH_4 p90 (% of total FCH_4)**	**Wilcoxon-Mann-Whitney test**
CN-Hgu	3.22 (1.79)	-0.12 (0.11)	3.0 (2.14, 55)	-0.07 (0.12, 93)	3.2 (2.21, 54)	0.04 (17)	5.69 (20)	*p*<0.001 (n_{EC} = 265, n_{CH} = 265)
FI-Si2	57.13 (18.74)	62.14 (37.85)	54.37 (21.48, 33)	49.46 (57.04, 61)	0.81 (30.53, 132)	98.37 (25)	77.5 (19)	*p*=0.737 (n_{EC} = 26, n_{CH} = 26)
SE-Deg	52.44 (20.75)	24.24 (15.76)	55.88 (39.7, 40)	21.39 (24.96, 65)	0.81 (30.53, 132)	48.56 (21)	78.16 (15)	*p*<0.001 (n_{EC} = 317, n_{CH} = 317)
US-Ho1	-0.43 (0.54)	-0.68 (1.67)	-0.45 (0.73, 96)	-1.01 (0.9, 130)	0.39 (1.22, 165)	2.04 (52)	0.4 (39)	*p*<0.001 (n_{EC} = 759, n_{CH} = 759)
US-La1	41.49 (29.79)	97.72 (65.37)	42.12 (53.85, 72)	116.91 (62.59, 67)	-45.43 (71.64, 115)	157.64 (37)	71.03 (34)	*p*=0.222 (n_{EC} = 5, n_{CH} = 5)
US-La2	163.74 (63.81)	191.35 (93.46)	150.22 (103.39, 39)	189.16 (117.65, 49)	5.75 (103.92, 141)	276.98 (32)	226.3 (30)	*p*=0.436 (n_{EC} = 10, n_{CH} = 10)
US-Los	35.37 (12.78)	9.61 (5.62)	38.75 (13.82, 36)	8.43 (4.09, 58)	27.75 (4.74, 37)	15.42 (38)	46.72 (28)	*p*=0.016 (n_{EC} = 5, n_{CH} = 5)

https://doi.org/10.5194/egusphere-2025-5023
Preprint. Discussion started: 27 October 2025

US-Owc	607.26 (289.11)	770.24 (766.66)	652.8 (490.18, 48)	579.95 (721.2, 100)	-108.22 (485.14, 169)	1306.07 (46)	936.62 (28)	p=0.988 (n_{EC} = 18, n_{CH} = 18)
US-StJ	39.2 (58.96)	13.98 (27.01)	16.4 (29.69, 150)	5.26 (8.31, 193)	9.15 (20.85, 202)	22.15 (63)	73.94 (54)	p=0.007 (n_{EC} = 16, n_{CH} = 16)
US-Uaf	3.5 (2.09)	2.15 (3.12)	3.49 (3.96, 60)	0.66 (2.0, 145)	1.27 (2.29, 111)	4.97 (25)	6.09 (20)	p<0.001 (n_{EC} = 458, n_{CH} = 458)

Table C9. Wilcoxon-Mann-Whitney test results for weekly aggregation. The EC and chamber data sample sizes in Wilcoxon-Mann-Whitney tests are reported as n_{EC} and n_{CH}, respectively. Proportions of annual chamber and EC CH_4 emission (i.e., $FCH_4 \leq 0$ excluded) above the 90th percentile (p90) are reported as the mean of year-specific 90th percentiles (not in parentheses) and percentages (in parentheses). This dataset contains all sites (n=10). Note: due to small sample sizes (n=5) in US-La1 and US-Los, the Wilcoxon-Mann-Whitney test results should be interpreted with caution. Abbreviations: IQR = interquartile range, CV = coefficient of variation (%).

Site	**Mean EC FCH_4 (SD),** ***nmol CH_4 $m^{-2}s^{-1}$***	**Mean chamber FCH_4 (SD),** ***nmol CH_4 $m^{-2}s^{-1}$***	**Median EC FCH_4 (IQR, CV),** ***nmol CH_4 $m^{-2}s^{-1}$***	**Median chamber FCH_4 (IQR, CV),** ***nmol CH_4 $m^{-2}s^{-1}$***	**Median ΔFCH_4 (IQR, CV),** ***nmol CH_4 $m^{-2}s^{-1}$***	**Chamber FCH_4 p90 (% of total FCH_4)**	**EC FCH_4 p90 (% of total FCH_4)**	**Wilcoxon-Mann-Whitney test**
CN-Hgu	3.02 (1.18)	-0.12 (0.11)	3.0 (1.98, 39)	-0.07 (0.13, 90)	3.08 (1.98, 39)	0.02 (59)	4.26 (20)	p<0.001 (n_{EC} = 40, n_{CH} = 40)
FI-Si2	55.43 (17.61)	59.55 (35.23)	53.36 (18.93, 32)	49.46 (48.82, 59)	1.45 (24.92, 139)	88.39 (27)	73.87 (22)	p=0.789 (n_{EC} = 22, n_{CH} = 22)
SE-Deg	50.17 (21.18)	22.73 (15.64)	50.94 (38.12, 42)	18.74 (22.04, 69)	24.83 (19.9, 43)	46.5 (27)	76.31 (19)	p<0.001 (n_{EC} = 50,

https://doi.org/10.5194/egusphere-2025-5023
Preprint. Discussion started: 27 October 2025

								$n_{CH} = 50$)
US-Ho1	-0.42 (0.48)	-0.69 (1.34)	-0.42 (0.72, 90)	-0.99 (0.91, 112)	0.32 (1.28, 146)	6.02 (43)	0.41 (27)	$p<0.001$ ($n_{EC} = 119$, $n_{CH} = 119$)
US-La1	41.49 (29.79)	97.72 (65.37)	42.12 (53.85, 72)	116.91 (62.59, 67)	-45.43 (71.64, 115)	157.64 (37)	71.03 (34)	$p=0.222$ ($n_{EC} = 5$, $n_{CH} = 5$)
US-La2	163.74 (63.81)	191.35 (93.46)	150.22 (103.39, 39)	189.16 (117.65, 49)	5.75 (103.92, 141)	276.98 (32)	226.3 (30)	$p=0.436$ ($n_{EC} = 10$, $n_{CH} = 10$)
US-Los	35.37 (12.78)	9.61 (5.62)	38.75 (13.82, 36)	8.43 (4.09, 58)	27.75 (4.74, 37)	15.42 (38)	46.72 (28)	$p=0.016$ ($n_{EC} = 5$, $n_{CH} = 5$)
US-Owc	561.44 (287.63)	753.88 (619.97)	642.45 (446.31, 51)	552.85 (657.0, 82)	47.22 (728.26, 145)	1185.44 (56)	828.1 (45)	$p=0.796$ ($n_{EC} = 9$, $n_{CH} = 9$)
US-StJ	39.2 (58.96)	13.98 (27.01)	16.4 (29.69, 150)	5.26 (8.31, 193)	9.15 (20.85, 202)	22.12 (63)	73.94 (54)	$p=0.007$ ($n_{EC} = 16$, $n_{CH} = 16$)
US-Uaf	3.4 (1.97)	2.01 (3.04)	3.46 (3.82, 58)	0.64 (1.87, 151)	1.18 (2.13, 107)	4.76 (29)	5.85 (23)	$p<0.001$ ($n_{EC} = 73$, $n_{CH} = 73$)

https://doi.org/10.5194/egusphere-2025-5023
Preprint. Discussion started: 27 October 2025

Table C10. Wilcoxon-Mann-Whitney test results for monthly aggregation. The EC and chamber data sample sizes in Wilcoxon-Mann-Whitney tests are reported as n_{EC} and n_{CH}, respectively. Proportions of annual chamber and EC CH_4 emission (i.e., $FCH_4 \leq 0$ excluded) above the 90th percentile (p90) are reported as the mean of year-specific 90th percentiles (not in parentheses) and percentages (in parentheses). This dataset contains all sites (n=10). Note: due to small sample sizes (n=5) in US-La1 and US-Los, the Wilcoxon-Mann-Whitney test results should be interpreted with caution. Abbreviations: IQR = interquartile range, CV = coefficient of variation (%). * CN-Hgu had only negative chamber FCH_4 values and chamber p90 was not calculated for this site.

Site	**Mean EC FCH_4 (SD),** ***nmol CH_4 $m^{-2}s^{-1}$***	**Mean chamber FCH_4 (SD),** ***nmol CH_4 $m^{-2}s^{-1}$***	**Median EC FCH_4 (IQR, CV),** ***nmol CH_4 $m^{-2}s^{-1}$***	**Median chamber FCH_4 (IQR, CV),** ***nmol CH_4 $m^{-2}s^{-1}$***	**Median ΔFCH_4 (IQR, CV),** ***nmol CH_4 $m^{-2}s^{-1}$***	**Chamber FCH_4 p90 (% of total FCH_4)**	**EC FCH_4 p90 (% of total FCH_4)**	**Wilcoxon-Mann-Whitney test**
CN-Hgu	3.1 (1.06)	-0.12 (0.1)	3.0 (1.08, 34)	-0.07 (0.14, 84)	3.05 (1.2, 34)	-*	4.14 (30)	$p<0.001$ (n_{EC} = 10, n_{CH} = 10)
FI-Si2	52.49 (16.25)	51.0 (26.4)	53.36 (23.22, 31)	47.79 (44.33, 52)	2.68 (26.17, 120)	73.18 (32)	68.51 (29)	p=0.635 (n_{EC} = 14, n_{CH} = 14)
SE-Deg	46.58 (22.45)	20.66 (15.23)	46.85 (44.64, 48)	15.7 (22.22, 74)	25.1 (11.52, 46)	40.22 (33)	73.06 (25)	p=0.002 (n_{EC} = 13, n_{CH} = 13)
US-Ho1	-0.44 (0.45)	-0.8 (0.97)	-0.46 (0.6, 86)	-1.05 (0.8, 88)	0.35 (1.12, 124)	2.86 (67)	0.28 (41)	$p<0.001$ (n_{EC} = 32, n_{CH} = 32)
US-La1	41.49 (29.79)	97.72 (65.37)	42.12 (53.85, 72)	116.91 (62.59, 67)	-45.43 (71.64, 115)	157.64 (37)	71.03 (34)	p=0.222 (n_{EC} = 5, n_{CH} = 5)
US-La2	163.74 (63.81)	191.35 (93.46)	150.22 (103.39, 39)	189.16 (117.65, 49)	5.75 (103.92, 141)	276.98 (32)	226.3 (30)	p=0.436 (n_{EC} = 10, n_{CH} = 10)
US-Los	32.8 (14.3)	7.78 (2.88)	38.75 (13.34, 44)	6.91 (2.78, 37)	27.75 (14.07, 57)	10.18 (47)	42.28 (44)	p=0.1 (n_{EC} = 3,

https://doi.org/10.5194/egusphere-2025-5023
Preprint. Discussion started: 27 October 2025

								n_{CH} = 3)
US-Owc	575.34 (301.58)	705.33 (549.45)	642.45 (446.31, 52)	667.58 (756.29, 78)	131.03 (524.49, 144)	1056.3 (58)	828.57 (47)	p=0.798 (n_{EC} = 8, n_{CH} = 8)
US-StJ	24.14 (19.65)	9.92 (11.72)	21.19 (22.71, 81)	6.0 (7.45, 118)	18.45 (22.01, 82)	20.73 (47)	44.15 (33)	p=0.105 (n_{EC} = 8, n_{CH} = 8)
US-Uaf	3.39 (1.87)	2.17 (3.15)	3.42 (3.87, 55)	0.65 (1.97, 145)	1.24 (1.84, 114)	4.5 (34)	5.52 (28)	p=0.006 (n_{EC} = 18, n_{CH} = 18)

https://doi.org/10.5194/egusphere-2025-5023
Preprint. Discussion started: 27 October 2025

Table C11. Wilcoxon-Mann-Whitney test results for annual aggregation. The EC and chamber data sample sizes in Wilcoxon-Mann-Whitney tests are reported as n_{EC} and n_{CH}, respectively. Annual chamber and EC FCH_4 90th percentiles were not calculated for this aggregation. This dataset contains all sites (n=10). Note: due to small sample sizes (n=5) in US-La1 and
1045 US-Los, the Wilcoxon-Mann-Whitney test results should be interpreted with caution. Abbreviations: IQR = interquartile range, CV = coefficient of variation (%).

Site	**Mean EC FCH_4 (SD),** ***nmol CH_4 $m^{-2}s^{-1}$***	**Mean chamber FCH_4 (SD),** ***nmol CH_4 $m^{-2}s^{-1}$***	**Median EC FCH_4 (IQR, CV),** ***nmol CH_4 $m^{-2}s^{-1}$***	**Median chamber FCH_4 (IQR, CV),** ***nmol CH_4 $m^{-2}s^{-1}$***	**Median ΔFCH_4 (IQR, CV),** ***nmol CH_4 $m^{-2}s^{-1}$***	**Wilcoxon-Mann-Whitney test**
CN-Hgu	3.04 (0.06)	-0.15 (0.14)	3.04 (0.04, 2)	-0.15 (0.1, 94)	3.2 (0.14, 6)	-
FI-Si2	55.7 (2.45)	53.01 (23.84)	55.19 (2.41, 4)	66.22 (20.91, 45)	-7.85 (21.73, 138)	p=0.7 (n_{EC} = 3, n_{CH} = 3)
SE-Deg	54.08 (3.69)	20.78 (0.59)	54.08 (2.61, 7)	20.78 (0.42, 3)	33.3 (2.19, 9)	-
US-Ho1	-0.38 (0.27)	-0.82 (0.45)	-0.51 (0.34, 70)	-0.77 (0.57, 55)	0.25 (0.78, 111)	p=0.095 (n_{EC} = 5, n_{CH} = 5)
US-La1	37.77 (-)	76.56 (-)	37.77 (-,-)	76.56 (-,-)	-38.79 (-,-)	-
US-La2	163.81 (49.76)	161.89 (74.25)	163.81 (35.19, 30)	161.89 (52.5, 46)	1.93 (87.69, 141)	-
US-Los	38.18 (-)	8.12 (-)	38.18 (-,-)	8.12 (-,-)	30.05 (-,-)	-
US-Owc	476.61 (209.52)	539.49 (445.72)	476.61 (148.15, 44)	539.49 (315.17, 83)	-62.88 (167.02, 141)	-
US-StJ	14.06 (-)	4.97 (-)	14.06 (-,-)	4.97 (-,-)	9.09 (-,-)	-

https://doi.org/10.5194/egusphere-2025-5023
Preprint. Discussion started: 27 October 2025

US-Uaf	3.38 (0.11)	0.65 (0.34)	3.42 (0.11, 3)	0.52 (0.32, 52)	2.95 (0.41, 16)	*p*=0.1 (n_{EC} = 3, n_{CH} = 3)

Table C12. Final linear mixed effects model results of significant predictors of ΔFCH_4 for the half-hourly model (site n=3) with soil temperature (TS) instead of Month as one of the predictors. Absolute ΔFCH_4 was Yeo-Johnson-transformed, centered and scaled, while all continuous predictors were only centered and scaled. The predictors are listed in decreasing order based on β-coefficients. The reference level in Hour was 0 and May in Month. Abbreviations: SE = standard error, Df = degrees of freedom of denominator, PA = air pressure (kPa), u* = friction velocity (m s^{-1}), WTL = water table level (cm), TS = soil temperature (°C), NEE = net ecosystem exchange (µmol CO_2 m^{-2} s^{-1}), VPD = vapor pressure deficit (hPa), vWD = *v* wind component (m s^{-1}), uWD = *u* wind component (m s^{-1}).

Predictors	**β-coefficient**	**SE**	***p*-value (*t*-test)**	**Marginal R^2**	**Conditional R^2**	**Df**	**Random effect variation explained, %**
Intercept	0.0581	0.5465	0.9153	0.0109	0.805	43522	
<u>**Fixed effects**</u>							
Hour							
- 5 AM	0.0838	0.0166	**0**			43522	
u*	0.0836	0.004	**0**			43522	
Hour	-0.0565	0.01	**0**			43522	
- 6 AM	0.0727	0.0163	**0**			43522	
PA	-0.0684	0.0105	**0**			43522	
Hour							
- 4 AM	0.0567	0.0163	**0.0005**			43522	
- 7 AM	0.0489	0.0165	**0.003**			43522	
- 10 AM	-0.0406	0.0169	**0.0161**			43522	
- 8 AM	0.0392	0.0166	**0.0181**			43522	
- 3 AM	0.0375	0.0166	**0.0238**			43522	
- 10 PM	-0.0311	0.0163	0.0559			43522	
- 5 PM	-0.0294	0.0166	0.0776			43522	
NEE	-0.0289	0.004	**0**			43522	
TS	-0.027	0.0068	**0.0001**			43522	
VPD	-0.0268	0.0054	**0**			43522	
Hour							

https://doi.org/10.5194/egusphere-2025-5023
Preprint. Discussion started: 27 October 2025

- 3 PM	-0.0248	0.0172	0.1498			43522	
- 9 PM	-0.0246	0.0168	0.1412			43522	
- 6 PM	-0.0221	0.0163	0.1741			43522	
- 8 PM	-0.0201	0.0165	0.2224			43522	
- 7 PM	-0.018	0.0165	0.2745			43522	
vWD	-0.018	0.0036	**0**			43522	
Hour							
- 2 AM	0.0175	0.0163	0.2827			43522	
- 1 PM	-0.0148	0.0173	0.394			43522	
- 12 PM	-0.0094	0.0172	0.5833			43522	
- 1 AM	0.0072	0.0166	0.6597			43522	
- 11 PM	-0.0054	0.0165	0.7413			43522	
- 2 PM	-0.0042	0.0171	0.8068			43522	
- 11 AM	-0.0028	0.0172	0.8698			43522	
- 9 AM	-0.0024	0.0171	0.8847			43522	
- 4 PM	-0.0013	0.0167	0.9376			43522	
Random effects							
Site							72.29
Date							8

Table C13. Half-hourly and hourly linear mixed effects model results after backward variable selection. In the models, absolute ΔFCH4 was Yeo-Johnson-transformed, centered and scaled, while all continuous predictors were only centered and scaled. Note that in both models temporal variables were included in nested random effects (see Text S3). In both models, the reference level in dominant vegetation type was *Sphagnum* moss, 0 in Hour and May in Month. Note that we excluded TS from the half-hourly model due to high multicollinearity with Month (VIF>3; see models with TS instead of Month in S17). The predictors are listed in a decreasing order according to their β-coefficients. SE = standard error, Df = degrees of freedom of denominator, PA = air pressure (kPa), u* = friction velocity (m s^{-1}), WTL = water table level (cm), TS = soil temperature (°C), NEE = net ecosystem exchange (μmol CO_2 m^{-2} s^{-1}), VPD = vapor pressure deficit (hPa), vWD = *v* wind component (m s^{-1}), uWD = *u* wind component (m s^{-1}).

Data set	Predictors	β-coefficient	SE	*p*-value (*t*-test)	Marginal R^2	Conditional R^2	Df	Random effect variation explained, %
Half-hourly	Intercept	-0.236	0.5259	0.6537	0.0329	0.7933	43522	

https://doi.org/10.5194/egusphere-2025-5023
Preprint. Discussion started: 27 October 2025

(n=3 sites)	**Fixed effects**				
	Month				
	- **Aug**	0.4626	0.0291	**0**	1408
	- **Jul**	0.4169	0.029	**0**	1408
	- **Sep**	0.3972	0.0294	**0**	1408
	- **Jun**	0.2157	0.0293	**0**	1408
	- Apr	0.1615	0.0164	0.6751	1408
	- **Oct**	0.1105	0.0316	**0.0005**	1408
	u*	0.0876	0.0039	**0**	43522
	Hour				
	- **5 AM**	0.0873	0.0166	**0**	43522
	- **6 AM**	0.0742	0.0163	**0**	43522
	WTL	0.0617	0.0121	**0**	43522
	Hour				
	- **4 AM**	0.0593	0.0163	**0.0003**	43522
	PA	-0.056	0.0097	**0**	43522
	Hour				
	- **7 AM**	0.0486	0.0165	**0.0032**	43522
	- **10 AM**	-0.0449	0.0168	**0.0075**	43522
	- **3 AM**	0.0409	0.0166	**0.0137**	43522
	VPD	-0.0394	0.0049	**0**	43522
	Hour				
	- **8 AM**	0.0376	0.0166	**0.0235**	43522
	Month				
	- Nov	0.0372	0.0535	0.4865	1408

https://doi.org/10.5194/egusphere-2025-5023
Preprint. Discussion started: 27 October 2025

	Hour							
	- 10 PM	-0.0323	0.0163	0.0476			43522	
	- 5 PM	-0.0323	0.0166	0.0515			43522	
	- 3 PM	-0.0297	0.0171	0.0825			43522	
	NEE	-0.0295	0.0039	**0**			43522	
	Hour							
	- 9 PM	-0.0259	0.0168	0.1221			43522	
	- 6 PM	-0.0245	0.0163	0.1319			43522	
	- 8 PM	-0.0207	0.0164	0.2072			43522	
	- 1 PM	-0.0206	0.0172	0.2309			43522	
	- 7 PM	-0.0198	0.0165	0.2293			43522	
	- 2 AM	0.0194	0.0163	0.2336			43522	
	vWD	-0.0179	0.0035	**0**			43522	
	Hour							
	- 12 PM	-0.0155	0.0171	0.363			43522	
	- 2 PM	-0.0095	0.017	0.5736			43522	
	- 1 AM	0.0089	0.0166	0.5925			43522	
	- 11 AM	-0.008	0.0171	0.6385			43522	
	- 11 PM	-0.0052	0.0165	0.7522			43522	
	- 4 PM	-0.0049	0.0166	0.7696			43522	
	- 9 AM	-0.0045	0.0171	0.7928			43522	
	Random effects							
	Site							72.39
	Date							6.23
Hourly (n=3 sites)	Intercept	-0.2978	0.5368	0.5791	0.0439	0.816	25231	
	Fixed effects							
	Month							
	- **Aug**	0.6418	0.0359	**0**			1405	

https://doi.org/10.5194/egusphere-2025-5023
Preprint. Discussion started: 27 October 2025

- **Jul**	0.5815	0.0365	**0**	1405
- **Sep**	0.5118	0.035	**0**	1405
- Apr	-0.3979	0.4686	0.3959	1405
- **Jun**	0.27	0.0354	**0**	1405
- **Oct**	0.1829	0.0373	**0**	1405
Hour				
- **5 AM**	0.1371	0.0208	**0**	25231
WTL	0.0936	0.0142	**0**	25231
Hour				
- **7 AM**	0.0926	0.0207	**0**	25231
- **3 AM**	0.0841	0.0206	**0**	25231
TS	-0.0838	0.0092	**0**	25231
Hour				
- **6 AM**	0.0831	0.0204	**0**	25231
u*	0.0687	0.0051	**0**	25231
Hour				
- **9 AM**	0.0657	0.0216	**0.0024**	25231
- **8 AM**	0.0656	0.0207	**0.0016**	25231
- **1 AM**	0.0594	0.0206	**0.0039**	25231
- **11 PM**	0.0578	0.0204	**0.0046**	25231
- **1 PM**	0.0488	0.0222	**0.028**	25231
- **7 PM**	0.0479	0.0206	**0.0197**	25231
- **11 AM**	0.0476	0.022	**0.0302**	25231
PA	-0.0458	0.0117	**0.0001**	25231
Hour				
- **4 AM**	0.0417	0.0201	**0.0383**	25231
- 3 PM	0.0417	0.0218	0.056	25231
- 2 AM	0.0377	0.0201	0.0612	25231
- 12 PM	0.0336	0.0219	0.1259	25231
- 2 PM	0.0272	0.0218	0.2113	25231
- 5 PM	0.0267	0.021	0.2039	25231
NEE	-0.0243	0.0052	**0**	25231
Hour				
- 10 AM	-0.0183	0.0215	0.3942	25231
VPD	-0.0181	0.0066	**0.0063**	25231

https://doi.org/10.5194/egusphere-2025-5023
Preprint. Discussion started: 27 October 2025

Month							
- Nov	0.0176	0.0628	0.7792			1405	
Hour							
- 6 PM	-0.0167	0.0204	0.4144			25231	
- 9 PM	0.0149	0.0207	0.4738			25231	
- 4 PM	0.0148	0.0212	0.4851			25231	
- 8 PM	-0.0129	0.0202	0.523			25231	
- 10 PM	-0.0121	0.0202	0.5514			25231	
vWD	-0.0081	0.0045	0.0705			25231	
Random effects							
Site							72.46
Date							8.29

Table C14. Full linear mixed effects model results. In the models, absolute ΔFCH$_4$ was Yeo-Johnson-transformed, centered and scaled, while all continuous predictors were only centered and scaled. This table presents the full models with both nonsignificant and significant predictors before backward variable selection. The final daily and monthly models were the full models which are shown in Table 3 of the main text. Note that in all models temporal variables were included in nested random effects (see methods and Text S3). In all models, the reference level in site dominant vegetation (VEG) was *Sphagnum* moss, 0 in Hour and May in Month. Annual models were not included due to an inadequate number of observations. Due to lack of complete case observations, US-Owc was not included in the weekly and monthly models (n=7 sites). We excluded TS from the half-hourly model due to high multicollinearity with Month (VIF>3). Due to multicollinearity in the weekly model, we built one model without NEE and one without VPD. Fixed effects are listed in decreasing order based on their β-coefficients. SE = standard error, Df = degrees of freedom of denominator, PA = air pressure (kPa), u* = friction velocity (m s^{-1}), WTL = water table level (cm), TS = soil temperature (°C), NEE = net ecosystem exchange (μmol CO$_2$ m^{-2} s^{-1}), VPD = vapor pressure deficit (hPa), vWD = v wind component (m s^{-1}), uWD = u wind component (m s^{-1}).

Data set	Predictors	β-coefficient	SE	*p*-value (*t*-test)	Marginal R^2	Conditional R^2	Df	Random effect variation explained, %
Half-hourly (n=3 sites)	Intercept	0.0962	0.7069	0.8917	0.2041	0.8518	43521	
	Fixed effects							
	VEG							

https://doi.org/10.5194/egusphere-2025-5023
Preprint. Discussion started: 27 October 2025

- Tree	-0.9969	1.2237	0.5648	1
Month				
- Aug	0.4629	0.029	**0**	1408
- Jul	0.4172	0.029	**0**	1408
- Sep	0.3974	0.0294	**0**	1408
- Jun	0.2161	0.0294	**0**	1408
- Apr	0.1613	0.3852	0.6753	1408
- Oct	0.1109	0.0316	**0.0005**	1408
u*	0.088	0.004	**0**	43521
Hour				
- 5 AM	0.0873	0.0166	**0**	43521
- 6 AM	0.0741	0.0163	**0**	43521
WTL	0.0615	0.0121	**0**	43521
Hour				
- 4 AM	0.0592	0.0163	**0.0003**	43521
PA	-0.056	0.0097	**0**	43521
Hour				
- 7 AM	0.0484	0.0165	**0.0033**	43521
- 10 AM	-0.0451	0.0168	**0.0073**	43521
- 3 AM	0.0409	0.0166	**0.0138**	43521
VPD	-0.0393	0.0049	**0**	43521
Month				
- Nov	0.0376	0.0535	0.4822	1408
Hour				
- 8 AM	0.0373	0.0166	**0.0244**	43521
- 5 PM	-0.0325	0.0166	0.0502	43521
- 10 PM	-0.0323	0.0163	0.0476	43521

https://doi.org/10.5194/egusphere-2025-5023
Preprint. Discussion started: 27 October 2025

	- 3 PM	-0.0299	0.0171	0.0808			43521	
	NEE	-0.0294	0.0039	**0**			43521	
	Hour							
	- 9 PM	-0.0259	0.0168	0.1219			43521	
	- 6 PM	-0.0247	0.0163	0.1296			43521	
	- 8 PM	-0.0208	0.0164	0.2056			43521	
	- 1 PM	-0.0207	0.0172	0.2282			43521	
	- 7 PM	-0.0199	0.0165	0.2267			43521	
	- 2 AM	0.0194	0.0163	0.234			43521	
	vWD	-0.0182	0.0036	**0**			43521	
	Hour							
	- 12 PM	-0.0156	0.0171	0.3593			43521	
	- 2 PM	-0.0097	0.017	0.5678			43521	
	- 1 AM	0.0089	0.0166	0.5925			43521	
	- 11 AM	-0.0082	0.0171	0.6317			43521	
	- 11 PM	-0.0052	0.0165	0.7538			43521	
	- 4 PM	-0.0051	0.0166	0.7589			43521	
	- 9 AM	-0.0047	0.0171	0.7818			43521	
	uWD	-0.0015	0.0035	0.6716			43521	
	Random effects							
	Site							75.96
	Date							5.43
Hourly (n=3 sites)	Intercept	0.0199	0.7487	0.9788	0.2116	0.8752	25230	
	Fixed effects							
	VEG							
	- Tree	-0.9517	1.2957	0.5967			1	
	Month							

https://doi.org/10.5194/egusphere-2025-5023
Preprint. Discussion started: 27 October 2025

- **Aug**	0.6413	0.036	**0**	1405
- **Jul**	0.5811	0.0366	**0**	1405
- **Sep**	0.5114	0.035	**0**	1405
- Apr	-0.3974	0.4686	0.3966	1405
- **Jun**	0.2697	0.0355	**0**	1405
- **Oct**	0.1826	0.0373	**0**	1405
Hour				
- **5 AM**	0.1371	0.0208	**0**	25230
WTL	0.0933	0.0142	**0**	25230
Hour				
- **7 AM**	0.0927	0.0207	**0**	25230
- **3 AM**	0.0841	0.0206	**0**	25230
TS	-0.0837	0.0093	**0**	25230
Hour				
- **6 AM**	0.0831	0.0204	**0**	25230
u*	0.0685	0.0052	**0**	25230
Hour				
- **9 AM**	0.0658	0.0217	**0.0024**	25230
- **8 AM**	0.0656	0.0207	**0.0015**	25230
- **1 AM**	0.0594	0.0206	**0.0039**	25230
- **11 PM**	0.0578	0.0204	**0.0046**	25230
- **1 PM**	0.0488	0.0222	**0.028**	25230
- **7 PM**	0.048	0.0206	**0.0196**	25230
- **11 AM**	0.0476	0.022	**0.0302**	25230
PA	-0.0455	0.0117	**0.0001**	25230
Hour				
- 3 PM	0.0417	0.0218	0.0558	25230
- **4 AM**	0.0417	0.0201	**0.0384**	25230

https://doi.org/10.5194/egusphere-2025-5023
Preprint. Discussion started: 27 October 2025

	- 2 AM	0.0377	0.0201	0.0611			25230	
	- 12 PM	0.0336	0.0219	0.126			25230	
	- 2 PM	0.0272	0.0218	0.2111			25230	
	- 5 PM	0.0268	0.021	0.2028			25230	
	NEE	-0.0244	0.0052	**0**			25230	
	Hour							
	- 10 AM	-0.0183	0.0215	0.3958			25230	
	VPD	-0.0182	0.0066	**0.0061**			25230	
	Month							
	- Nov	0.0177	0.0628	0.7786			1405	
	Hour							
	- 6 PM	-0.0166	0.0204	0.4159			25230	
	- 4 PM	0.0149	0.0212	0.4826			25230	
	- 9 PM	0.0149	0.0207	0.4738			25230	
	- 8 PM	-0.0129	0.0202	0.5236			25230	
	- 10 PM	-0.0121	0.0202	0.5505			25230	
	vWD	-0.0079	0.0045	0.0833			25230	
	uWD	0.0009	0.0044	0.8346			25230	
	Random effects							
	Site							77.36
	Date							6.82
Weekly (no NEE, n=9 sites)	Intercept	0.3046	0.3665	0.407	0.5468	0.8357	180	
	Fixed effects							
	VEG							
	- Tree	-1.4712	0.702	0.0903			5	
	- Aerenchymatous	0.9949	0.5112	0.1092			5	
	- Ericaceous shrub	0.5253	0.7163	0.4962			5	

https://doi.org/10.5194/egusphere-2025-5023
Preprint. Discussion started: 27 October 2025

	Month							
	- Apr	0.3907	0.416	0.3502			86	
	- Nov	0.3193	0.2602	0.2232			86	
	- Dec	0.316	0.6993	0.6524			86	
	- Jul	0.3104	0.142	**0.0315**			86	
	- Aug	0.3012	0.1442	**0.0396**			86	
	- Sep	0.2964	0.14	**0.0371**			86	
	- Jun	0.2082	0.1388	0.1373			86	
	- Oct	0.169	0.1457	0.2492			86	
	WTL	-0.0727	0.0551	0.1887			180	
	PA	-0.0604	0.0407	0.14			180	
	VPD	-0.0352	0.0318	0.2701			180	
	u*	0.0317	0.0272	0.244			180	
	Month							
	- Mar	-0.0234	0.5319	0.9649			86	
	vWD	-0.0167	0.0175	0.3418			180	
	TS	-0.0104	0.06	0.862			180	
	uWD	-0.0081	0.0198	0.6819			180	
	Random effects							
	Site							63.74
	Year-month							$6.38e^{-07}$
Weekly (no VPD, n=9 sites)	Intercept	0.3008	0.3724	0.4202	0.5423	0.8365	180	
	Fixed effects							
	VEG							
	- Tree	-1.4642	0.713	0.0952			5	

- Aerenchymatous	0.9763	0.5228	0.1208	5	
- Ericaceous shrub	0.4435	0.7268	0.5684	5	
Month					
- Apr	0.3611	0.4145	0.386	86	
- Dec	0.3525	0.7059	0.6188	86	
- Nov	0.3375	0.263	0.2029	86	
- Aug	**0.317**	**0.1484**	**0.0355**	86	
- Jul	**0.3144**	**0.1438**	**0.0315**	86	
- Sep	**0.3086**	**0.1408**	**0.0311**	86	
- Jun	0.2001	0.141	0.1596	86	
- Oct	0.1847	0.1473	0.2134	86	
- Mar	-0.0786	0.5287	0.8822	86	
PA	-0.0737	0.039	0.0603	180	
WTL	-0.07	0.0546	0.2046	180	
u*	0.032	0.0276	0.2464	180	
TS	-0.019	0.0637	0.7663	180	
vWD	-0.0184	0.0175	0.2962	180	
uWD	-0.0137	0.0201	0.4953	180	
NEE	0.01	0.0266	0.7117	180	
Random effects					
Site					64.27
Year-month					$5.04e^{-07}$

Data availability

The timestamp-aligned data sets containing ecosystem and plot-scale CH_4 flux and environmental data at half-hourly, hourly, daily, weekly, monthly, and annual scales can be accessed via Zenodo (Määttä et al., 2025; doi: 10.5281/zenodo.17312404).

Author contribution

TM, AM, SB, KD, AD, SF, EFC, RJ, SK, GM, LM, ZO, OS, MU, RV, EW, ZZ, AT, and MH conceptualized the study. Data was provided by AD, GB, JJ, AK, KK, LM, MN, SN, MP, KS, ET, MU, RV, JW, EW, and ZZ, and data curation was conducted by TM, AM, AD, GB, KD, EFC, JJ, SK, AK, KK, GM, MN, SN, MP, KS, ET, MU, RV, JW, EW, and ZZ. Formal analysis (data processing and statistical analyses) and visualization were done by TM. Investigation was conducted by TM and AM. AM supervised the study. Project administration was done by TM, AM and RJ. Funding acquisition for the study was done by AM and RJ. TM and AM prepared the original manuscript draft and TM, AM, AD, GB, SB, KD, SF, EFC, RJ, JJ, SK, LM, MN, ZO, MP, OS, ET, MU, RV, JW, EW, ZZ, AT, and MH contributed to the review and editing.

Competing interests

The authors declare that they have no conflict of interest.

Acknowledgements

We acknowledge funding from the University of Zurich Stiftung für Wissenschaftliche Forschung (STWF-22-028) and the Swiss National Science Foundation (SNSF) (project 200021_215214) awarded to AM. This work was also supported by COMPASS-FME, a multi-institutional project supported by the U.S. Department of Energy, Office of Science, Biological and Environmental Research as part of the Environmental System Science Program. The Pacific Northwest National Laboratory is operated for DOE by Battelle Memorial Institute under contract DE-AC05-76RL01830. RBJ acknowledges support from the Gordon and Betty Moore Foundation through Grants GBMF5439 'Advancing Understanding of the Global Methane Cycle' and GBMF11519 'Advancing the understanding of methane emissions from tropical wetlands' to Stanford University and from the USGS Powell Synthesis Center (Scaling tropical wetland methane fluxes regionally and globally). SB was funded by the USGS Ecosystems Land Change Science Program and U.S. Department of Energy, Office of Science, Office of Biological and Environmental Research (Grant DE-SC0023084). Any use of trade, firm, or product names is for descriptive purposes only and does not imply endorsement by the U.S. Government. MU was supported by the Arctic Challenge for Sustainability II and III (JPMXD1420318865; JPMXD1720251001). ZO was supported by the US Department of the Treasury (grant no. DISL-MESC-ALCOE-06). ARD acknowledges support for the US Dept of Energy Ameriflux Management Project support to ChEAS core site cluster. OS acknowledges financial support through the Canada Research Chair program (CRC-2018-00259) and the NSERC Discovery Grants program (DGPIN-2018-05743). EJW acknowledges support from the US Greenhouse Gas Center and the NASA Terrestrial Ecology Program. We thank Yang Qi for assistance in preliminary PlanetScope data processing.

References

Alduchov, O. A. and Eskridge, R.: Improved Magnus form approximation of saturation vapor pressure, Journal of Applied

https://doi.org/10.5194/egusphere-2025-5023
Preprint. Discussion started: 27 October 2025

Meteorology, 35, 601–609, https://doi.org/10.1175/1520-0450(1996)035<0601:IMFAOS>2.0.CO;2, 1996.

Alekseychik, P., Korrensalo, A., Mammarella, I., Launiainen, S., Tuittila, E.-S., Korpela, I., and Vesala, T.: Carbon balance of a Finnish bog: temporal variability and limiting factors based on 6 years of eddy-covariance data, Biogeosciences, 18, 4681–4704, https://doi.org/10.5194/bg-18-4681-2021, 2021.

Anthony, T. L. and Silver, W. L.: Hot moments drive extreme nitrous oxide and methane emissions from agricultural peatlands, Glob. Chang. Biol., 27, 5141–5153, https://doi.org/10.1111/gcb.15802, 2021.

Anthony, T. L. and Silver, W. L.: Hot spots and hot moments of greenhouse gas emissions in agricultural peatlands, Biogeochemistry, 167, 461–477, https://doi.org/10.1007/s10533-023-01095-y, 2023.

Aubinet, M.: Eddy covariance CO2 flux measurements in nocturnal conditions: an analysis of the problem, Ecol. Appl., 18, 1368–1378, https://doi.org/10.1890/06-1336.1, 2008.

Aubinet, M., Vesala, T., and Papale, D.: Eddy Covariance: A Practical Guide to Measurement and Data Analysis, Springer Science & Business Media, 438 pp., https://doi.org/10.1007/978-94-007-2351-1, 2012.

Baldocchi, D.: Assessing the eddy covariance technique for evaluating carbon dioxide exchange rates of ecosystems: past, present and future: carbon balance and eddy covariance, Glob. Chang. Biol., 9, 479–492, https://doi.org/10.1046/j.1365-2486.2003.00629.x, 2003.

Baldocchi, D., Detto, M., Sonnentag, O., Verfaillie, J., Teh, Y. A., Silver, W., and Kelly, N. M.: The challenges of measuring methane fluxes and concentrations over a peatland pasture, Agric. For. Meteorol., 153, 177–187, https://doi.org/10.1016/j.agrformet.2011.04.013, 2012.

Bansal, S., Post van der Burg, M., Fern, R. R., Jones, J. W., Lo, R., McKenna, O. P., Tangen, B. A., Zhang, Z., and Gleason, R. A.: Large increases in methane emissions expected from North America's largest wetland complex, Sci. Adv., 9, eade1112, https://doi.org/10.1126/sciadv.ade1112, 2023a.

Bansal, S., Creed, I. F., Tangen, B. A., Bridgham, S. D., Desai, A. R., Krauss, K. W., Neubauer, S. C., Noe, G. B., Rosenberry, D. O., Trettin, C., Wickland, K. P., Allen, S. T., Arias-Ortiz, A., Armitage, A. R., Baldocchi, D., Banerjee, K., Bastviken, D., Berg, P., Bogard, M. J., Chow, A. T., Conner, W. H., Craft, C., Creamer, C., DelSontro, T., Duberstein, J. A., Eagle, M., Fennessy, M. S., Finkelstein, S. A., Göckede, M., Grunwald, S., Halabisky, M., Herbert, E., Jahangir, M. M. R., Johnson, O. F., Jones, M. C., Kelleway, J. J., Knox, S., Kroeger, K. D., Kuehn, K. A., Lobb, D., Loder, A. L., Ma, S., Maher, D. T., McNicol, G., Meier, J., Middleton, B. A., Mills, C., Mistry, P., Mitra, A., Mobilian, C., Nahlik, A. M., Newman, S., O'Connell, J. L., Oikawa, P., van der Burg, M. P., Schutte, C. A., Song, C., Stagg, C. L., Turner, J., Vargas, R., Waldrop, M. P., Wallin, M. B., Wang, Z. A., Ward, E. J., Willard, D. A., Yarwood, S., and Zhu, X.: Practical guide to measuring wetland carbon pools and fluxes, Wetlands (Wilmington), 43, 105, https://doi.org/10.1007/s13157-023-01722-2, 2023b.

Barba, J., Cueva, A., Bahn, M., Barron-Gafford, G. A., Bond-Lamberty, B., Hanson, P. J., Jaimes, A., Kulmala, L., Pumpanen, J., Scott, R. L., Wohlfahrt, G., and Vargas, R.: Comparing ecosystem and soil respiration: Review and key challenges of tower-based and soil measurements, Agric. For. Meteorol., 249, 434–443, https://doi.org/10.1016/j.agrformet.2017.10.028, 2018.

Bartoń, K.: MuMIn: Multi-Model Inference, https://doi.org/10.32614/CRAN.package.MuMIn, 2024

Becker, R. A., Allan R. Wilks, A. R., Brownrigg Ray Minka Thomas, and Deckmyn, A.: maps: Draw Geographical Maps, 2023.

https://doi.org/10.5194/egusphere-2025-5023
Preprint. Discussion started: 27 October 2025

van den Berg, M., van den Elzen, E., Ingwersen, J., Kosten, S., Lamers, L. P. M., and Streck, T.: Contribution of plant-induced pressurized flow to CH_4 emission from a Phragmites fen, Sci. Rep., 10, 12304, https://doi.org/10.1038/s41598-020-69034-7, 2020.

Bohrer, G., Ju, Y., Arend, K., Morin, T., Rey-Sanchez, C., Wrighton, K., and Villa, J.: Methane and CO_2 chamber fluxes and porewater concentrations US-OWC Ameriflux wetland site, 2015-2018, https://doi.org/10.15485/1568865, 2019.

Bohrer, G., Kerns, J., Morin, T., Rey-Sanchez, A., Villa, J., and Ju, Y.: FLUXNET-CH_4 US-OWC Old Woman Creek, https://doi.org/10.18140/FLX/1669690, 2020.

Bond-Lamberty, B., Christianson, D. S., Malhotra, A., Pennington, S. C., Sihi, D., AghaKouchak, A., Anjileli, H., Altaf Arain, M., Armesto, J. J., Ashraf, S., Ataka, M., Baldocchi, D., Andrew Black, T., Buchmann, N., Carbone, M. S., Chang, S.-C., Crill, P., Curtis, P. S., Davidson, E. A., Desai, A. R., Drake, J. E., El-Madany, T. S., Gavazzi, M., Görres, C.-M., Gough, C. M., Goulden, M., Gregg, J., Gutiérrez Del Arroyo, O., He, J.-S., Hirano, T., Hopple, A., Hughes, H., Järveoja, J., Jassal, R., Jian, J., Kan, H., Kaye, J., Kominami, Y., Liang, N., Lipson, D., Macdonald, C. A., Maseyk, K., Mathes, K., Mauritz, M., Mayes, M. A., McNulty, S., Miao, G., Migliavacca, M., Miller, S., Miniat, C. F., Nietz, J. G., Nilsson, M. B., Noormets, A., Norouzi, H., O'Connell, C. S., Osborne, B., Oyonarte, C., Pang, Z., Peichl, M., Pendall, E., Perez-Quezada, J. F., Phillips, C. L., Phillips, R. P., Raich, J. W., Renchon, A. A., Ruehr, N. K., Sánchez-Cañete, E. P., Saunders, M., Savage, K. E., Schrumpf, M., Scott, R. L., Seibt, U., Silver, W. L., Sun, W., Szutu, D., Takagi, K., Takagi, M., Teramoto, M., Tjoelker, M. G., Trumbore, S., Ueyama, M., Vargas, R., Varner, R. K., Verfaillie, J., Vogel, C., Wang, J., Winston, G., Wood, T. E., Wu, J., Wutzler, T., Zeng, J., Zha, T., Zhang, Q., and Zou, J.: COSORE: A community database for continuous soil respiration and other soil-atmosphere greenhouse gas flux data, Glob. Chang. Biol., 26, 7268–7283, https://doi.org/10.1111/gcb.15353, 2020.

Budishchev, A., Mi, Y., van Huissteden, J., Belelli-Marchesini, L., Schaepman-Strub, G., Parmentier, F. J. W., Fratini, G., Gallagher, A., Maximov, T. C., and Dolman, A. J.: Evaluation of a plot-scale methane emission model using eddy covariance observations and footprint modelling, Biogeosciences, 11, 4651–4664, https://doi.org/10.5194/bg-11-4651-2014, 2014.

Cernusak, L. A., Ubierna, N., Jenkins, M. W., Garrity, S. R., Rahn, T., Powers, H. H., Hanson, D. T., Sevanto, S., Wong, S. C., McDowell, N. G., and Farquhar, G. D.: Unsaturation of vapour pressure inside leaves of two conifer species, Sci. Rep., 8, 7667, https://doi.org/10.1038/s41598-018-25838-2, 2018.

Chaichana, N., Bellingrath-Kimura, S. D., Komiya, S., Fujii, Y., Noborio, K., Dietrich, O., and Pakoktom, T.: Comparison of Closed Chamber and Eddy Covariance Methods to Improve the Understanding of Methane Fluxes from Rice Paddy Fields in Japan, Atmosphere, 9, 356, https://doi.org/10.3390/atmos9090356, 2018.

Chamberlain, S. D., Verfaillie, J., Eichelmann, E., Hemes, K. S., and Baldocchi, D. D.: Evaluation of density corrections to methane fluxes measured by open-path eddy covariance over contrasting landscapes, Boundary Layer Meteorol., 165, 197–210, https://doi.org/10.1007/s10546-017-0275-9, 2017.

Chen, W., Zhang, F., Wang, B., Wang, J., Tian, D., Han, G., Wen, X., Yu, G., and Niu, S.: Diel and seasonal dynamics of ecosystem-scale methane flux and their determinants in an alpine meadow, J. Geophys. Res. Biogeosci., 124, 1731–1745, https://doi.org/10.1029/2019jg005011, 2019.

Chen, W., Wang, B., Zhang, F., Li, Z., Wang, J., Yu, G., Wen, X., and Niu, S.: Hysteretic relationship between plant productivity and methane uptake in an alpine meadow, Agric. For. Meteorol., 288-289, 107982, https://doi.org/10.1016/j.agrformet.2020.107982, 2020.

Cho, R., Schroth, M. H., and Zeyer, J.: Circadian methane oxidation in the root zone of rice plants, Biogeochemistry, 111,

https://doi.org/10.5194/egusphere-2025-5023
Preprint. Discussion started: 27 October 2025

317–330, https://doi.org/10.1007/s10533-011-9651-6, 2012.

Christiansen, J. R., Outhwaite, J., and Smukler, S. M.: Comparison of CO2, CH4 and N2O soil-atmosphere exchange measured in static chambers with cavity ring-down spectroscopy and gas chromatography, Agric. For. Meteorol., 211-212, 48–57, https://doi.org/10.1016/j.agrformet.2015.06.004, 2015.

Chu, H., Luo, X., Ouyang, Z., Chan, W. S., Dengel, S., Biraud, S. C., Torn, M. S., Metzger, S., Kumar, J., Arain, M. A., Arkebauer, T. J., Baldocchi, D., Bernacchi, C., Billesbach, D., Black, T. A., Blanken, P. D., Bohrer, G., Bracho, R., Brown, S., Brunsell, N. A., Chen, J., Chen, X., Clark, K., Desai, A. R., Duman, T., Durden, D., Fares, S., Forbrich, I., Gamon, J. A., Gough, C. M., Griffis, T., Helbig, M., Hollinger, D., Humphreys, E., Ikawa, H., Iwata, H., Ju, Y., Knowles, J. F., Knox, S. H., Kobayashi, H., Kolb, T., Law, B., Lee, X., Litvak, M., Liu, H., Munger, J. W., Noormets, A., Novick, K., Oberbauer, S. F., Oechel, W., Oikawa, P., Papuga, S. A., Pendall, E., Prajapati, P., Prueger, J., Quinton, W. L., Richardson, A. D., Russell, E. S., Scott, R. L., Starr, G., Staebler, R., Stoy, P. C., Stuart-Haëntjens, E., Sonnentag, O., Sullivan, R. C., Suyker, A., Ueyama, M., Vargas, R., Wood, J. D., and Zona, D.: Representativeness of Eddy-Covariance flux footprints for areas surrounding AmeriFlux sites, Agric. For. Meteorol., 301-302, 108350, https://doi.org/10.1016/j.agrformet.2021.108350, 2021.

Chu, H., Christianson, D. S., Cheah, Y.-W., Pastorello, G., O'Brien, F., Geden, J., Ngo, S.-T., Hollowgrass, R., Leibowitz, K., Beekwilder, N. F., Sandesh, M., Dengel, S., Chan, S. W., Santos, A., Delwiche, K., Yi, K., Buechner, C., Baldocchi, D., Papale, D., Keenan, T. F., Biraud, S. C., Agarwal, D. A., and Torn, M. S.: AmeriFlux BASE data pipeline to support network growth and data sharing, Sci. Data, 10, 614, https://doi.org/10.1038/s41597-023-02531-2, 2023.

Clement, R. J., Verma, S. B., and Verry, E. S.: Relating chamber measurements to eddy correlation measurements of methane flux, J. Geophys. Res. D: Atmos., 100, 21047–21056, https://doi.org/10.1029/95JD02196, 1995.

Davidson, E. A., Savage, K., Verchot, L. V., and Navarro, R.: Minimizing artifacts and biases in chamber-based measurements of soil respiration, Agric. For. Meteorol., 113, 21–37, https://doi.org/10.1016/s0168-1923(02)00100-4, 2002.

Davidson, S. J., Santos, M. J., Sloan, V. L., Reuss-Schmidt, K., Phoenix, G. K., Oechel, W. C., and Zona, D.: Upscaling CH4 Fluxes Using High-Resolution Imagery in Arctic Tundra Ecosystems, Remote Sensing, 9, 1227, https://doi.org/10.3390/rs9121227, 2017.

Delwiche, K. B., Knox, S. H., Malhotra, A., Fluet-Chouinard, E., McNicol, G., Feron, S., Ouyang, Z., Papale, D., Trotta, C., Canfora, E., and Others: FLUXNET-CH4: A global, multi-ecosystem dataset and analysis of methane seasonality from freshwater wetlands, Earth System Science Data Discussions, 2021, 1–111, 2021.

Desai, A. R.: AmeriFlux BASE US-Los Lost Creek, Ver. 33-5, AmeriFlux AMP, https://doi.org/10.17190/AMF/1246071, 2025a.

Desai, A. R.: In Situ Carbon Dioxide and Methane Flux Measurements Using Opaque Chambers in a Sedge Fen Wetland (US-Los Lost Creek AmeriFlux Site, Wisconsin, Summer 2015) ver 1. Environmental Data Initiative (1), https://doi.org/10.6073/pasta/fc48a416ab7c580f2fd0d5450668a23a, 2025b.

Desai, A. R. and Thom, J.: FLUXNET-CH4 US-Los Lost Creek, https://doi.org/10.18140/FLX/1669682, 2020.

Desai, A. R., Xu, K., Tian, H., Weishampel, P., Thom, J., Baumann, D., Andrews, A. E., Cook, B. D., King, J. Y., and Kolka, R.: Landscape-level terrestrial methane flux observed from a very tall tower, Agric. For. Meteorol., 201, 61–75, https://doi.org/10.1016/j.agrformet.2014.10.017, 2015.

Detto, M., Verfaillie, J., Anderson, F., Xu, L., and Baldocchi, D.: Comparing laser-based open- and closed-path gas analyzers

https://doi.org/10.5194/egusphere-2025-5023
Preprint. Discussion started: 27 October 2025

to measure methane fluxes using the eddy covariance method, Agric. For. Meteorol., 151, 1312–1324, https://doi.org/10.1016/j.agrformet.2011.05.014, 2011.

Deventer, M. J., Griffis, T. J., Roman, D. T., Kolka, R. K., Wood, J. D., Erickson, M., Baker, J. M., and Millet, D. B.: Error characterization of methane fluxes and budgets derived from a long-term comparison of open- and closed-path eddy covariance systems, Agric. For. Meteorol., 278, 107638, https://doi.org/10.1016/j.agrformet.2019.107638, 2019.

Dinno, A.: conover.test: Conover-Iman Test of Multiple Comparisons Using Rank Sums, https://doi.org/10.32614/CRAN.package.conover.test, 2024.

Erkkilä, K.-M., Ojala, A., Bastviken, D., Biermann, T., Heiskanen, J. J., Lindroth, A., Peltola, O., Rantakari, M., Vesala, T., and Mammarella, I.: Methane and carbon dioxide fluxes over a lake: comparison between eddy covariance, floating chambers and boundary layer method, Biogeosciences, 15, 429–445, https://doi.org/10.5194/bg-15-429-2018, 2018.

Forbrich, I., Kutzbach, L., Hormann, A., and Wilmking, M.: A comparison of linear and exponential regression for estimating diffusive CH4 fluxes by closed-chambers in peatlands, Soil Biol. Biochem., 42, 507–515, https://doi.org/10.1016/j.soilbio.2009.12.004, 2010.

Forbrich, I., Kutzbach, L., Wille, C., Becker, T., Wu, J., and Wilmking, M.: Cross-evaluation of measurements of peatland methane emissions on microform and ecosystem scales using high-resolution landcover classification and source weight modelling, Agric. For. Meteorol., 151, 864–874, https://doi.org/10.1016/j.agrformet.2011.02.006, 2011.

Fox, J. and Weisberg, S.: An R companion to applied regression, 3rd ed., SAGE Publications, Thousand Oaks, CA, 608 pp., https://www.john-fox.ca/Companion/, 2018.

Griebel, A., Bennett, L. T., Metzen, D., Cleverly, J., Burba, G., and Arndt, S. K.: Effects of inhomogeneities within the flux footprint on the interpretation of seasonal, annual, and interannual ecosystem carbon exchange, Agric. For. Meteorol., 221, 50–60, https://doi.org/10.1016/j.agrformet.2016.02.002, 2016.

Grossiord, C., Buckley, T. N., Cernusak, L. A., Novick, K. A., Poulter, B., Siegwolf, R. T. W., Sperry, J. S., and McDowell, N. G.: Plant responses to rising vapor pressure deficit, New Phytol., 226, 1550–1566, https://doi.org/10.1111/nph.16485, 2020.

Hargreaves, K. J., Fowler, D., Pitcairn, C. E. R., and Aurela, M.: Annual methane emission from Finnish mires estimated from eddy covariance campaign measurements, Theor. Appl. Climatol., 70, 203–213, https://doi.org/10.1007/s007040170015, 2001.

Hartley, I. P., Hill, T. C., Wade, T. J., Clement, R. J., Moncrieff, J. B., Prieto-Blanco, A., Disney, M. I., Huntley, B., Williams, M., Howden, N. J. K., Wookey, P. A., and Baxter, R.: Quantifying landscape-level methane fluxes in subarctic Finland using a multiscale approach, Glob. Chang. Biol., 21, 3712–3725, https://doi.org/10.1111/gcb.12975, 2015.

Heusinkveld, B. G., Jacobs, A. F. G., and Holtslag, A. A. M.: Effect of open-path gas analyzer wetness on eddy covariance flux measurements: A proposed solution, Agric. For. Meteorol., 148, 1563–1573, https://doi.org/10.1016/j.agrformet.2008.05.010, 2008.

Hill, A. C. and Vargas, R.: Carbon dioxide and methane chamber flux data from temperate S. alterniflora salt-marsh, https://doi.org/10.6084/M9.FIGSHARE.20099321.V1, 2022a.

Hill, A. C. and Vargas, R.: Methane and carbon dioxide fluxes in a temperate tidal salt marsh: Comparisons between plot and ecosystem measurements, J. Geophys. Res. Biogeosci., 127, https://doi.org/10.1029/2022jg006943, 2022b.

https://doi.org/10.5194/egusphere-2025-5023
Preprint. Discussion started: 27 October 2025

Hollinger, D. Y. and Richardson, A. D.: Uncertainty in eddy covariance measurements and its application to physiological models, Tree Physiol., 25, 873–885, https://doi.org/10.1093/treephys/25.7.873, 2005.

Holm, G., Perez, B., McWhorter, D., Krauss, K., Raynie, R., and Killebrew, C.: FLUXNET-CH4 US-LA1 Pointe-aux-Chenes Brackish Marsh, https://doi.org/10.18140/FLX/1669680, 2020a.

Holm, G., Perez, B., McWhorter, D., Krauss, K., Raynie, R., and Killebrew, C.: FLUXNET-CH4 US-LA2 Salvador WMA Freshwater Marsh, https://doi.org/10.18140/FLX/1669681, 2020b.

Intergovernmental Panel on Climate Change (IPCC): Climate Change 2021 – the physical science basis, Cambridge University Press, https://doi.org/10.1017/9781009157896, 2023.

Irvin, J., Zhou, S., McNicol, G., Lu, F., Liu, V., Fluet-Chouinard, E., Ouyang, Z., Knox, S. H., Lucas-Moffat, A., Trotta, C., Papale, D., Vitale, D., Mammarella, I., Alekseychik, P., Aurela, M., Avati, A., Baldocchi, D., Bansal, S., Bohrer, G., Campbell, D. I., Chen, J., Chu, H., Dalmagro, H. J., Delwiche, K. B., Desai, A. R., Euskirchen, E., Feron, S., Goeckede, M., Heimann, M., Helbig, M., Helfter, C., Hemes, K. S., Hirano, T., Iwata, H., Jurasinski, G., Kalhori, A., Kondrich, A., Lai, D. Y. F., Lohila, A., Malhotra, A., Merbold, L., Mitra, B., Ng, A., Nilsson, M. B., Noormets, A., Peichl, M., Rey-Sanchez, A. C., Richardson, A. D., Runkle, B. R. K., Schäfer, K. V. R., Sonnentag, O., Stuart-Haëntjens, E., Sturtevant, C., Ueyama, M., Valach, A. C., Vargas, R., Vourlitis, G. L., Ward, E. J., Wong, G. X., Zona, D., Alberto, M. C. R., Billesbach, D. P., Celis, G., Dolman, H., Friborg, T., Fuchs, K., Gogo, S., Gondwe, M. J., Goodrich, J. P., Gottschalk, P., Hörtnagl, L., Jacotot, A., Koebsch, F., Kasak, K., Maier, R., Morin, T. H., Nemitz, E., Oechel, W. C., Oikawa, P. Y., Ono, K., Sachs, T., Sakabe, A., Schuur, E. A., Shortt, R., Sullivan, R. C., Szutu, D. J., Tuittila, E.-S., Varlagin, A., Verfaillie, J. G., Wille, C., Windham-Myers, L., Poulter, B., and Jackson, R. B.: Gap-filling eddy covariance methane fluxes: Comparison of machine learning model predictions and uncertainties at FLUXNET-CH4 wetlands, Agric. For. Meteorol., 308-309, 108528, https://doi.org/10.1016/j.agrformet.2021.108528, 2021.

Iwata, H., Kosugi, Y., Ono, K., Mano, M., Sakabe, A., Miyata, A., and Takahashi, K.: Cross-validation of open-path and closed-path eddy-covariance techniques for observing methane fluxes, Boundary Layer Meteorol., 151, 95–118, https://doi.org/10.1007/s10546-013-9890-2, 2014.

Iwata, H., Ueyama, M., and Harazono, Y.: FLUXNET-CH4 US-Uaf University of Alaska, Fairbanks, https://doi.org/10.18140/FLX/1669701, 2020.

Järveoja, J., Nilsson, M. B., Gažovič, M., Crill, P. M., and Peichl, M.: Partitioning of the net CO2 exchange using an automated chamber system reveals plant phenology as key control of production and respiration fluxes in a boreal peatland, Glob. Chang. Biol., 24, 3436–3451, https://doi.org/10.1111/gcb.14292, 2018.

Jentzsch, K., van Delden, L., Fuchs, M., and Treat, C. C.: An expert survey on chamber measurement techniques and data handling procedures for methane fluxes, Earth System Science Data, 17, 2331–2372, https://doi.org/10.5194/essd-17-2331-2025, 2025.

Knapp, A. K. and Yavitt, J. B.: Evaluation of a closed-chamber method for estimating methane emissions from aquatic plants, Tellus B Chem. Phys. Meteorol., 44, 63–71, https://doi.org/10.1034/j.1600-0889.1992.00006.x, 1992.

Knox, S. H., Matthes, J. H., Sturtevant, C., Oikawa, P. Y., Verfaillie, J., and Baldocchi, D.: Biophysical controls on interannual variability in ecosystem-scale CO 2 and CH 4 exchange in a California rice paddy: Interannual variability rice CH4 fluxes, J. Geophys. Res. Biogeosci., 121, 978–1001, https://doi.org/10.1002/2015jg003247, 2016.

Knox, S. H., Jackson, R. B., Poulter, B., McNicol, G., Fluet-Chouinard, E., Zhang, Z., Hugelius, G., Bousquet, P., Canadell,

J. G., Saunois, M., Papale, D., Chu, H., Keenan, T. F., Baldocchi, D., Torn, M. S., Mammarella, I., Trotta, C., Aurela, M., Bohrer, G., Campbell, D. I., Cescatti, A., Chamberlain, S., Chen, J., Chen, W., Dengel, S., Desai, A. R., Euskirchen, E., Friborg, T., Gasbarra, D., Goded, I., Goeckede, M., Heimann, M., Helbig, M., Hirano, T., Hollinger, D. Y., Iwata, H., Kang, M., Klatt, J., Krauss, K. W., Kutzbach, L., Lohila, A., Mitra, B., Morin, T. H., Nilsson, M. B., Niu, S., Noormets, A., Oechel, W. C., Peichl, M., Peltola, O., Reba, M. L., Richardson, A. D., Runkle, B. R. K., Ryu, Y., Sachs, T., Schäfer, K. V. R., Schmid, H. P., Shurpali, N., Sonnentag, O., Tang, A. C. I., Ueyama, M., Vargas, R., Vesala, T., Ward, E. J., Windham-Myers, L., Wohlfahrt, G., and Zona, D.: FLUXNET-CH4 Synthesis Activity: Objectives, Observations, and Future Directions, Bull. Am. Meteorol. Soc., 100, 2607–2632, https://doi.org/10.1175/BAMS-D-18-0268.1, 2019.

Knox, S. H., Bansal, S., McNicol, G., Schafer, K., Sturtevant, C., Ueyama, M., Valach, A. C., Baldocchi, D., Delwiche, K., Desai, A. R., Euskirchen, E., Liu, J., Lohila, A., Malhotra, A., Melling, L., Riley, W., Runkle, B. R. K., Turner, J., Vargas, R., Zhu, Q., Alto, T., Fluet-Chouinard, E., Goeckede, M., Melton, J. R., Sonnentag, O., Vesala, T., Ward, E., Zhang, Z., Feron, S., Ouyang, Z., Alekseychik, P., Aurela, M., Bohrer, G., Campbell, D. I., Chen, J., Chu, H., Dalmagro, H. J., Goodrich, J. P., Gottschalk, P., Hirano, T., Iwata, H., Jurasinski, G., Kang, M., Koebsch, F., Mammarella, I., Nilsson, M. B., Ono, K., Peichl, M., Peltola, O., Ryu, Y., Sachs, T., Sakabe, A., Sparks, J. P., Tuittila, E.-S., Vourlitis, G. L., Wong, G. X., Windham-Myers, L., Poulter, B., and Jackson, R. B.: Identifying dominant environmental predictors of freshwater wetland methane fluxes across diurnal to seasonal time scales, Glob. Chang. Biol., 27, 3582–3604, https://doi.org/10.1111/gcb.15661, 2021.

Koebsch, F., Jurasinski, G., Koch, M., Hofmann, J., and Glatzel, S.: Controls for multi-scale temporal variation in ecosystem methane exchange during the growing season of a permanently inundated fen, Agric. For. Meteorol., 204, 94–105, https://doi.org/10.1016/j.agrformet.2015.02.002, 2015.

Korkiakoski, M., Tuovinen, J.-P., Aurela, M., Koskinen, M., Minkkinen, K., Ojanen, P., Penttilä, T., Rainne, J., Laurila, T., and Lohila, A.: Methane exchange at the peatland forest floor – automatic chamber system exposes the dynamics of small fluxes, Biogeosciences, 14, 1947–1967, https://doi.org/10.5194/bg-14-1947-2017, 2017.

Korrensalo, A., Männistö, E., Alekseychik, P., Mammarella, I., Rinne, J., Vesala, T., and Tuittila, E.-S.: Small spatial variability in methane emission measured from a wet patterned boreal bog, Biogeosciences, 15, 1749–1761, https://doi.org/10.5194/bg-15-1749-2018, 2018.

Krauss, K. W., Holm, G. O., Perez, B. C., McWhorter, D. E., Cormier, N., Moss, R. F., Johnson, D. J., Neubauer, S. C., and Raynie, R. C.: Component greenhouse gas fluxes and radiative balance from two deltaic marshes in Louisiana: Pairing chamber techniques and eddy covariance, Journal of Geophysical Research: Biogeosciences, 121, 1503–1521, https://doi.org/10.1002/2015JG003224, 2016.

Kroon, P. S., Hensen, A., Jonker, H. J. J., Zahniser, M. S., van 't Veen, W. H., and Vermeulen, A. T.: Suitability of quantum cascade laser spectroscopy for CH_4 and N_2O eddy covariance flux measurements, Biogeosciences, 4, 715–728, https://doi.org/10.5194/bg-4-715-2007, 2007.

Kroon, P. S., Hensen, A., Jonker, H. J. J., Ouwersloot, H. G., Vermeulen, A. T., and Bosveld, F. C.: Uncertainties in eddy covariance flux measurements assessed from CH4 and N2O observations, Agric. For. Meteorol., 150, 806–816, https://doi.org/10.1016/j.agrformet.2009.08.008, 2010.

Kuhn, M. A., Varner, R. K., Bastviken, D., Crill, P., MacIntyre, S., Turetsky, M., Walter Anthony, K., McGuire, A. D., and Olefeldt, D.: BAWLD-CH_4: a comprehensive dataset of methane fluxes from boreal and arctic ecosystems, Earth System Science Data, 13, 5151–5189, https://doi.org/10.5194/essd-13-5151-2021, 2021.

Kutzbach, L., Wagner, D., and Pfeiffer, E.-M.: Effect of microrelief and vegetation on methane emission from wet polygonal

https://doi.org/10.5194/egusphere-2025-5023
Preprint. Discussion started: 27 October 2025

tundra, Lena Delta, Northern Siberia, Biogeochemistry, 69, 341–362, https://doi.org/10.1023/B:BIOG.0000031053.81520.db, 2004.

Lai, D. Y. F., Roulet, N. T., Humphreys, E. R., Moore, T. R., and Dalva, M.: The effect of atmospheric turbulence and chamber deployment period on autochamber CO_2 and CH_4 flux measurements in an ombrotrophic peatland, Biogeosciences, 9, 3305–3322, https://doi.org/10.5194/bg-9-3305-2012, 2012.

Langensiepen, M., Kupisch, M., van Wijk, M. T., and Ewert, F.: Analyzing transient closed chamber effects on canopy gas exchange for optimizing flux calculation timing, Agric. For. Meteorol., 164, 61–70, https://doi.org/10.1016/j.agrformet.2012.05.006, 2012.

Lawrence, M. G.: The relationship between relative humidity and the dewpoint temperature in moist air: A simple conversion and applications, Bull. Am. Meteorol. Soc., 86, 225–234, https://doi.org/10.1175/bams-86-2-225, 2005.

Levy, P. E., Gray, A., Leeson, S. R., Gaiawyn, J., Kelly, M. P. C., Cooper, M. D. A., Dinsmore, K. J., Jones, S. K., and Sheppard, L. J.: Quantification of uncertainty in trace gas fluxes measured by the static chamber method, Eur. J. Soil Sci., 62, 811–821, https://doi.org/10.1111/j.1365-2389.2011.01403.x, 2011.

Livingston, G. P. and Hutchinson, G. L.: Enclosure-based measurement of trace gas exchange: applications and sources of error, in: Methods in ecology: biogenic trace gas emissions from soil and water, Blackwell Scientific Publications Inc., 14–51, 1995.

Long, K. D., Flanagan, L. B., and Cai, T.: Diurnal and seasonal variation in methane emissions in a northern Canadian peatland measured by eddy covariance, Glob. Chang. Biol., 16, 2420–2435, https://doi.org/10.1111/j.1365-2486.2009.02083.x, 2010.

Marushchak, M. E., Friborg, T., Biasi, C., Herbst, M., Johansson, T., Kiepe, I., Liimatainen, M., Lind, S. E., Martikainen, P. J., Virtanen, T., Soegaard, H., and Shurpali, N. J.: Methane dynamics in the subarctic tundra: combining stable isotope analyses, plot- and ecosystem-scale flux measurements, Biogeosciences, 13, 597–608, https://doi.org/10.5194/bg-13-597-2016, 2016.

McGuire, A. D., Christensen, T. R., Hayes, D., Heroult, A., Euskirchen, E., Kimball, J. S., Koven, C., Lafleur, P., Miller, P. A., Oechel, W., Peylin, P., Williams, M., and Yi, Y.: An assessment of the carbon balance of Arctic tundra: comparisons among observations, process models, and atmospheric inversions, Biogeosciences, 9, 3185–3204, https://doi.org/10.5194/bg-9-3185-2012, 2012.

McNicol, G., Fluet-Chouinard, E., Ouyang, Z., Knox, S., Zhang, Z., Aalto, T., Bansal, S., Chang, K.-Y., Chen, M., Delwiche, K., Feron, S., Goeckede, M., Liu, J., Malhotra, A., Melton, J. R., Riley, W., Vargas, R., Yuan, K., Ying, Q., Zhu, Q., Alekseychik, P., Aurela, M., Billesbach, D. P., Campbell, D. I., Chen, J., Chu, H., Desai, A. R., Euskirchen, E., Goodrich, J., Griffis, T., Helbig, M., Hirano, T., Iwata, H., Jurasinski, G., King, J., Koebsch, F., Kolka, R., Krauss, K., Lohila, A., Mammarella, I., Nilson, M., Noormets, A., Oechel, W., Peichl, M., Sachs, T., Sakabe, A., Schulze, C., Sonnentag, O., Sullivan, R. C., Tuittila, E.-S., Ueyama, M., Vesala, T., Ward, E., Wille, C., Wong, G. X., Zona, D., Windham-Myers, L., Poulter, B., and Jackson, R. B.: Upscaling wetland methane emissions from the FLUXNET-CH4 eddy covariance network (UpCH4 v1.0): Model development, network assessment, and budget comparison, AGU Adv., 4, https://doi.org/10.1029/2023av000956, 2023.

Meijide, A., Manca, G., Goded, I., Magliulo, V., di Tommasi, P., Seufert, G., and Cescatti, A.: Seasonal trends and environmental controls of methane emissions in a rice paddy field in Northern Italy, Biogeosci. Discuss., 8, 8999–9032, https://doi.org/10.5194/bgd-8-8999-2011, 2011.

https://doi.org/10.5194/egusphere-2025-5023
Preprint. Discussion started: 27 October 2025

Metzger, S.: Surface-atmosphere exchange in a box: Making the control volume a suitable representation for in-situ observations, Agric. For. Meteorol., 255, 68–80, https://doi.org/10.1016/j.agrformet.2017.08.037, 2018.

Montaldo, N. and Oren, R.: The way the wind blows matters to ecosystem water use efficiency, Agric. For. Meteorol., 217, 1–9, https://doi.org/10.1016/j.agrformet.2015.11.002, 2016.

Morin, T. H.: Advances in the eddy covariance approach to CH_4 monitoring over two and a half decades, J. Geophys. Res. Biogeosci., 124, 453–460, https://doi.org/10.1029/2018jg004796, 2019.

Morin, T. H., Bohrer, G., Frasson, R. P. d., Naor-Azreli, L., Mesi, S., Stefanik, K. C., and Schäfer, K. V. R.: Environmental drivers of methane fluxes from an urban temperate wetland park, Journal of Geophysical Research: Biogeosciences, 119, 2188–2208, https://doi.org/10.1002/2014JG002750, 2014.

Morin, T. H., Bohrer, G., Stefanik, K. C., Rey-Sanchez, A. C., Matheny, A. M., and Mitsch, W. J.: Combining eddy-covariance and chamber measurements to determine the methane budget from a small, heterogeneous urban floodplain wetland park, Agric. For. Meteorol., 237-238, 160–170, https://doi.org/10.1016/j.agrformet.2017.01.022, 2017.

Määttä, T., Desai, A., Ueyama, M., Vargas, R., Ward, E. J., Zhang, Z., Bohrer, G., Delwiche, K., Fluet-Chouinard, E., Järveoja, J., Knox, S., Melling, L., Nilsson, M. B., Peichl, M., Tang, A. C. I., Tuittila, E.-S., Wang, J., Bansal, S., Feron, S., Helbig, M., Korrensalo, A., Krauss, K. W., McNicol, G., Niu, S., Ouyang, Z., Savage, K., Sonnentag, O., Jackson, R., and Malhotra, A.: Cross-site comparison of ecosystem- and plot-scale methane fluxes from wetlands and uplands (Version v1), Zenodo [data set], https://doi.org/10.5281/zenodo.17312404, 2025.

Nadeau, D. F., Rousseau, A. N., Coursolle, C., Margolis, H. A., and Parlange, M. B.: Summer methane fluxes from a boreal bog in northern Quebec, Canada, using eddy covariance measurements, Atmos. Environ. (1994), 81, 464–474, https://doi.org/10.1016/j.atmosenv.2013.09.044, 2013.

Nakano, T.: A comparison of regression methods for estimating soil–atmosphere diffusion gas fluxes by a closed-chamber technique, Soil Biol. Biochem., 36, 107–113, https://doi.org/10.1016/j.soilbio.2003.07.005, 2004.

van der Nat, F.-F. W. A., Middelburg*, J. J., Van Meteren, D., and Wielemakers, A.: Diel methane emission patterns from Scirpus lacustris and Phragmites australis, Biogeochemistry, 41, 1–22, https://doi.org/10.1023/a:1005933100905, 1998.

Nilsson, M. and Peichl, M.: FLUXNET-CH4 SE-Deg Degero, https://doi.org/10.18140/FLX/1669659, 2020.

Niu, S. and Chen, W.: FLUXNET-CH4 CN-Hgu Hongyuan, https://doi.org/10.18140/FLX/1669632, 2020.

Niu, S., Luo, Y., Fei, S., Montagnani, L., Bohrer, G., Janssens, I. A., Gielen, B., Rambal, S., Moors, E., and Matteucci, G.: Seasonal hysteresis of net ecosystem exchange in response to temperature change: patterns and causes: SEASONAL HYSTERESIS OF NET ECOSYSTEM EXCHANGE, Glob. Chang. Biol., 17, 3102–3114, https://doi.org/10.1111/j.1365-2486.2011.02459.x, 2011.

Oikawa, P. Y., Sihi, D., Forbrich, I., Fluet-Chouinard, E., Najarro, M., Thomas, O., Shahan, J., Arias-Ortiz, A., Russell, S., Knox, S. H., McNicol, G., Wolfe, J., Windham-Myers, L., Stuart-Haentjens, E., Bridgham, S. D., Needelman, B., Vargas, R., Schäfer, K., Ward, E. J., Megonigal, P., and Holmquist, J.: A new coupled biogeochemical modeling approach provides accurate predictions of methane and carbon dioxide fluxes across diverse tidal wetlands, J. Geophys. Res. Biogeosci., 129, https://doi.org/10.1029/2023jg007943, 2024.

Parmentier, F. J. W., van Huissteden, J., van der Molen, M. K., Schaepman-Strub, G., Karsanaev, S. A., Maximov, T. C., and

https://doi.org/10.5194/egusphere-2025-5023
Preprint. Discussion started: 27 October 2025

Dolman, A. J.: Spatial and temporal dynamics in eddy covariance observations of methane fluxes at a tundra site in northeastern Siberia, J. Geophys. Res., 116, https://doi.org/10.1029/2010jg001637, 2011.

Peltola, O., Hensen, A., Helfter, C., Belelli Marchesini, L., Bosveld, F. C., van den Bulk, W. C. M., Elbers, J. A., Haapanala, S., Holst, J., Laurila, T., Lindroth, A., Nemitz, E., Röckmann, T., Vermeulen, A. T., and Mammarella, I.: Evaluating the performance of commonly used gas analysers for methane eddy covariance flux measurements: the InGOS inter-comparison field experiment, Biogeosciences, 11, 3163–3186, https://doi.org/10.5194/bg-11-3163-2014, 2014.

Peltola, O., Vesala, T., Gao, Y., Räty, O., Alekseychik, P., Aurela, M., Chojnicki, B., Desai, A. R., Dolman, A. J., Euskirchen, E. S., Friborg, T., Göckede, M., Helbig, M., Humphreys, E., Jackson, R. B., Jocher, G., Joos, F., Klatt, J., Knox, S. H., Kowalska, N., Kutzbach, L., Lienert, S., Lohila, A., Mammarella, I., Nadeau, D. F., Nilsson, M. B., Oechel, W. C., Peichl, M., Pypker, T., Quinton, W., Rinne, J., Sachs, T., Samson, M., Schmid, H. P., Sonnentag, O., Wille, C., Zona, D., and Aalto, T.: Monthly gridded data product of northern wetland methane emissions based on upscaling eddy covariance observations, Earth Syst. Sci. Data, 11, 1263–1289, https://doi.org/10.5194/essd-11-1263-2019, 2019.

Peterson, R.: Finding optimal normalizing transformations via bestNormalize, R J., 13, 310, https://doi.org/10.32614/rj-2021-041, 2021.

Phillips, C. L., Bond-Lamberty, B., Desai, A. R., Lavoie, M., Risk, D., Tang, J., Todd-Brown, K., and Vargas, R.: The value of soil respiration measurements for interpreting and modeling terrestrial carbon cycling, Plant Soil, 413, 1–25, https://doi.org/10.1007/s11104-016-3084-x, 2017.

Pihlatie, M. K., Christiansen, J. R., Aaltonen, H., Korhonen, J. F. J., Nordbo, A., Rasilo, T., Benanti, G., Giebels, M., Helmy, M., Sheehy, J., Jones, S., Juszczak, R., Klefoth, R., Lobo-do-Vale, R., Rosa, A. P., Schreiber, P., Serça, D., Vicca, S., Wolf, B., and Pumpanen, J.: Comparison of static chambers to measure CH4 emissions from soils, Agric. For. Meteorol., 171-172, 124–136, https://doi.org/10.1016/j.agrformet.2012.11.008, 2013.

Pinheiro J, Bates D, R Core Team: nlme: Linear and Nonlinear Mixed Effects Models, https://doi.org/10.32614/CRAN.package.nlme, 2023.

Pinheiro, J. C. and Bates, D. M.: Mixed-Effects Models in S and S-PLUS, Springer, New York, https://doi.org/10.1007/b98882, 2000.

Räsänen, A., Manninen, T., Korkiakoski, M., Lohila, A., and Virtanen, T.: Predicting catchment-scale methane fluxes with multi-source remote sensing, Landsc. Ecol., 36, 1177–1195, https://doi.org/10.1007/s10980-021-01194-x, 2021.

R Core Team: R: A Language and Environment for Statistical Computing. R Foundation for Statistical Computing, Vienna, Austria, https://www.R-project.org, 2024.

Rebmann, C., Göckede, M., Foken, T., Aubinet, M., Aurela, M., Berbigier, P., Bernhofer, C., Buchmann, N., Carrara, A., Cescatti, A., Ceulemans, R., Clement, R., Elbers, J. A., Granier, A., Grünwald, T., Guyon, D., Havránková, K., Heinesch, B., Knohl, A., Laurila, T., Longdoz, B., Marcolla, B., Markkanen, T., Miglietta, F., Moncrieff, J., Montagnani, L., Moors, E., Nardino, M., Ourcival, J.-M., Rambal, S., Rannik, Ü., Rotenberg, E., Sedlak, P., Unterhuber, G., Vesala, T., and Yakir, D.: Quality analysis applied on eddy covariance measurements at complex forest sites using footprint modelling, Theor. Appl. Climatol., 80, 121–141, https://doi.org/10.1007/s00704-004-0095-y, 2005.

Rey-Sanchez, C., Morin, T. H., Stefanik, K. C., Wrighton, K., and Bohrer, G.: Determining total emissions and environmental drivers of methane flux in a Lake Erie estuarine marsh, Ecol. Eng., 114, 7–15, https://doi.org/10.1016/j.ecoleng.2017.06.042, 2018.

Rey-Sanchez, C., Arias-Ortiz, A., Kasak, K., Chu, H., Szutu, D., Verfaillie, J., and Baldocchi, D.: Detecting hot spots of methane flux using footprint-weighted flux maps, J. Geophys. Res. Biogeosci., 127, e2022JG006977, https://doi.org/10.1029/2022JG006977, 2022.

Rey-Sanchez, C., Arias-Ortiz, A., Kasak, K., Shortt, R., Szutu, D., Verfaillie, J., Lorenson, T., Liira, M., Somelar, P., Espenberg, M., and Baldocchi, D.: Explaining hot spots of methane flux in a restored wetland: the role of water level, soil disturbance, and methanotrophy, Environ. Res. Lett., 20, 074064, https://doi.org/10.1088/1748-9326/ade45b, 2025.

Richardson, A. D. and Hollinger, D.: FLUXNET-CH4 US-Ho1 Howland Forest (main tower), https://doi.org/10.18140/FLX/1669675, 2020.

Richardson, A. D., Hollinger, D. Y., Burba, G. G., Davis, K. J., Flanagan, L. B., Katul, G. G., William Munger, J., Ricciuto, D. M., Stoy, P. C., Suyker, A. E., Verma, S. B., and Wofsy, S. C.: A multi-site analysis of random error in tower-based measurements of carbon and energy fluxes, Agric. For. Meteorol., 136, 1–18, https://doi.org/10.1016/j.agrformet.2006.01.007, 2006.

Richardson, A. D., Mahecha, M. D., Falge, E., Kattge, J., Moffat, A. M., Papale, D., Reichstein, M., Stauch, V. J., Braswell, B. H., Churkina, G., Kruijt, B., and Hollinger, D. Y.: Statistical properties of random CO2 flux measurement uncertainty inferred from model residuals, Agric. For. Meteorol., 148, 38–50, https://doi.org/10.1016/j.agrformet.2007.09.001, 2008.

Richardson, A. D., Hollinger, D. Y., Shoemaker, J. K., Hughes, H., Savage, K., and Davidson, E. A.: Six years of ecosystem-atmosphere greenhouse gas fluxes measured in a sub-boreal forest, Sci. Data, 6, 117, https://doi.org/10.1038/s41597-019-0119-1, 2019.

Rinne, J., Riutta, T., Pihlatie, M., Aurela, M., Haapanala, S., Tuovinen, J.-P., Tuittila, E.-S., and Vesala, T.: Annual cycle of methane emission from a boreal fen measured by the eddy covariance technique, Tellus B Chem. Phys. Meteorol., 59, https://doi.org/10.3402/tellusb.v59i3.17009, 2007.

Riutta, T., Laine, J., Aurela, M., Rinne, J., Vesala, T., Laurila, T., Haapanala, S., Pihlatie, M., and Tuittila, E.-S.: Spatial variation in plant community functions regulates carbon gas dynamics in a boreal fen ecosystem, Tellus B Chem. Phys. Meteorol., 59, 838, https://doi.org/10.1111/j.1600-0889.2007.00302.x, 2007.

Rößger, N., Wille, C., Holl, D., Göckede, M., and Kutzbach, L.: Scaling and balancing carbon dioxide fluxes in a heterogeneous tundra ecosystem of the Lena River Delta, Biogeosciences, 16, 2591–2615, https://doi.org/10.5194/bg-16-2591-2019, 2019.

Sachs, T., Wille, C., Boike, J., and Kutzbach, L.: Environmental controls on ecosystem-scale CH4emission from polygonal tundra in the Lena River Delta, Siberia, J. Geophys. Res., 113, https://doi.org/10.1029/2007jg000505, 2008.

Saunois, M., Martinez, A., Poulter, B., Zhang, Z., Raymond, P., Regnier, P., Canadell, J. G., Jackson, R. B., Patra, P. K., Bousquet, P., Ciais, P., Dlugokencky, E. J., Lan, X., Allen, G. H., Bastviken, D., Beerling, D. J., Belikov, D. A., Blake, D. R., Castaldi, S., Crippa, M., Deemer, B. R., Dennison, F., Etiope, G., Gedney, N., Höglund-Isaksson, L., Holgerson, M. A., Hopcroft, P. O., Hugelius, G., Ito, A., Jain, A. K., Janardanan, R., Johnson, M. S., Kleinen, T., Krummel, P., Lauerwald, R., Li, T., Liu, X., McDonald, K. C., Melton, J. R., Mühle, J., Müller, J., Murguia-Flores, F., Niwa, Y., Noce, S., Pan, S., Parker, R. J., Peng, C., Ramonet, M., Riley, W. J., Rocher-Ros, G., Rosentreter, J. A., Sasakawa, M., Segers, A., Smith, S. J., Stanley, E. H., Thanwerdas, J., Tian, H., Tsuruta, A., Tubiello, F. N., Weber,

T. S., van der Werf, G., Worthy, D. E., Xi, Y., Yoshida, Y., Zhang, W., Zheng, B., Zhu, Q., Zhu, Q., and Zhuang, Q.: Global Methane Budget 2000–2020, Earth System Science Data Discussions, https://doi.org/10.5194/essd-2024-115, 2024.

Schrier-Uijl, A. P., Kroon, P. S., Hensen, A., Leffelaar, P. A., Berendse, F., and Veenendaal, E. M.: Comparison of chamber and eddy covariance-based CO2 and CH4 emission estimates in a heterogeneous grass ecosystem on peat, Agric. For. Meteorol., 150, 825–831, https://doi.org/10.1016/j.agrformet.2009.11.007, 2010.

Sha, C., Mitsch, W. J., Mander, Ü., Lu, J., Batson, J., Zhang, L., and He, W.: Methane emissions from freshwater riverine wetlands, Ecol. Eng., 37, 16–24, https://doi.org/10.1016/j.ecoleng.2010.07.022, 2011.

Smeets, C. J. P. P., Holzinger, R., Vigano, I., Goldstein, A. H., and Röckmann, T.: Eddy covariance methane measurements at a Ponderosa pine plantation in California, Atmos. Chem. Phys., 9, 8365–8375, https://doi.org/10.5194/acp-9-8365-2009, 2009.

Stewart, G. A., Sharp, S. J., Taylor, A. K., Williams, M. R., and Palmer, M. A.: High spatial variability in wetland methane fluxes is tied to vegetation patch types, Biogeochemistry, https://doi.org/10.1007/s10533-024-01188-2, 2024.

Subke, J.-A., Kutzbach, L., and Risk, D.: Soil chamber measurements, in: Springer Handbook of Atmospheric Measurements, Springer International Publishing, Cham, 1603–1624, https://doi.org/10.1007/978-3-030-52171-4_60, 2021.

Tokida, T., Miyazaki, T., Mizoguchi, M., Nagata, O., Takakai, F., Kagemoto, A., and Hatano, R.: Falling atmospheric pressure as a trigger for methane ebullition from peatland, Global Biogeochem. Cycles, 21, https://doi.org/10.1029/2006GB002790, 2007.

Tuovinen, J.-P., Aurela, M., Hatakka, J., Räsänen, A., Virtanen, T., Mikola, J., Ivakhov, V., Kondratyev, V., and Laurila, T.: Interpreting eddy covariance data from heterogeneous Siberian tundra: land-cover-specific methane fluxes and spatial representativeness, Biogeosciences, 16, 255–274, https://doi.org/10.5194/bg-16-255-2019, 2019.

Turetsky, M. R., Kotowska, A., Bubier, J., Dise, N. B., Crill, P., Hornibrook, E. R. C., Minkkinen, K., Moore, T. R., Myers-Smith, I. H., Nykänen, H., Olefeldt, D., Rinne, J., Saarnio, S., Shurpali, N., Tuittila, E.-S., Waddington, J. M., White, J. R., Wickland, K. P., and Wilmking, M.: A synthesis of methane emissions from 71 northern, temperate, and subtropical wetlands, Glob. Chang. Biol., 20, 2183–2197, https://doi.org/10.1111/gcb.12580, 2014.

Ueyama, M., Iwata, H., and Harazono, Y.: CO2 and CH4 fluxes data based on an automated-closed chamber system for a black spruce forest on permafrost in Fairbanks, Alaska, https://doi.org/10.17592/001.2021093001, 2022.

Ueyama, M., Iwata, H., Endo, R., and Harazono, Y.: Methane and carbon dioxide emissions from the forest floor of a black spruce forest on permafrost in interior Alaska, Polar Sci., 35, 100921, https://doi.org/10.1016/j.polar.2022.100921, 2023a.

Ueyama, M., Knox, S. H., Delwiche, K. B., Bansal, S., Riley, W. J., Baldocchi, D., Hirano, T., McNicol, G., Schafer, K., Windham-Myers, L., Poulter, B., Jackson, R. B., Chang, K.-Y., Chen, J., Chu, H., Desai, A. R., Gogo, S., Iwata, H., Kang, M., Mammarella, I., Peichl, M., Sonnentag, O., Tuittila, E.-S., Ryu, Y., Euskirchen, E. S., Göckede, M., Jacotot, A., Nilsson, M. B., and Sachs, T.: Modeled production, oxidation, and transport processes of wetland methane emissions in temperate, boreal, and Arctic regions, Glob. Chang. Biol., 29, 2313–2334, https://doi.org/10.1111/gcb.16594, 2023b.

Vargas, R. and Le, V. H.: The paradox of assessing greenhouse gases from soils for nature-based solutions, Biogeosciences, 20, 15–26, https://doi.org/10.5194/bg-20-15-2023, 2023.

https://doi.org/10.5194/egusphere-2025-5023
Preprint. Discussion started: 27 October 2025

Vázquez-Lule, A. and Vargas, R.: Biophysical drivers of net ecosystem and methane exchange across phenological phases in a tidal salt marsh, Agric. For. Meteorol., 300, 108309, https://doi.org/10.1016/j.agrformet.2020.108309, 2021.

Venterea, R. T., Spokas, K. A., and Baker, J. M.: Accuracy and precision analysis of chamber-based nitrous oxide gas flux estimates, Soil Sci. Soc. Am. J., 73, 1087–1093, https://doi.org/10.2136/sssaj2008.0307, 2009.

Vesala, T., Kljun, N., Rannik, U., Rinne, J., Sogachev, A., Markkanen, T., Sabelfeld, K., Foken, T., and Leclerc, M. Y.: Flux and concentration footprint modelling: state of the art, Environ. Pollut., 152, 653–666, https://doi.org/10.1016/j.envpol.2007.06.070, 2008.

Vesala, T., Tuittila, E.-S., Mammarella, I., and Alekseychik, P.: FLUXNET-CH4 FI-Si2 Siikaneva-2 Bog, https://doi.org/10.18140/FLX/1669639, 2020.

Villa, J. A., Ju, Y., Yazbeck, T., Waldo, S., Wrighton, K. C., and Bohrer, G.: Ebullition dominates methane fluxes from the water surface across different ecohydrological patches in a temperate freshwater marsh at the end of the growing season, Sci. Total Environ., 767, 144498, https://doi.org/10.1016/j.scitotenv.2020.144498, 2021.

Virkkala, A.-M., Virtanen, T., Lehtonen, A., Rinne, J., and Luoto, M.: The current state of CO2 flux chamber studies in the Arctic tundra: A review, Progress in Physical Geography: Earth and Environment, 42, 162–184, https://doi.org/10.1177/0309133317745784, 2018.

Voigt, C., Virkkala, A.-M., Hould Gosselin, G., Bennett, K. A., Black, T. A., Detto, M., Chevrier-Dion, C., Guggenberger, G., Hashmi, W., Kohl, L., Kou, D., Marquis, C., Marsh, P., Marushchak, M. E., Nesic, Z., Nykänen, H., Saarela, T., Sauheitl, L., Walker, B., Weiss, N., Wilcox, E. J., and Sonnentag, O.: Arctic soil methane sink increases with drier conditions and higher ecosystem respiration, Nat. Clim. Chang., 13, 1095–1104, https://doi.org/10.1038/s41558-023-01785-3, 2023.

Vroom, R. J. E., van den Berg, M., Pangala, S. R., van der Scheer, O. E., and Sorrell, B. K.: Physiological processes affecting methane transport by wetland vegetation – A review, Aquat. Bot., 182, 103547, https://doi.org/10.1016/j.aquabot.2022.103547, 2022.

Wang, J., Luo, Y., Quan, Q., Ma, F., Tian, D., Chen, W., Wang, S., Yang, L., Meng, C., and Niu, S.: Effects of warming and clipping on CH4 and N2O fluxes in an alpine meadow, Agric. For. Meteorol., 297, 108278, https://doi.org/10.1016/j.agrformet.2020.108278, 2021.

Wang, J. M., Murphy, J. G., Geddes, J. A., Winsborough, C. L., Basiliko, N., and Thomas, S. C.: Methane fluxes measured by eddy covariance and static chamber techniques at a temperate forest in central Ontario, Canada, Biogeosciences, 10, 4371–4382, https://doi.org/10.5194/bg-10-4371-2013, 2013.

Wang, P., Wang, J., Elberling, B., Yang, L., Chen, W., Song, L., Yan, Y., Wang, S., Pan, J., He, Y., and Niu, S.: Increased annual methane uptake driven by warmer winters in an alpine meadow, Glob. Chang. Biol., 28, 3246–3259, https://doi.org/10.1111/gcb.16120, 2022.

Whiting, G. J. and Chanton, J. P.: Control of the diurnal pattern of methane emission from emergent aquatic macrophytes by gas transport mechanisms, Aquat. Bot., 54, 237–253, https://doi.org/10.1016/0304-3770(96)01048-0, 1996.

Wille, C., Kutzbach, L., Sachs, T., Wagner, D., and Pfeiffer, E.-M.: Methane emission from Siberian arctic polygonal tundra: eddy covariance measurements and modeling: methane emission from Siberian arctic tundra. Glob. Chang. Biol., 14, 1395–1408, https://doi.org/10.1111/j.1365-2486.2008.01586.x, 2008.

https://doi.org/10.5194/egusphere-2025-5023
Preprint. Discussion started: 27 October 2025

Xu, K., Metzger, S., and Desai, A. R.: Surface-atmosphere exchange in a box: Space-time resolved storage and net vertical fluxes from tower-based eddy covariance, Agric. For. Meteorol., 255, 81–91, https://doi.org/10.1016/j.agrformet.2017.10.011, 2018.

Yeo, I. and Johnson, R. A.: A new family of power transformations to improve normality or symmetry, Biometrika, 87, 954–959, https://doi.org/10.1093/BIOMET/87.4.954, 2000.

Yuan, K., Li, F., McNicol, G., Chen, M., Hoyt, A., Knox, S., Riley, W. J., Jackson, R., and Zhu, Q.: Boreal-Arctic wetland methane emissions modulated by warming and vegetation activity, Nat. Clim. Chang., 14, 282–288, https://doi.org/10.1038/s41558-024-01933-3, 2024.

Yu, L., Wang, H., Wang, G., Song, W., Huang, Y., Li, S.-G., Liang, N., Tang, Y., and He, J.-S.: A comparison of methane emission measurements using Eddy Covariance and manual and automated chamber-based techniques in Tibetan Plateau alpine wetland, Environ. Pollut., 181, 81–90, https://doi.org/10.1016/j.envpol.2013.06.018, 2013.

Zhang, Y., Sachs, T., Li, C., and Boike, J.: Upscaling methane fluxes from closed chambers to eddy covariance based on a permafrost biogeochemistry integrated model, Glob. Chang. Biol., 18, 1428–1440, https://doi.org/10.1111/j.1365-2486.2011.02587.x, 2012.

Zhao, K., Ma, B., Xu, Y., Stirling, E., and Xu, J.: Light exposure mediates circadian rhythms of rhizosphere microbial communities, ISME J., 15, 2655–2664, https://doi.org/10.1038/s41396-021-00957-3, 2021.

Zhu, Q., Yuan, K., Li, F., Riley, W. J., Hoyt, A., Jackson, R., McNicol, G., Chen, M., Knox, S. H., Briner, O., Beerling, D., Gedney, N., Hopcroft, P. O., Ito, A., Jain, A. K., Jensen, K., Kleinen, T., Li, T., Liu, X., McDonald, K. C., Melton, J. R., Miller, P. A., Müller, J., Peng, C., Poulter, B., Qin, Z., Peng, S., Tian, H., Xu, X., Yao, Y., Xi, Y., Zhang, Z., Zhang, W., Zhu, Q., and Zhuang, Q.: Critical needs to close monitoring gaps in pan-tropical wetland CH_4 emissions, Environ. Res. Lett., 19, 114046, https://doi.org/10.1088/1748-9326/ad8019, 2024.